Høgskulen på Vestlandet

MMO5017 - Master thesis

MMO5017-MOPPG-1-2023-VÅR-FLOWassign

Predefinert informasjon

Startdato:	16-05-2023 00:00 CEST	**Termin:**	2023 VÅR
Sluttdato:	02-06-2023 14:00 CEST	**Vurderingsform:**	Norsk 6-trinns skala (A-F)
Eksamensform:	Master thesis		
Flowkode:	203 MMO5017 1 MOPPG-1 2023 VÅR		
Intern sensor:	(Anonymisert)		

Deltaker

Navn:	Lucky Chukwuladi Masi
Kandidatnr.:	211
HVL-id:	602237@hvl.no

Informasjon fra deltaker

Antall ord *:	22000

Egenerklæring *:	Ja	**Inneholder besvarelsen konfidensielt materiale?:**	Nei
Jeg bekrefter at jeg har registrert oppgavetittelen på norsk og engelsk i StudentWeb og vet at denne vil stå på vitnemålet mitt *:	Ja		

Gruppe

Gruppenavn:	One-person group
Gruppenummer:	9
Andre medlemmer i gruppen:	Deltakeren har innlevert i en enkeltmannsgruppe

Jeg godkjenner avtalen om publisering av masteroppgaven min *

Ja

Er masteroppgaven skrevet som del av et større forskningsprosjekt ved HVL? *

Nei

Er masteroppgaven skrevet ved bedrift/virksomhet i næringsliv eller offentlig sektor? *

Nei

Lucky Chukwuladi Masi

Installation Analysis of Offshore Structures in Swell Dominant Sea States: with Focus on Southern Nigerain Waters - using Hybrid Modelling Technique (HMT)

Master's thesis in Marine Operations, Technology, and Management

Supervisor: Prof. Ove Tobias Gudmestad

June 2023

Western Norway University of Applied Science
Faculty of Natural Sciences

Department of Marine Technology

Abstract

This research comprehensively models swell sea states in Southern Nigerian water. It investigates the response and nature of the sea loads experienced by installation vessels in a typical Southern Nigerian Sea state. Further, it assesses the implication of swells on the response of an installation vessel and the significance of the response to the planning and execution of installation operations in Southern Nigeria.

Due to their high energy and long periods, swells have been identified to pose some challenges to vessel motions concerning particularly around vessel's resonance period. With the identification of swell as the dominant spectra in Southern Nigeria and seemingly limited scholarly studies on the motion characteristics of vessels in this region, the master's thesis deemed it necessary to embark on this research to uncover the spectra-response relationship and provide additional insight into existing knowledge.

Through hybrid modelling techniques (HMT), which combined extensive literature studies, mathematical modelling of ocean waves, spectra modelling, 3D modelling, and numerical simulations using ShipX, a frequency-domain spectra analysis was carried out for the Asabo deep-water field, Forcados, and Bonga field. In total, 19 spectra with varying significant wave heights (H_s) and peak periods (T_P) were analysed.

Apart from the consistency seen in the data where swells dominate Southern Nigerian waters, the vessel motion analysis demonstrates significant motion amplification in beams seas, particularly at about 8 seconds of spectra peak period. Hence, roll motion is found to be more significant in the first instance where viscous effects and damping from bilge keels were neglected. Subsequently, with the inclusion of viscous effects and bilge keels in the rolling regime, a significant reduction in the roll motion was recorded, but motion amplification around 8s shows persistency.

With the further assessment of crew comfort using motion-induced sickness as a criterion, the findings correlate with roll motion as the primary contributor to the recorded motion sickness dose value (MSDV). This highlights and underscores the need for an adequate roll-stabilizing mechanism to be incorporated in the design of installation vessels. At the same time, reliance on data and favourable weather windows would be used for a safe planning and execution of installation operations.

Overall, this thesis contributes to the advancement of sea state modelling in Southern Nigerian waters and provides valuable insight for the design of offshore structures, planning and execution of installation operations in Southern Nigeria.

Preface

This document is a master's thesis report authored by Masi, Lucky Chukwuladi and supervised by Professor Ove Tobias Gudmestad. The thesis constitutes parts of the 120 European Credit Transfer System (E.C.T.S) for the international master's degree in maritime technology, operations and management option jointly conducted by the Western Norway University of Applied Sciences and the University of Applied Science Emden/Leer.

Sign:

Masi, Lucky Chukwuladi Masi

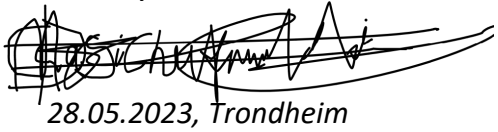

28.05.2023, Trondheim

Dedication

With pleasure, I dedicate this thesis project to the loving and eternal memories of my late parents and all those who have and continue to inspire and challenge me in this life journey.

Acknowledgement

I wish to acknowledge and appreciate the thesis supervisor Professor Ove Tobias Gudmestad, whose immense and rich knowledge proved a source of inspiration. Further acknowledgement is also extended to my employer Boa Offshores in Trondheim, and its engineering leadership for providing the software license.

Glossary of Terms

Symbol / Acronym	Meaning
A	The amplitude of the Diffracted Components of wave potential
A_{xx}	Added Mass
ABL	Above Base Line
B	Damping Coefficient
BL	Baseline
C	Restoring Coefficient
C_a	Coefficient of Added Mass
C_g	Wave Group Velocity
CL	Centre Line
C_p	Wave phase velocity
CDF	Cumulative Density Function
D	Depth
EEZ	Exclusive Economic Zone
F_{xx}	Force
g	Gravitational Acceleration
H_s	Significant Wave Height
h	Seabed Depth
I_{xx}	Moment of Inertia
JONSWAP	Joint North Sea Wave Project
k	Wave Number
L_{pp}	Length between Perpendiculars
M, m	Mass
m_0	Spectra / Response Moment
MSL	Mean Sea Level
n	Number of occurrences
nm	Nautical Mile
P, p	Pressure
PDF / pdf	Probability Distribution Function
PM	Pierson-Moskowitz
T	Draft
Tp	Wave Peak Period
Tz	Zero Up- Crossing Period
U, u	Longitudinal Component of Velocity
V, v	Transverse Component of Velocity
W, w	Vertical Component of Velocity
Z	Transfer Function
ρ	Sea Water Density
π	Pi (22/7)
ω	Angular Wave Frequency

ξ	Response amplitude
ø	Wave Potential
θ	Wave Heading
γ	Spectra Peak Parameter

List of Tables

Table 4-1: Vessel Geometric Properties (Ref. /Appendix 1/).....38
Table 4-2: Summary of Vessel Properties for Installation Ballast Condition.....39
Table 4-3: Radii of Gyration for a Typical Monohull (Ref. /Appendix 1/).....40
Table 4-4: Derived Radius of Gyration (Ref. /Table 4-3/) 41
Table 4-5: 0.5-2.5m H_s & 6s-17s T_p for Asabo Field Offshore Nigeria. Adapted from (Agbakwuru et al., 2020) 44
Table 4-6: 0.5-2.2m H_s & 6s-14.4s T_p for Asabo Field Offshore Nigeria. Adapted from (Agbakwuru et al., 2020).....46
Table 4-7: 0.5-2.2m H_s & 6s-14.4s T_p for Bonga Field Offshore Nigeria. Adapted from (Olugbenga et al., 2017).....48

List of Figures

Figure 1-1: Thesis Outline / Structure 4
Figure 2-1: Map of Nigeria (Source:(UN Geospatial, 2014)) 6
Figure 2-2: An illustration of a Bi-Modal Seas Source: (Olagnon et al., 2013) 7
Figure 2-3: West African Swell Sea Sate Fitted to Different Spectra Models Source:(Olagnon et al., 2013) 8
Figure 2-4: Variance Density Frequency Spectra of Swells for Asabo Field Akwa Ibom, State Nigeria. Source: (Agbakwuru., et al., 2020) 8
Figure 2-2: A Lognormal Distribution of 4m Hs, 0.1 f_p & Multiple Standard Deviations Source: (Forristall et al., 2013). 10
Figure 3-1: Depiction of Ocean Surface Wave. Source: (Krogstad & Arntsen, 2000b) 20
Figure 3-2: Wave Regimes (Source: https://manoa.hawaii.edu) 22
Figure 3-3: Limits of Wave Theory Validity. Adapted from (Wilson, 2003) 23
Figure 3-4: Depiction of Barge in a Typical Flow Field 26
Figure 3-5: Schematic of Ship's Degrees of Freedom 28
Figure 3-6: Decomposition of body motion in a seaway 30
Figure 3-7: VERES Wave Period & Heading Dialogue Box 33
Figure 3-8: Transfer Function H(w) Connecting Source Signal & Response 35
Figure 4-1: Analysis Set-Up 37
Figure 4-2: Semi-Submersible Hull Lines Generated with ShipShape 38
Figure 4-3: Typical Installation Ballast Condition with Cargo on Deck 39
Figure 4-4: Asabo Field Location Source: Google Maps 2023 43
Figure 4-5: 3-Year Time History Plot of Significant Wave Height at Asabo Field. 43
Figure 4-6: Scatter Plot of Hs(m) Vs Tp (S) for Asabo 1981-1983 Source: (Agbakwuru et al., 2020) 44
Figure 4-7: Scatter Plot of Hs & Tp for Forcados Offshore Delta State, Nigeria. Source:(Agbakwuru & Bernard, 2019) 45
Figure 4-8: Time History of Hs between Sept. 1980-May 1982 45
Figure 4-9: Location of Bonga Field, Offshore Nigeria. Source: (Xiao et al., 2016) 46
Figure 4-10: Scatter Plot for Bonga Field July 1998 - Sept. 1999. Source: (Olugbenga et al., 2017) 47
Figure 4-11: Time History of Swells for Bonga Field July 1998 - Sept. 1999. Source: (Olugbenga et al., 2017) 47
Figure 4-12: Graph of the Relationship Between γ, T_p & H_s. Source: (Fathi & Hoff, 2004) 50
Figure 5-1: RAO in Heave - 0^0 Wave Direction 53
Figure 5-2: RAO in Heave - 15^0 Wave Direction 53
Figure 5-3: RAO in Heave - 30^0 Wave Direction 54
Figure 5-4: RAO in Heave - 45^0 Wave Direction 54
Figure 5-5: RAO in Heave - 60^0 Wave Direction 54

Figure 5-6: RAO in Heave - 75^0 Wave Direction 54
Figure 5-7: RAO in Heave - 90^0 Wave Direction 55
Figure 5-8: RAO in Roll - 0^0 Wave Direction 55
Figure 5-9: RAO in Roll - 15^0 Wave Direction 55
Figure 5-10: RAO in Roll - 30^0 Wave Direction 56
Figure 5-11: RAO in Roll - 45^0 Wave Direction 56
Figure 5-12: RAO in Roll - 60^0 Wave Direction 56
Figure 5-13: RAO in Roll - 75^0 Wave Direction 56
Figure 5-14: RAO in Roll - 90^0 Wave Direction 57
Figure 5-15: RAO in Roll - 0^0 & 90^0 Wave Direction 57
Figure 5-16: RAO Heave Vel. - 0^0 Wave Direction 57
Figure 5-17: RAO Heave Vel. - 90^0 Wave Direction 57
Figure 5-18: RAO Roll Vel. - 0^0 Wave Direction 58
Figure 5-19: RAO Roll Vel. - 90^0 Wave Direction 58
Figure 5-20: RAO Heave Acc. - 0^0 Wave Direction 58
Figure 5-21: RAO Heave Acc. - 90^0 Wave Direction 58
Figure 5-22: RAO Roll Acc. - 0^0 Wave Direction 59
Figure 5-23: RAO Roll Acc. - 90^0 Wave Direction 59
Figure 5-24: Heave Response Spectrum. - 0^0 Wave Direction HS: 0.5m / Tp: 6 sec 60
Figure 5-25: Heave Response Spectrum. - 15^0 Wave Direction HS: 0.5m / Tp: 6 sec 60
Figure 5-26: Heave Response Spectrum. - 0^0 Wave Direction HS: 0.5m / Tp: 6 sec 61
Figure 5-27: Heave Response Spectrum. - 90^0 Wave Direction HS: 0.5m / Tp: 6 sec 61
Figure 5-28: Heave Response Spectrum. -9 0^0 Wave Direction HS: 2.2 / Tp: 16.2 sec 61
Figure 5-29: Heave Response Spectrum. - 15^0 Wave Direction HS: 2.3m / Tp: 10.2 sec 61
Figure 5-30: Roll Response Spectrum. - 0^0 Wave Direction H_S: 0.5m / T_p: 6 sec 62
Figure 5-31: Roll Response Spectrum. - 90^0 Wave Direction H_S: 2.3 m / T_p: 10.2 sec 62
Figure 5-32: Roll Response Spectrum. - 90^0 Wave Direction HS: 2.2m / Tp: 16.1 sec 62
Figure 5-33: Roll Response Spectrum. - 90^0 Wave Direction HS: 2.0m / Tp: 8 sec 62
Figure 5-34: Roll Response Spectrum. - 75^0 Wave Direction HS: 2.0m / Tp: 10.0 sec 63
Figure 5-35: Roll Response Spectrum. - 75^0 Wave Direction HS: 2.2m / Tp: 16.1 sec 63
Figure 5-36: Roll Response Spectrum. - 75^0 Wave Direction HS: 2.0m / Tp: 10.0 sec 63
Figure 5-37: Roll Response Spectrum. - 45^0 Wave Direction HS: 2.3m / Tp: 10.2 sec 63
Figure 5-38: Heave Response Spectrum 60^0 Wave Direction HS: 2.2m / Tp: 14 sec 64
Figure 5-39: Heave Response Spectrum 90^0 Wave Direction HS: 2.2m / Tp: 14 sec 64
Figure 5-40: Heave Response Spectrum 90^0 Wave Direction HS: 1.52m / Tp: 6 sec 65
Figure 5-41: Heave Response Spectrum 60^0 Wave Direction HS: 2.0m / Tp: 10 sec 65
Figure 5-42: Heave Response Spectrum 45^0 Wave Direction HS: 2.20m / Tp:12.0 sec 65
Figure 5-43: Heave Response Spectrum 30^0 Wave Direction HS: 2.20m / Tp:14.0 sec 65
Figure 5-44: Roll Response Spectrum - 30^0 Wave Direction HS: 2.0m / Tp: 10.0 sec. 66
Figure 5-45: Roll Response Spectrum - 45^0 Wave Direction HS: 2.0m / Tp: 8.0 sec 66

Figure 5-46: Roll Response Spectrum - 90^0 Wave Direction HS: 2.0m / Tp: 8.0 sec. 66
Figure 5-47: Roll Response Spectrum - 90^0 Wave Direction HS: 2.2m / Tp: 14.0 sec. 66
Figure 5-48: Heave Response Spectrum 0^0 Wave Direction HS: 0.75m / Tp: 12 sec 67
Figure 5-49: Heave Response Spectrum 15^0 Wave Direction HS: 1.9m / Tp: 22 sec 67
Figure 5-50: Heave Response Spectrum 90^0 Wave Direction HS: 2.0m / Tp: 20 sec 68
Figure 5-51: Heave Response Spectrum 90^0 Wave Direction HS: 2.0m / Tp: 18 sec 68
Figure 5-52: Heave Response Spectrum 60^0 Wave Direction HS: 1.8m / Tp: 21 sec 68
Figure 5-53: Heave Response Spectrum 45^0 Wave Direction HS: 2.0m / Tp: 20 sec 68
Figure 5-54: Roll Response Spectrum - 90^0 Wave Direction HS: 2.0m / Tp: 20.0 sec. 69
Figure 5-55: Roll Response Spectrum - 90^0 Wave Direction HS: 2.0m / Tp: 18.0 sec. 69
Figure 5-56: Roll Response Spectrum - 90^0 Wave Direction HS: 1.8m / Tp: 23.0 sec 69
Figure 5-57: Roll Response Spectrum - 45^0 Wave Direction HS: 2.0m / Tp: 20.0 sec 69
Figure 5-58: Roll Response Spectrum - 90^0 Wave Direction HS: 2.0m / Tp: 20.0 sec 70
Figure 5-59: Roll Response Spectrum - 90^0 Wave Direction HS: 0.75m / Tp: 12.0 sec 70
Figure 5-60: Roll Response Spectrum - 90^0 Wave Direction HS:1.9m / Tp: 14.0 sec 70
Figure 5-60: Roll Response Spectrum - 0^0 Wave Direction HS:2.0m / Tp: 18.0 sec 70
Figure 6-1: Contour Plot of the Roll RAO 72
Figure 6-2: Contour Plot of the Heave RAO 72
Figure 6-3: Roll RAO for Head & Beam Seas 73
Figure 6-4: Sway RAO for Head & beam Seas 73
Figure 6-5: MSDV 20-26S Tp 75
Figure 6-6: MSI 20-26S Tp 75
Figure 6-7: MSI Polar Plot 20-26S Tp 75
Figure 6-8: MSDV Polar Plot 20-26S Tp 75
Figure 6-9: Plot of damped & and undamped Roll Displacement RAO at Head Seas 77
Figure 6-10: Plot of damped & and undamped Roll Velocities RAO in Beam Seas 78

List of Equations

Equ. 1 10
Equ. 2 10
Equ. 3 11
Equ. 4 11
Equ. 5 11
Equ. 6 11
Equ. 7 13
Equ. 8 13
Equ. 9 14
Equ. 10 14
Equ. 11 14
Equ. 12 14
Equ. 13 14
Equ. 14 14
Equ. 15 15
Equ. 16 20
Equ. 17 20
Equ. 18 21
Equ. 19 21
Equ. 20 21
Equ. 21 21
Equ. 22 21
Equ. 23 21
Equ. 24 21
Equ. 25 22
Equ. 26 22
Equ. 27 22
Equ. 28 23
Equ. 30 23
Equ. 31 24
Equ. 32 24
Equ. 33 24
Equ. 34 24
Equ. 35 24
Equ. 36 24
Equ. 37 24
Equ. 38 25
Equ. 39 25

Equ. 42 27
Equ. 43 27
Equ. 46 29
Equ. 47 29
Equ. 48 29
Equ. 49 30
Equ. 50 30
Equ. 51 30
Equ. 52 31
Equ. 53 31
Equ. 54 31
Equ. 55 32
Equ. 56 32
Equ. 57 32
Equ. 58 33
Equ. 59 33
Equ. 63 34
Equ. 64 35
Equ. 65 35
Equ. 66 35
Equ. 67 35
Equ. 68 40
Equ. 69 40
Equ. 74 41
Equ. 75 41
Equ. 76 41
Equ. 77 41
Equ. 78 41
Equ. 79 42

Table of Contents

1 Chapter One – Introduction 1
1.1 Background 1
1.2 Research Question 3
1.3 Research Objectives 3
1.4 Significance of Research 3
1.5 Hybrid Modelling Technique 3
1.6 Thesis Structure 4
2 Chapter Two – Literature Review 5
2.1 Seas of Southern Nigeria 6
2.1.1 West African Sea State Model 7
2.1.2 The Lognormal Distribution 10
2.2 Offshore Structures in Swell Sea States 11
2.3 Sea States Modelling 13
2.4 Response & Wave-Induced Loads 16
2.5 Hybrid Modeling Technique (HMT) 18
3 Chapter Three – Wave Theory & Formulation 19
3.1 Airy Wave Model 20
3.2 Swells as Irregular Ocean Waves 25
3.3 Flow Around Fixed-Floating Objects 26
3.4 Vessel Response in Waves 28
3.4.1 Ship Frame of Reference & Degrees of Freedom 28
3.4.2 Motion & Excitation Forces 29
3.4.3 Response Amplitude Operators (RAOs) 35
4 Chapter Four – Analysis Set-Up 37
4.1 Analysis Set-Up 37
4.2 Vessel Modelling 37
4.2.1 Installation Ballast Condition 38
4.2.2 Mass Model 39
4.2.3 Radius of Gyration 40

4.2.4 Moment of Inertia 41
4.2.5 Natural Frequency & Period 41
4.2.6 Forward Speed 42
4.3 Analysis software – ShipX 42
4.4 Environmental Wave Data 43
4.4.1 Location 1 – Asabo Oil and Gas Field, Offshore Nigeria 43
4.4.2 Location 2 – Forcados Field, Delta State, Offshore Nigeria 45
4.4.3 Location 3 – Bonga Field, Offshore Nigeria 46
4.4.4 Swell – Barge Interaction & Natural Periods: Analysing Implications 48
4.5 Idealized Wave Spectrum 50
4.5.1 Short-Term Statistical Model 51
4.6 Simulation Run 51
5 Chapter Five – Results 52
5.1 RAOs in Regular Wave 53
5.1.1 RAOs – Heave Displacements 53
5.1.2 RAOs – Roll Displacement 55
5.1.3 RAOs – Heave Velocity 57
5.1.4 RAOs – Roll Velocity 58
5.1.5 RAOs – Heave Acceleration 58
5.1.6 RAOs – Roll Acceleration 59
5.2 Response Spectrum – Asabo Field 59
5.2.1 Heave Response Spectrum – Asabo Field 60
5.2.2 Roll Response Spectrum – Asabo Field 62
5.3 Response Spectrum – Forcados Field 64
5.3.1 Heave Response Spectrum – Forcados Field 64
5.3.2 Roll Response Spectrum – Forcados Field 66
5.4 Response Spectrum – Bonga Field 67
5.4.1 Heave Response Spectrum – Bonga Field 67
5.4.2 Roll Response Spectrum – Bonga Field 69
6 Chapter Six – Results Discussion 71
6.1 Spectra–Response Correlation: Emerging Lessons 72

6.2 Implications – Design & Planning of Marine Operations 74
6.2.1 Roll Motion Control 76
6.3 Extending Lessons to Jack-Ups 78
7 Chapter Seven – Conclusion 79
7.1 Conclusion 79
7.2 Contribution to Knowledge 80
7.3 Limitation of Study 80
7.4 Future Work 80
References 81
Appendix 1 – Computer Software ShipX 89
Appendix 2 – Derivation of Gamma (γ) 91
Asabo Field 91
Forcados Field 92
Bonga Field 92
JONSWAP Spectrum Classification 93
Appendix 3 – Selected Results 94

1 Chapter One – Introduction

1.1 Background

Maritime and offshore operations are often exposed to various environmental loads. These environmental loads can be attributed to winds, waves, currents, tides, storm surges or even tsunamis. Due to these, the design of offshore structures becomes constrained as they must conform to the different stringent regulatory regimes regarding strength, stability, and general system safety. Furthermore, the planning and execution of maritime operations are also limited by weather and other prevailing environmental conditions, requiring that operations be performed within an acceptable weather window for the case of weather-restricted operations or within operability-limiting criteria for weather-unrestricted operations. To address these challenges, it is essential to have adequate and accurate modelling and computation of environmental forces and their impact on offshore structures.

The topic and focus of this thesis are the "installation analysis of offshore operations in long period swell dominant sea states in the Southern Coast of Nigeria using Hybrid Modelling Techniques". Ocean Swells are waves created by storms occurring miles from the locations where the waves are observed. Unlike wind-generated waves, swells are long-crested, long-travelling, and highly energised ocean waves with long periods typically within the range of 14s – 22s of peak period (T_p).

In the southern coast of Nigeria, part of the greater offshore West Africa, swell waves originate from the South Atlantic or the North Atlantic during the Austral winter and summer(Olugbenga et al., 2017; Prevosto et al., 2013; Toualy et al., 2015). These swells, according to (Prevosto et al., 2013), are described as being created by moderate storms with a significant wave height (H_S) of 8m, while the South-West swell is said to be generated by severe storms, with an initial significant wave height of 13m around South America, gradually decaying to produce swells of 8 meters significant wave height as it approaches closer to South Africa, and subsequently to around 2.2m of H_s around offshore West Africa with a corresponding long period of 25s, and lastly, the North-West swell generated during the winter by storms at the North Atlantic storm with a significant wave height (Hs) of 0.3m.

The Southern region of Nigeria hosts significant offshore; oil and gas activities where swell sea states are believed to be dominant (Prevosto et al., 2013; L. Zhang et al., 2013). According to (Z. Zhang & Li, 2017), swell waves can impose specific threats to the safety of sailing vessels, particularly when such vessels have natural periods within or coincides with the periods of the sea state. For (L. Zhang et al., 2013), which studied the low-frequency drift forces and horizontal motions of a moored FPSO in bi-directional swell and wind-sea in offshore West Africa (OWA), a

conclusion was reached that; swell induced large drift forces than wind-sea at surge/sway natural frequency, with swell and wind-generated seas both contributing equally to low-frequency responses. This, therefore, forms the basis for identifying the impact of the swell sea on both the design and operation of offshore structures used for installation and other related offshore operations in this part of the world.

Previous studies related to swell in this region include but are not limited to; the development of a swell wave model for the Bonga field (Olugbenga et al., 2017), "the West African swell project" (Forristall et al., 2013), "Motion Analysis of FPSO in Multidirectional Seas: The West African Offshore Region" (Ugochukwu, 2019), "Analysis of Coupling Characteristics of the Offloading Buoy System in West Africa Seas" (He, 2018), "Ocean State projection: A review of the West African marine environment" (Foli et al., 2022), "Ocean swell variability along the northern coast of the Gulf of Guinea" (Toualy et al., 2015), (Gang et al., 2014) on the "Effects on Hydrodynamic performance of FPSO in Swell Condition of West Africa", etc. While these studies provide a decent body of knowledge, for the most part, they are focused on modelling/describing the nature of swells in offshore West Africa or investigating the response of an FPSO. Further searches suggest that there is an unfilled knowledge gap in studies relating swells to the response of installation vessels and installation operations in general for offshore West Africa.

Also, building on the stated future works in (Olugbenga et al., 2017), this thesis focuses on the "installation analysis of offshore structures in long-period swell dominating sea state in the Southern Coast of Nigeria using Hybrid Modelling Techniques." The research investigates the response of offshore installation aspect of maritime operation under the wave actions of swell seas in lower Southern Nigeria, within the proximity of the Gulf of Guinea and the Bight of Biafra. This would mean the waters of Rivers, Bayelsa, Delta, and Akwa Ibom before terminating at Kumba, Cameroon.

The study will use wave theories, relevant wave statistics and existing methods for modelling swell seas in this region to accurately model the swell spectrum offshore West Africa (Southern Nigeria). With a 3D-generated model of a typical installation vessel, a numerical hydrodynamic simulation of the ship under swell seas is performed using the hydrodynamic software ShipX. The results of this simulation, or response form the basis for interpreting the characteristics of an installation under swell-dominant sea states.

Further discussions and examination for the Southern Coast of Nigeria are assessed in the view of learning if topological factors, sheltering and bathymetry of the southern coast of Nigeria could have implications on the generic understanding of the West African swell sea states and the effects on the accuracy of the spectrum and the response obtained.

1.2 Research Question

To properly undertake this research, three research questions whose answers will provide the needed insights have been proposed. These are:

1. What are the dynamics and nature of loads experienced by installation vessels during long-period swells in the seas of Southern Nigeria?
2. How can the wave spectrum in this part of Offshore West Africa be modelled and described?
3. How are these sea loads and the contributory sea state likely to affect the design, planning and execution of maritime operations in this region?

1.3 Research Objectives

The objective of this research is to investigate the response of offshore installation vessels and the installation aspect of maritime operations under swell sea states in Offshore West Africa (Southern Nigeria) by developing a model of a typical installation vessel and simulating it using the combination of wave theories, and a hydrodynamic software. The result will be analysed to understand the impact of swell seas on the design, operations, and planning of maritime operations in Offshore West Africa.

1.4 Significance of Research

This research is significant as it aims to fill the knowledge gap related to the impact of long-crested swell sea states on offshore installation vessels and installation operations on the southern coast of Nigeria, a significant area for offshore oil and gas activities. The research will provide a better understanding of the nature of swells in offshore West Africa and their impact on the design, operation, and planning of maritime operations, which will eventually help improve operation safety for offshore structures in this region. The research assesses theoretically if seabed bathymetry, topography, sheltering and other location-specific properties could alter the generic understanding of the swell sea states and what possible implications it could mean for the experience and future spectrum modelling for this region.

1.5 Hybrid Modelling Technique

Hybrid Modelling Techniques (HMT) (Fu et al., 2019; Londhe et al., 2016; Janssen et al., 2003) refers to the use of a combination of different modelling techniques, such as numerical and experimental approaches to obtain a more comprehensive understanding of a system or phenomenon. For this research, the use of the term hybrid modelling is justified through the combination of 3D modelling, wave theories and modelling of the swell spectrum, the use of a

hydrodynamic (numerical) software, and the theoretical assessment of the impact of topography, sheltering, bathymetry on the computation and accuracy of the results.

This approach could allow for a more accurate and detailed model of the sea loads experienced by installation vessels and a better understanding of the sea state and its impact on maritime operations in this region. In addition, the use of HMT can also enable the integration of various data sources (if needed) and the incorporation of different uncertainties into the modelling and simulation process.

1.6 Thesis Structure

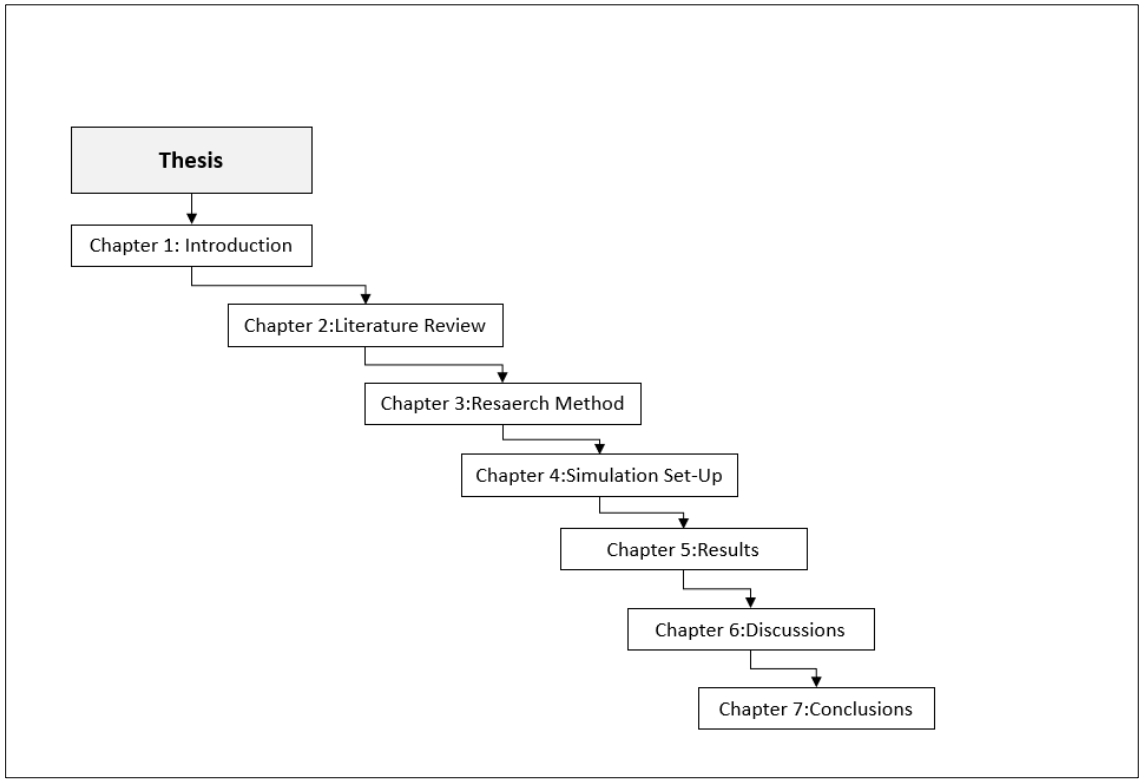

Figure 1-1: Thesis Outline / Structure

The master's thesis is structured into seven chapters. Chapter one contains the introduction and a presentation of the problem. Chapter two presents the literature survey on the subject, while Chapter three discusses the research method. Chapter four presents the simulation setup in the computer software ShipX, and the result presentation is contained in chapter five. Chapter six contains the discussion, and finally, the conclusion and recommendations are included in chapter seven. These descriptions of the thesis build-up have been summarised according to Figure 1-1

2 Chapter Two – Literature Review

The stability, safety, and reliability of offshore structures, such as ships, floating production, offloading facilities (FPSOs), oil rigs, wind farms, etc., are critical for sustaining the global energy supply. Offshore structures, in general, are not immune from the impact of forces of the sea within their operational proximity or those resulting from distant occurrences.

The southern coast of Nigeria, primarily known for its high offshore activities, hosts numerous offshore structures and assets. Swells possess an enormous amount of energy and cause severe impacts on maritime operations and floating constructions (Olugbenga et al., 2017). The seas around Southern Nigeria are part of the greater offshore West Africa dominated by swells, not ignoring contributions from waves generated by local winds. In this circumstance, a challenge emerges for offshore structures as they must provide adequate structural integrity with minimal response to swell-induced dynamic loads.

Swells are described as surface waves that propagate beyond their origin (Ardhuin et al., 2009), have a high amount of energy, fast travelling, with long and regular periods (Olugbenga et al., 2017), and are typically caused by distant storms (Forristall et al., 2013; pp. 35).

This chapter is a literature review which aims to provide an overview of existing knowledge on the "installation analysis of offshore structures in long-period swell dominant sea state" and an assessment of the feasibility of using the Hybrid Modeling Technique (HMT) to perform the analysis.

Hybrid Modelling Techniques (HMT), which have been discussed in (Fu et al., 2019; Londhe et al., 2016; P. A. E. M. Janssen et al., 2003) and section 1.5 of this document, refer to the coupling of a continuous and discrete approach in the modelling of a complex phenomenon that cannot be necessarily described using standardised homogenous method due to a multiscale nature of the phenomenon (Stéphanou & Volpert, 2016). In this respect, (Stéphanou & Volpert, 2016) argues that any research where multiple methods of conducting research are coupled and mixed into a single research method qualifies to be termed a Hybrid.

This literature review aims to synthesise knowledge on offshore structures in long-period swell dominant sea states and to assess the feasibility of using Hybrid Modelling Techniques (HMT). By evaluating and summarising existing literature, the chapter aims to identify the knowledge gap in this subject and set the foundation for the proposed research in this thesis.

To begin, the literature review discusses the nature of the sea state on the southern coast of Nigeria, the challenges, and characteristics of offshore structures under long-period swells, existing methods for modelling and computing hydrodynamic loads resulting from swells, the concept of HMT, and the justification for its use in this research.

2.1 Seas of Southern Nigeria

The Federal Republic of Nigeria (Figure 2-1) is a country located on the West coast of Africa, lying between latitudes $3^0$15' to $13^0$30' N and longitude $2^0$59' to $15^0$00' E (Federal Department of Forestry 2019) with about 853 km of coastline bordering the Atlantic ocean in the Gulf of Guinea (Ajao E.A., 1996).

Figure 2-1: Map of Nigeria (Source:(UN Geospatial, 2014)*)*

Nigeria's sovereign waters are defined by the United Nations Convention on the Laws of the Sea (Chircop et al., 2016; Churchill et al., 2022; United Nations, 1982). As enshrined in (United Nations, 1982), the maritime borders include 12nm of territorial waters, a 24nm extension from the coastal baseline, 200nm of an exclusive economic zone (EEZ), and a continental shelf coextensive with the exclusive economic zone, and an additional 350nm extending from the coastal baseline (Chircop et al., 2016; United Nations, 1982). Southern Nigerian seas, as seen from the map (UN Geospatial, 2014), will infer the maritime space between the boundary of Nigeria and Benin Republic along the Bight of Benin through the core southern states (Delta, Bayelsa, Rivers, Akwa Ibom) up to the coast of Kumba in Cameroon which seats at the Bight of Biafra.

This ocean space is part of the greater West Africa continental margin (Ceraldi et al., 2017). According to (LeBlanc et al. 2011; Reijers et al., 1997; Ugochukwu, 2019), the region has substantial reserves of petroleum deposits and a large installation of offshore structures (Ugochukwu, 2019). Offshore West Africa is benign compared to other areas like the North Sea (Forristall et al., 2013; Olugbenga et al., 2017). It is said to have a persistent swell (see figure 2-2) that can reach high amplitudes with very low periods (Forristall et al., 2013).

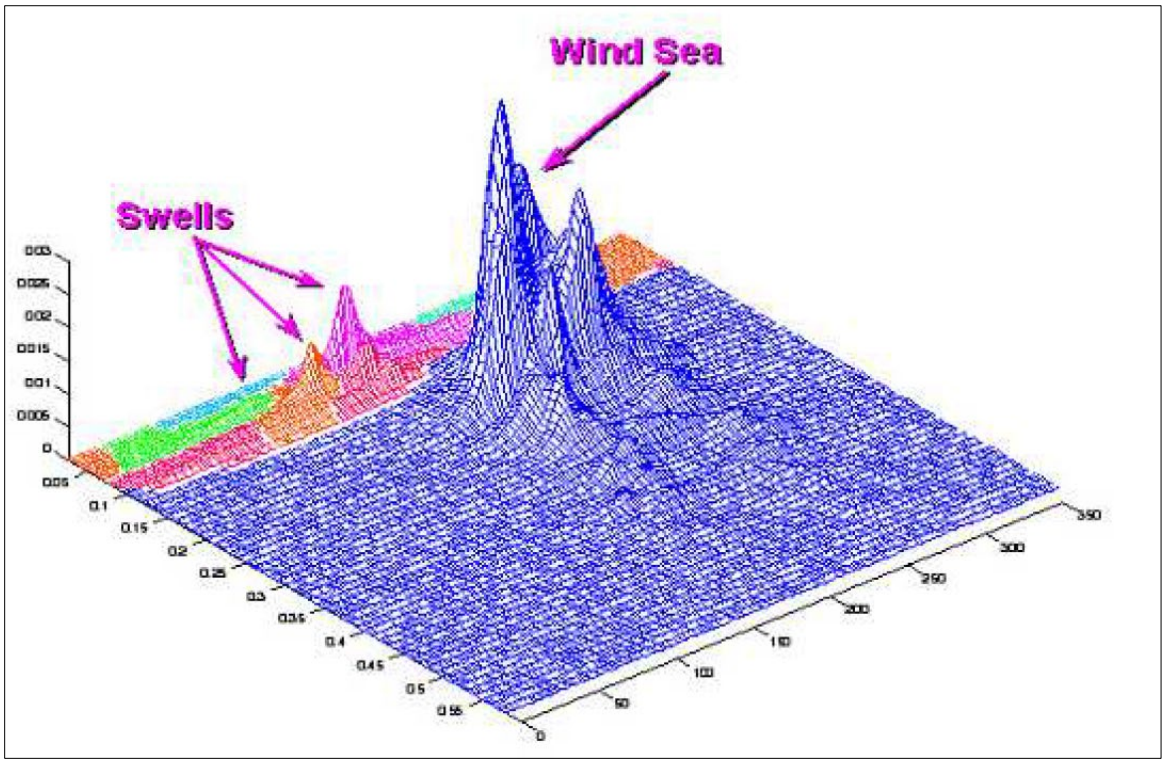

Figure 2-2: An illustration of a Bi-Modal Seas Source: (Olagnon et al., 2013)

As opined by (Forristall et al., 2013), floating structures are said to be sensitive to the amplitude, frequency, and shape of the swell peak in the spectrum. Spectrum is a term used to describe a sea state about its frequency and direction (Forristall et al., 2013). In the following subsection, a review of the spectrum and representation of the sea state for this region will be presented.

2.1.1 West African Sea State Model

To specify a sea state, knowledge of the wave frequency spectrum with a given significant wave height, a representative frequency, a mean propagation direction, and a spreading function are needed (Mackay, 2012; Norske Veritas, 2010).

A sea state model describes the superimposition of various wave systems (Bitner-Gregersen et al., 2016). These wave systems may include components of wind-generated seas and one or more swells (Bitner-Gregersen et al., 2016; Section 2.2.17, Det Norske Veritas, 2011) and often

combines mathematical, probabilistic, empirical, and statistical models to describe the stochastic nature of ocean waves.

Regardless of if the sea states are measured, or parametrised analytically, a proper representation of a sea state or spectrum considers the geographical location, the bathymetry, and the severity of the sea state (Det Norske Veritas, 2011). With this, it's plausible to argue that no two sea states can have the same properties unless they both possess the same location properties, similar bathymetry, and severity - the number of embedded energies and duration.

Perhaps, this necessitated the West African Swell Project (Forristall et al., 2013). The project, amongst other factors, sought to provide an insight into the actual nature of the sea state in offshore West Africa. Using in-situ data obtained at Bonga, Kundu, Ekoundou, Cabinda and Malabo over a cumulative period of 5.58 years (Forristall et al., 2013; pp. 3), the study prescribed for the first time, the nature of the West African sea state and described the spectrum for both wind-generated seas and swells.

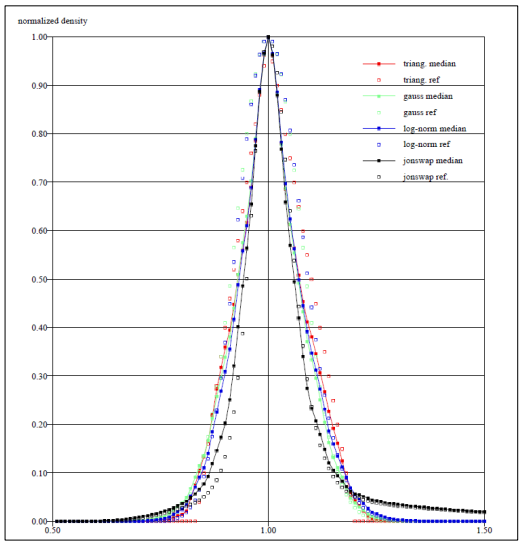

Figure 2-3: West African Swell Sea Sate Fitted to Different Spectra Models Source:(Olagnon et al., 2013)

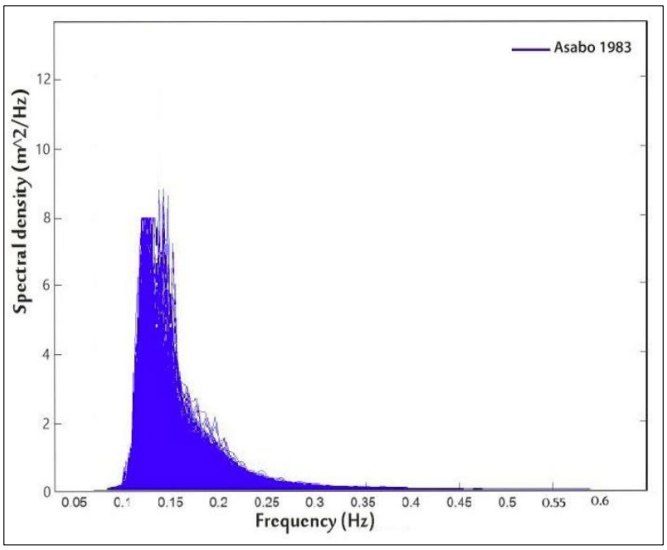

Figure 2-4: Variance Density Frequency Spectra of Swells for Asabo Field Akwa Ibom, State Nigeria. Source: (*Agbakwuru.,* et al., 2020)

According to the study, the best fit compared to other models for describing the swell component offshore West Africa is the lognormal or triangular spectra distribution (Forristall et al., 2013; pp. 183 Orji, 2019; pp. 239). A follow-up study exemplified this position (Olagnon et al., 2013) on the shape of swell spectra in West Africa; figure 2-3 shows the swell shape fitted with different spectra models. Other similar studies like (Agbakwuru et al., 2020), who studied the spectra shape for the Asabo field in Akwa Ibom State (figure 2-4), and the paper published by (Agbakwuru & Bernard, 2019) on the swell spectra shape for Forcados, offshore Warri, Delta

State Nigeria are all good bodies of knowledge on the spectra shape for this part of the world ocean.

Although, the study noted that the JONGlenn, a modified JONSWAP spectrum (Orji, 2019), was marginally better when compared to the lognormal and, on some occasions, provided a better fit. On a cautionary tune, (Forristall et al., 2013) suggested that the choice of "best spectra" for modelling swell in this region depends on the application.

In the concluding part of the study, the authors argued that for analysis, studies, or investigative purposes where the interest lies in obtaining the response of floating structures, the lognormal distribution provided a better description of the sea state than JONSWAP. The key reason was that the low-frequency tail of the JONSWAP spectrum fell off faster than the fitted in-situ data when compared (Forristall et al., 2013). In a separate study conducted by (Olugbenga et al., 2017) on the swell nature at the Bonga field offshore of Nigeria, the authors appear to agree with the position of (Forristall et al., 2013) on the nature of swell in offshore West Africa. But from the studies carried out by (Lucas & Guedes Soares, 2015) on the general modelling of swell spectra using data sets for the Bonga field in Nigeria and the A platform-Maui off the coast of New Zealand, Lucas & Guedes showed that the JONSWAP spectrum model represented more accurately, the nature of the swell spectra as opposed to a Gaussian model.

As seen from the positions of (Forristall et al., 2013), (Lucas & Guedes Soares, 2015), and (Olugbenga et al., 2017), a dual paradigm emerges on the proper spectra model for a typical swell sea state. One holds that the lognormal distribution represented the ideal swell nature in offshore West Africa, while the other paradigm is that the JONSWAP fitted the character of swell in general. Reflecting on the work of (Orji, 2019; pp. 266), the deviations in the values of the significant roll response of an FPSO calculated using either JONSWAP or Brettschneider spectrum were more than 1-23% when compared to a lognormal distribution.

While one study such as that by (Orji, 2019) may not represent an extensive array of studies to be used as a basis for concluding the best spectrum, it can provide a reasonable ground to support an opinion on the nature of swell in southern Nigeria and offshore West Africa by extension as being lognormally distributed.

2.1.2 The Lognormal Distribution

In section 2.1.1, the thesis document established that the sea state in offshore West Africa has a lognormal distribution (figure 2-2). While it seems outside this thesis's framework to delve into probability theory and randomness, perhaps presenting a contextual overview of a lognormal distribution may be beneficial.

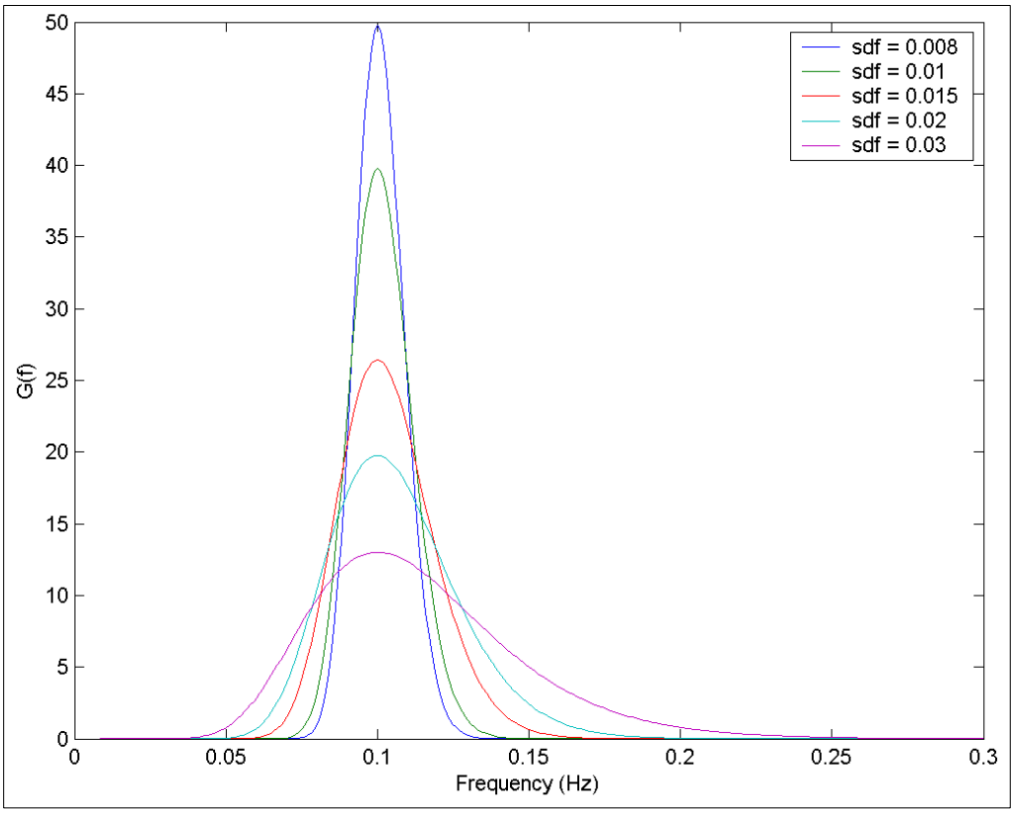

Figure 2-5: A Lognormal Distribution of 4m Hs, 0.1 f_p & Multiple Standard Deviations Source: (Forristall et al., 2013).

As stated by (Dennis & Patil, 2018), for a random variable, in this case, a sea state, to be lognormally distributed, the probability distribution of the logarithm of the random variable must follow a normal distribution. Mathematically, following probabilistic theorems, this is presented thus:

If $X = LogN$ *Equ. 1*

It follows that Equ. 1 has a normal distribution with a probability distribution function (pdf) given by:

$$f_X(x) = \frac{1}{(\sigma^2 2\pi)^{1/2}} \exp[-\frac{(x-\mu)^2}{2\sigma^2}] \qquad \textit{Equ. 2}$$

Where -∞ < x < +∞ is satisfied only if Equ. 3 holds.

X~normal (μ, σ^2). *Equ. 3*

The terms μ and σ represent the location and scale parameters of the normal distribution.

Then,

$$N = e^x \quad \textit{Equ. 4}$$

Hence Equ.3 has a lognormal distribution with a probability distribution function as follows:

$$f_N(n) = \frac{1}{n(\sigma^2 2\pi)^{1/2}} \exp[-\frac{(\log n - \mu)^2}{2\sigma^2}] \quad \textit{Equ. 5}$$

Where,

N~lognormal (μ, σ^2) *Equ. 6*

2.2 Offshore Structures in Swell Sea States

The behaviour of offshore structures in wave conditions attracted lots of interest from a broad spectrum of researchers in naval architecture, ocean engineering, coastal engineering, and maritime operations. Numerous research articles in different scholarly databases support this claim. Some of the interest areas on these subject deals with the dynamic response of offshore structures and methods of computation of the responses, resonance, fatigue failure etc., resulting from wind, wave, tidal currents, earthquakes, etc. (Goda, 2010). As highlighted by (Rana et al., 2014), offshore structures are highly susceptible to damage caused by long-period ocean waves, especially in the peak region of the swell spectra.

According to (Sarpkaya & Isaacson, 1981), the significant challenges faced by offshore structures within the peak region of the swell spectra include the generation of large hydrodynamic forces, increased structural vibrations, and fatigue damage, which can ultimately lead to the failure of the structure.

Using numerical simulations, (Wang et al., 2019) evaluated the performance of a deep-water semi-submersible platform under long-period swell. The authors concluded that the long-period swell can cause significant wave-induced motion in pitch, heave, and roll (Wang et al., 2019). Using Newman's approximation, (L. Zhang et al., 2013) showed that the swell seas induced large drift forces at the natural frequency of an FPSO in sway and surge degrees of freedom in offshore West Africa compared to wind seas.

At the peak regions of swell spectra, a significant amount of high amplitude and low-frequency motions can be induced, resulting in a high probability of damage to offshore structures. This can have severe consequences for offshore structures. For example, the Ocean Ranger drilling platform accident 1982, which resulted in multiple fatalities, was attributed to wave loading during an extreme storm event (Heising & Grenzebach, 1989). Swell waves in the same order possess high energy like that which struck the Ocean Ranger drilling platform. According to (Kaminski & Rigo, 2018), swells are almost present in about 80% of the world's oceans. Their effects are not limited to offshore structures but also affect marine operations and shipping and account for the sea loads acting on them.

For the ocean space in Southern Nigeria, (Abam et al., 2016) stated that the effect of swell-induced loads on offshore structures operating in the region created certain limitations in terms of heave motion, which can inhibit drilling operations, as well as caused some adverse effects on subsea risers. Swells have also been found to induce more heave motion on TLPs, and in general, TLPs tend to show a more significant response to swell waves than standard wind-generated waves (Rijken, 2013). Furthermore, according to (Rijken, 2013), the swell characteristics in offshore West Africa present a unique challenge in achieving the optimum lock-off gap during the installations of TLPs due to changes in draft occasioned by swell presence.

A study by (Wang et al., 2019) investigated the response of offshore structures under swell waves and found that swell induced significant dynamic responses in the system, leading to increased stress levels which can be a precursor to fatigue damage over time. This position by (Wang et al., 2019) aligns with the paradigm held by (Rana et al., 2014), who noted that the dynamic response of an offshore structure to long-period waves is an essential factor in both the fatigue and ultimate failure of offshore structures.

Through field observation, Shin et al. (2017) showed that sea walls and rails were vulnerable to high energy swells on the coast of Jundonjin Beach, located on the east coast of Korea. In the same study, the authors showed that because of swell waves on sedimentary movement, the bathymetry of the region was altered significantly. Changes in bathymetry may be irrelevant for shipping operations in deep waters. Still, for shallow water regions, such variations may pose some challenges to safe navigation resulting from a reduced under-keel clearance.

As described by (Yoshimi Goda, 2010), for ship-shaped structures that are either moored to a multiple-buoy berth or a floating breakwater, the basis for determining the mooring force is that of a constant wave drift force. However, as (Yoshimi Goda, 2010) pointed out, wave drift force in random sea states such as swell is only partially constant. It fluctuates slowly in time-domain response to the gradual variations in wave height when a particular wave terrain is considered. The effect of such slow variation in wave drift force is long-period oscillations of the moored vessel (Yoshimi Goda, 2010). Such long-period fluctuation can eventually lead to fatigue of the moored object.

As the literature survey in this section shows, swells can significantly challenge offshore structures, maritime operations, and shipping activities. Its high energy and spectra shape have

been identified to have a specific contribution to the response of offshore structures. In the next section, the literature review explores the various methods of modelling sea states and the computation of the hydrodynamic force responsible for inducing the response on offshore structures.

2.3 Sea States Modelling

Large volume offshore structures such as ships, GBS platforms, FPSOs, TLPS, Spars, or Semi-submersibles are often generalised as "offshore structures" (Det Norske Veritas, 2010b), have high inertia, with less drag force in comparison to wave-induced loads. Wave-induced loads are the dominant loads these offshore structures are exposed to throughout their lifecycle (Det Norske Veritas, 2010b). The magnitudes of these loads vary depending on whether they are small or huge waves. According to (ABS, 2016), the most practical way to represent the wave conditions that create these loads would be to divide the sea state up and use short-term wave statistics to describe stochastic scenarios where specific wave properties over each sea state and long-erm wave statistics in the form of wave scatter diagram and wave directional spreading to denote the rate at which the sea states occur.

Short-term wave statistics describe an irregular sea state that is assumed to have a stationary sea surface elevation within a limited period of 20 minutes to 3-6 hours (Norske Veritas, 2010b). With such fixed assumptions, the sea state can be parametrised using significant wave height, spectra peak periods or zero up-crossing periods (Krogstad & Arntsen, 2000), while for long-term statistics where directional wave spreading is applicable, the sea state is represented by a wave scatter diagram, wave directionality (ABS, 2016), and considered to vary over season or yearly (Krogstad & Arntsen, 2000).

As discussed by (Krogstad & Arntsen, 2000), for short-term wave statistics, where the wave heights and periods are considered stochastic variables, an N-numbers of waves will yield an N-number of pairs of wave heights (H) and wave period (T). The cumulative probability distribution function of the wave height will follow a Rayleigh distribution.

$$P(H \leq h) = 1 - exp.^{-2\left(\frac{h}{H_{m0}}\right)^2} \qquad \textit{Equ. 7}$$

Classically available mathematical models representing a sea state include the ISSC Wave Spectrum, the Brettschneider Spectrum or Pierson-Moskowitz spectrum, the JONSWAP spectrum, or Ochi's six-parameter spectrum (ABS, 2016).

Pierson-Moskowitz spectrum, which is used to model fully developed, wind-generated sea states, and a single peak parameter wave (Ryabkova et al., 2019), can be represented using Equ. 8

$$S_{pm}(\omega) = \frac{ag^2}{\omega^5} exp.^{-\beta(\omega_{max}/\omega_p)^4} \qquad \textit{Equ. 8}$$

Where;

$\omega_p = 2(\frac{\pi}{T_P})$ is the angular spectra peak frequency

As expressed in Equ. 8, the PM spectrum is suitable for modelling open-ocean areas with an unlimited fetch (ABS, 2016). The spectrum, as observed, does not appear to follow a Rayleigh distribution. However, statistically, the observed wave amplitude could follow a Rayleigh distribution sufficiently (Newman, 2018).

Another approach to modelling random ocean waves is the JONSWAP spectrum (Hasselmann et al., 1973; Ryabkova et al., 2019). The JONSWAP spectrum evolved from the works of (Hasselmann et al., 1973), which measured the spectrum of developing wind waves in the North Sea. The authors did show that the spectra density at the maximum angular frequency was more significant than the spectrum approximation by the Pierson-Moskowitz spectrum (Equ. 8).

$$S(\omega) = \frac{ag^2}{\omega^5}(2\pi)exp.^{(-1.25\left(\frac{\omega_{max}}{\omega}\right)^4 \gamma^e\left(\frac{(\omega-\omega_{max})^2}{2\sigma^2\omega_{max}^2}\right)} \quad \textit{Equ. 9}$$

$$\sigma = \begin{cases}\sigma_a, \omega \leq \omega_{\max,} \\ \sigma_b, \omega > \omega_{max}.\end{cases} \quad \textit{Equ. 10}$$

According to (Ryabkova et al., 2019), the developing sea state can be described by the dimensionless wave fetch and dimensionless frequency as expressed in Equ. 11a and Equ. 11b.

$$x^* = \frac{xg}{U_{10}^2}, \quad \textit{Equ. 11}$$

$$\omega = \frac{\omega u_{10}}{g}, \quad \textit{Equ. 12}$$

Concerning Equ. 8 and Equ. 9, the difference between the Pierson-Moskowitz and JONSWAP spectrum is the introduction of the wave peakness parameter (γ); hence the JONSWAP spectrum can be said to be a modified version of the Pierson-Moskowitz spectrum (Norske Veritas, 2010b),.

Sea states that can be characterised as mild or gentle swell (Neumann, 1953; Ryabkova et al., 2019) provided a mathematical model (Equ. 13) that can describe the swell spectrum.

$$S_{swell}(\omega) = 6m_0\left(\frac{\omega_m}{\omega}\right)^5 \omega^{-1} exp.\left(\left(-1.2(\frac{\omega_m}{\omega}\right)^5\right) \quad \textit{Equ. 13}$$

Where;

M_0 is the zeroth moment of the swell spectra which is related to the swell significant height given in Equ. 14, while for a mixed sea state, the total spectrum can be described by summing up the swell spectrum and wind spectrum (Ryabkova et al., 2019) as shown in Equ. 15.

$$H_{s_{swell}} = 4 * \sqrt{m_0} \quad \textit{Equ. 14}$$

$$S(\omega) = S_{wind}(\omega) + S_{swell}(\omega) \qquad \textit{Equ. 15}$$

(Torsethaugen, 1993) published a double-peak spectra model obtained by extending two JONSWAP spectra where each peak represents the wind-generated seas, and the other peak represents the swell sea states. It is mainly suited for modelling bimodal seas (Garcia-Gabin, 2015). In a parametrised fashion, the spectra model depends on the significant wave height and the spectra peak period and is divided into site-dependent and site-independent parameters (Torsethaugen, 1993). Utilising a partitioning method, the wave is divided into two frequency bands, where the swell component is obtained through a low-frequency band and the wind sea through a high-frequency band (Garcia-Gabin, 2015). According to (Garcia-Gabin, 2015), this method of partitioning waves into pieces is said to have been inspired by the concept proposed by (Strekalov et al., 1972), where a high-frequency band was used for describing the wind sea and a Gaussian spectrum for the swell component.

(Ochi & E. Nadine Hubble., 1976) is a generalised sea state spectrum which describes combined sea states. Decomposition (Garcia-Gabin, 2015) divides the spectrum into two Gamma distributions; each distribution has significant wave height, spectra peak period, and a shape parameter (Norske Veritas, 2010b). The total spectrum is obtained by summing the two distributions, with one containing a low-frequency component and the other containing a high-frequency component (Garcia-Gabin, 2015). As seen in (Ochi & Hubble., 1976), the Ochi & Hubble spectrum uses two JONSWAP spectra, one for modelling the wind seas and the swell component.

For location-specific spectrums, the sea state can be represented via energy concentration around a single or, at most, two modal frequencies with an assigned direction (Orji, 2019). The sea state around southern Nigeria consists of several swells and at least a wind sea at any collection (Orji, 2019). Therefore, accurately computing the sea state will require a multi-parameter spectrum that can express the distinct parameters of the swell and wind sea components (Forristall et al., 2013; Orji, 2019).

The West African swell project (Forristall et al., 2013; Orji, 2019) highlighted the discrepancies in using bimodal spectrums to model the spectrum in offshore West Africa. The difference included an excessive value for the shape peak parameter when using the classical JONSWAP spectrum for modelling the sea state around the north of the Gulf of Guinea. The underlying implication buttresses the point that spectrums like JONSWAP or PM were native to wind seas alone, thereby making them somewhat inapplicable to modelling the swell spectrum for Offshore West Africa (Forristall et al., 2013; Orji, 2019).

Through portioning and fitting, (Forristall et al., 2013), did show that the most optimal way of modelling the sea state in offshore West Africa required the partitioning of the sea state into its respective swell components, which were best described using a lognormal distribution, and JONSWAP-Glenn for the wind sea component (Orji, 2019). This position also aligns with (Olugbenga et al., 2017), who fitted a series of wave data collected for the Bonga field in offshore

Southern Nigeria. The authors show that the lognormal distribution (2.1.2) better includes the collated wave data.

2.4 Response & Wave-Induced Loads

The waves and environmentally induced loads on ships and offshore structures have interested engineers and scientists for decades (Ohkusu, 1998). As (Wilson, 2003, p. 1) pointed out, "the design of structures compatible with the extremes of the offshore environment is a most creative and challenging task for the contemporary engineer."

The effects of loads on an offshore structure could be motion, acceleration, stresses, or deformation (Bergdahl, 2009, p. 149). In terms of motion, according to (Norske Veritas, 2010), floating structures respond to wave action in six distinct degrees of motion with both translation and rotation inclusive, in addition to wave-induced loads that can cause high-frequency springing and whipping (elastic) response. In some respect, where there are non-linear load effects, the offshore structure may be subjected to responding at its natural frequency (Chakrabarti, 1990, p. 169; Norske Veritas, 2011). Non-linear wave effects alongside forces from wind and current impose wave drift forces on offshore structures, which implies the constant mean displacement of the structure from its mean position (Abam et al., 2016, p. 2).

Literature about marine hydrodynamics dedicated to this subject of wave loads, effects and responses include but is not limited to; (Baso et al., 2013; Bergdahl, 2009; Chakrabarti, 1990; Faltinsen, 1990; Abam et al., 2016; Manners & Rainey, 1992; Newman, 2018; Oberhagemann, 2017; Ogilvie & Tuck, 1969; Ohkusu, 1998; Oliver, 1990; Wilson, 2003) suggesting that this subject has received considerable attention. Yet, it cannot be said that the need for more knowledge in this field has been exhausted. After all, as (Olugbenga et al., 2017) pointed out in the concluding section of their studies, there is a need to investigate the response of offshore structures in swell sea states within offshore West Africa. This is true since offshore structures respond differently to different wave systems, particularly in circumstances where location affects the type of wave regime.

Bergdahl (2009) discussed two main approaches to calculating the wave-induced force on an offshore structure at sea. According to (Bergdahl, 2009), in one method, the offshore structure is viewed as a whole, with the total wave load assessed from an empirical perspective or computed coefficients are applied to water velocities and acceleration in an undisturbed wave motion, while the other method is approached by integrating the calculated pressure distribution resulting from the disturbed motion around the hull of the offshore structure.

For ships moving with a forward speed, (Ohkusu, 1998) discussed and reviewed different methods that can be used to predict wave-induced motion and wave loads with a corresponding experimental validation of the discussed methods. As opined by (Oberhagemann, 2017), linear potential flow theory can be used to calculate the response of ships and other similar structures

in waves of small steepness where the corresponding response of the structure becomes a linear function of the wave. (BASO et al., 2013) discussed the application of strip theory to calculating wave forces and motion of a three-dimensional body.

According to (BASO et al., 2013), the ship consists of finite numbers of 2D dimensional strips of transverse cross-sections connected through the strip theory method. According to (Ogilvie & Tuck, 1969), the solution to the strip theory problem is obtained by solving a boundary-value problem (BVP) numerically in two dimensions with the assumption that the ship is a cylinder oscillating vertically on the free surface. When enhanced non-linearly, strip theory could be used to predict sectional hydrodynamic force for the motion of structures and hull girder loading (Oliver, 1990).

Oliver (1990) stated that using strip theory, it is possible to decompose the hydrodynamic force acting on an offshore structure into the Froude-Krylov component, the diffracted component, and a third component due to a self-induced motion. Manners & Rainey (1992) discussed a method for calculating the wave load on a cylindrical member of lattice-type offshore having a small cross-section relative to the incident waves. As their article (Geng et al., 2010; Abam et al., 2016; Manners & Rainey, 1992) highlighted, the Morrison equation (Cao & Jun Zhang, 1996; Wilson, 2003), which according to (Geng et al., 2010), is a semi-theoretical and empirical formula, centring on the principle of conservation of linear fluid momentum is the conventional method used for the calculation of the wave-induced force for these types of offshores structures.

In (Norske Veritas, 2010b), wave loads on an offshore structure in an irregular sea state can be computed through a frequency domain analysis. Frequency domain analysis requires that the offshore structure's motion be described by coupled ordinary differential equation (Chakrabarti, 1990, p. 185). According to (Det Norske Veritas, 2010b), frequency domain analysis involves linear superimposition of the loads due to regular wave components, with the assumption of a steady state where all the transient effect of the wave is neglected, such that the wave loads and the dynamic response of the structure oscillate harmonically with the same frequency as the incident wave or with the frequency of encounter in the case of a vessel moving with a forward speed.

Through Fourier transformation, the hydrodynamic properties of the structure, such as the added mass and damping coefficients in the frequency domain, can be represented in the time domain through a suitable Fourier integral transform (Chakrabarti, 1990).

Fonseca & Soares (1998) studied the vertical response and wave-induced loads on ships with a forward speed in the time domain, considering non-linear wave effects due to significant amplitude excitation. (Xia et al., 1998) developed a generalised time-domain strip theory approach for calculating ships' responses and vertical wave loads, while (Wu & Hermundstad, 2002) discussed a time-domain formulation for predicting ship motion, wave loads and long-term statistics.

Other methods for calculating an offshore structure's hydrodynamic load and response involve numerical methods, as demonstrated by (Bunnik & Buchner, 2004; Guanche et al., 2009; Newman, 2004; Schellin & Moctar, 2007).

Oberhagemann (2017) discussed the concept of using the numerical method for the computation of the wave-induced load on a ship. According to him (Oberhagemann, 2017), one of the numerical methods is based on the solution of the Reynolds-Averaged Navier-Stokes (RANS) equation in combination with a multiphase fluid problem formulation. The use of numerical methods for solving engineering problems, in general, is an evolving technology. Still, it is worth mentioning that the accuracy of the computation can be limited by individual skill and other factors such as computer hardware.

The following section reviews the hybrid modelling technique in the context of ocean wave modelling and response calculation.

2.5 Hybrid Modeling Technique (HMT)

A hybrid system is analogous to a system or method where two or more different subsystems are employed or assembled to serve the same purpose. This concept has been applied to automotive (Manwell et al., 2006), an artificial neural network for the prediction of location-specific wave forecast (Londhe et al., 2016), modelling of an ocean swell and wind sea state (P. A. E. M. Janssen, 2003), sea level anomaly prediction (Fu et al., 2019), and in biology (Stéphanou & Volpert, 2016).

A hybrid model is therefore expected to be drawn from a multiplicity of models and fused. As a method for conducting research, a Hybrid Modeling Technique (see section 1.5) combines different modelling techniques, such as numerical and experimental, to obtain a comprehensive understanding of a system or phenomenon. This research focuses on understanding and establishing the behaviour of offshore structures (loads and response) when subjected to the forces induced by swell sea states in Southern Nigeria.

To capture and represent swell spectra, a mathematical or analytical means will be employed, computer software used for the modelling of a conceived offshore structure, including an idealised mathematical formulation for the design, if need be, and the use of a hydrodynamic workbench (ShipX) for the simulation of the response and likely MatLab or Microsoft Excel additional post-processing. Combining these methods to arrive at findings qualifies the description of the technique, which is presented in chapters three and four as a hybrid.

3 Chapter Three – Wave Theory & Formulation

This chapter presents the research method. Typically, the role of a methodology in research is to document the approach and processes employed by the researcher in answering proposed research questions (Williams, 2011). If this holds, it is essential to present and document the methods adopted in answering the research questions described in section 1.2 of this thesis document.

Regarding chapter two of this thesis document, an extensive study of swell and other related topics was presented. Taking a derivation from the knowledge from there, it is consistent to refer to swells as irregular waves distinguishable from wind-generated waves based on their frequency band, wavelength, spectra peak periods and other relevant wave properties.

Irregular waves are conceived as waves resulting from the superimposition or combination of different regular waves. But to understand correctly how to formulate and represent this irregular wave phenomenon, the approach adopted would be to navigate from the known formulation of regular waves to that of irregular waves. In the field of ocean engineering, naval architecture, coastal engineering, or oceanographic studies, waves are described mathematically using either linear wave theory, Stokes 2^{nd} order wave, or other higher order waves such as the Stokes 2^{nd}, 3^{rd}, $4^{th,}$ and 5^{th} order wave (Dean & Dalrymple, 1991; Haritos, 2007).

As noted by (Dean & Dalrymple, 1991, p. 56), irregular sea states resulting from stormy ocean conditions are often represented as a superimposition of multiple Airy or linear waves having varying wave properties and directions of propagation.

With this as a foundational basis, this research conceived the ocean swell present in Southern Nigerian waters as a superimposition of different regular waves and modelled using the Airy wave theory. With this (Dean & Dalrymple, 1991, p. 56), the thesis idealises the motion of a regular wave packet as that which can be described using an Airy wave model.

With an Airy wave model formulated, the mathematics of regular waves will be further introduced, allowing for the arrival at a model suitable for describing swell as an irregular wave. Recall that earlier, following the works of (Forristall et al., 2013), which were later corroborated by (Olugbenga et al., 2017), the sea state around Southern Nigeria following the findings for the Bonga field and the WASP, was described as a log-normally distributed spectrum.

This can be viewed as a partial answer to one of the research questions proposed in section 1.2 but with little justice to understanding the combinatorial processes of regular waves that result in such stochastic described as a log-normal distribution.

Lastly, the mathematical formulations examine flow around a fixed or floating object from the context of fluid-body interaction (force and response paradigm). Such a theorem is vital in

understanding the relationships between fluid kinetics and vessel movement within a floating structure's six degrees of freedom.

3.1 Airy Wave Model

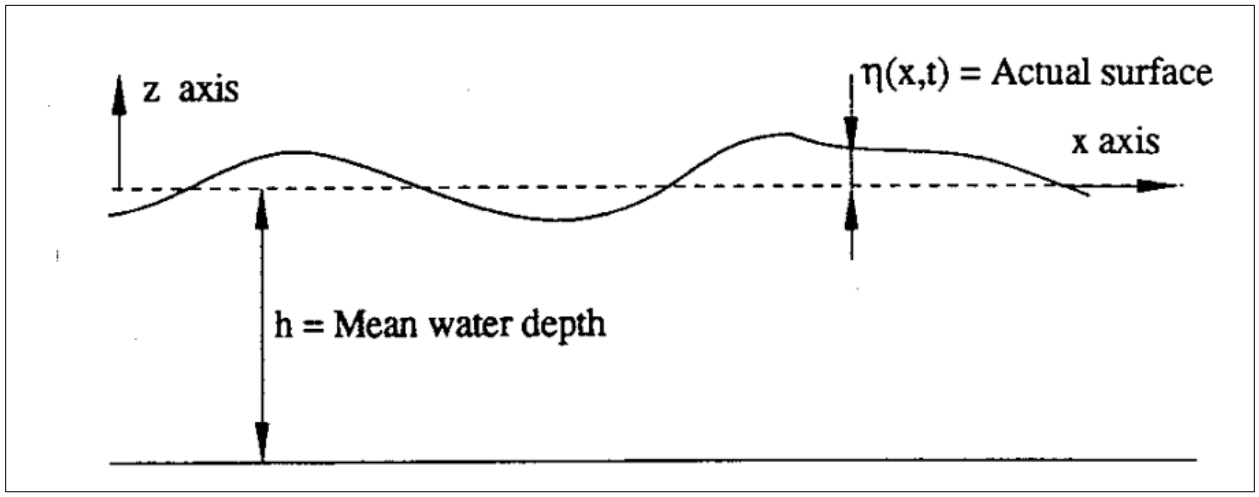

Figure 3-1: Depiction of Ocean Surface Wave. Source: (Krogstad & Arntsen, 2000b)

Figure 3-2 represents a progressive plane wave along the x-direction, where the surface elevation Etta(η) in space is a function of the longitudinal position and time (t). The dotted line represents the mean sea level (MSL), the seabed depth is given by "h", and the vertical axis is measured positively upward of the MSL. The application of Airy wave theory requires certain limitations that must be introduced regarding the nature of the waves. These are:

The waves are regular and harmonic and must satisfy equation 27 (Equ. 27).

I. The wave must be considered a small amplitude wave (i.e., the wave amplitude to wavelength ratio is negligible).
II. The waves must fall within the zone where the Airy wave is applicable (see figure 3-3).

These assumptions imply that the wave motion at the sea surface (MSL, z = 0) is so small that Bernoulli's equation (Equ. 16) can be linearised with specific boundary conditions applied.

One such boundary condition is the dynamic boundary condition, which says that at the free surface, the pressure of a plane progressive wave is equal to the atmospheric pressure. When applied to Equ. 16, the surface elevation can be expressed in terms of the partial derivative of the velocity potential with respect to time (t), giving rise to equation 17.

$$\frac{\partial \phi}{\partial t} + \frac{p}{\rho} + gz = 0 \qquad \text{Equ. 16}$$

$$\eta = -\frac{1}{g}\frac{\partial \phi}{\partial t}, where\ z = 0 \qquad \text{Equ. 17}$$

Further assumptions on formulating the Airy wave theory hold that the flow regime is irrotational. A fluid regime must satisfy the Laplace equation stated in Equ 18 to be classified as irrotational.

$$\frac{\partial^2 ø}{\partial x^2} + \frac{\partial^2 ø}{\partial y^2} + \frac{\partial^2 ø}{\partial z^2} = 0 \qquad \text{Equ. 18}$$

At the seabed, often referred to as the bottom boundary condition (z = -h), the seabed is impermeable and fixed. Therefore, the water particle velocity at the se bottom equals zero. Mathematically, this implies that the partial derivative of the velocity potential at the bottom boundary condition with respect to z equals zero (equation 199).

$$-\frac{\partial ø}{\partial z}(x, y, z, t) = 0 \qquad \text{Equ. 19}$$

Finally, the kinematic free surface boundary condition is applied. It holds that the velocity of the fluid normal to the surface must be equal to the velocity of the surface normal to itself. If, for example, the free surface is given by;

$$f(x, y, z, t) = \eta(x, y, t) - (z - z_s) = 0 \qquad \text{Equ. 2021}$$

Where x, y, and z are arbitrary points on the fluid domain along the direction of wave propagation, and z_s is a point on the fluid surface, then it holds that the partial differentiation of equation 19 (Equ. 19) with respect to time (t) can be expressed as equation 21 (Equ. 21).

$$\frac{\partial \eta}{\partial t} - \frac{\partial z}{\partial t} = 0 \qquad \text{Equ. 22}$$

But recall that Airy wave theory without modifications is only valid for small amplitude waves ($\lambda >> \eta_{max}$). Since the wave amplitude is small compared to the wavelength, it holds that;

$$\frac{\partial \eta}{\partial t} - v_z = \frac{\partial \eta}{\partial t} - \frac{\partial ø}{\partial z} = 0 \qquad \text{Equ. 23}$$

Note: v_z is the vertical velocity of the fluid normal to the surface, and v_s is the velocity of the fluid particle at the surface. Hence;

$$v_z = v_s \qquad \text{Equ. 24}$$

If η is eliminated from Equ. 17 and Equ. 22, the resulting equation can be expressed in terms of velocity potential, as shown in equation 24 (Equ. 24).

$$\frac{\partial^2 ø}{\partial t^2} + g\frac{\partial ø}{\partial z} = 0 \qquad \text{Equ. 25}$$

At z_{bottom}, where z = -h, the bottom boundary condition is expressed in Equ. 17 where $v_z = 0$.

Equations 16 and 24 represent the general basis or background for formulating Airy wave theory. According to (Krogstad & Arntsen, 2000a), the solutions to these equations are lengthy.

However, (Gjevik et al., 2015; Krogstad & Arntsen, 2000a) provided helpful insight on how to approach the problem. For (Krogstad & Arntsen, 2000a), a solution which expresses the velocity potential for a regular harmonic wave can be obtained using dimensional analysis and scaling method. The resulting equation for the velocity potential can then be obtained as follows;

$$ø = -gH\left(\frac{T}{4\pi}\right)\left\{\frac{cosh\left\{\left(\frac{2\pi}{L}\right)(h+z)\right\}}{cosh\left\{\left(\frac{2\pi}{L}\right)h\right\}}\right\}\sin\left(\frac{2\pi}{L}-2\pi t/T\right) \qquad \text{Equ. 26}$$

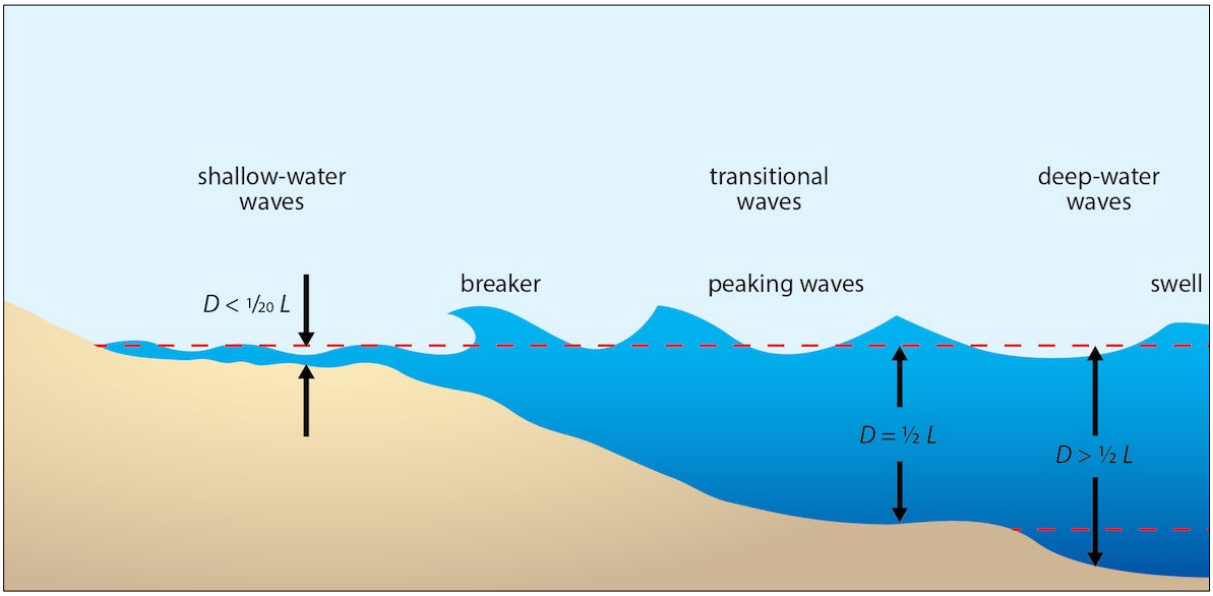

Figure 3-2: Wave Regimes (Source: https://manoa.hawaii.edu)

The term 2π/L can be equated to the wave number "k" in the above equation (Equ. 25). With some mathematical manipulation, as demonstrated by (Krogstad & Arntsen, 2000a), the velocity potential can be further represented as shown in equation 26 for a wave-particle motion described according to equation 27 (Equ. 27).

$$ø(x,z,t) = \left[-\frac{ag}{\omega}\frac{1}{\cosh(kh)}\right]\cosh\left(\left(k(h+z)\right)\right)(-\cos(\omega t - kx) \qquad \text{Equ. 27}$$

$$\eta(x,t) = \text{asin}\,(\omega t - kx + \varepsilon) \qquad \text{Equ. 28}$$

If equation 27 (Equ. 27) represents a particular wave with wave number (k) and wave frequency (w), the dispersion relationship states that for every wave with a frequency, there is a corresponding wavelength (Krogstad & Arntsen, 2000a) and thus expressed as;

$$\omega^2 = gk \tanh(kh) \qquad \text{Equ. 29}$$

$$\omega = \pm(\mathrm{gktanh(kh)}^{\frac{1}{2}} \qquad \text{Equ. 29}$$

Equation 28 has different implications for deep, intermediate, and shallow water conditions (see Figure 3-2). For this research, whose interest is in purely swell sea states, it follows that swells are to be treated as deep-water waves, according to Figure 4. For intermediate water conditions, where the swells begin to form peaking waves, equation 31 describes the dispersion relation for any given wave packet. In shallow water conditions, where the h < 1/20 λ, the dispersion relation is given in equation 31 (Equ. 30). While for deep water Conditions, the relationship

$$\omega = \pm(gh)^{\frac{1}{2}}k \qquad \text{Equ. 3031}$$

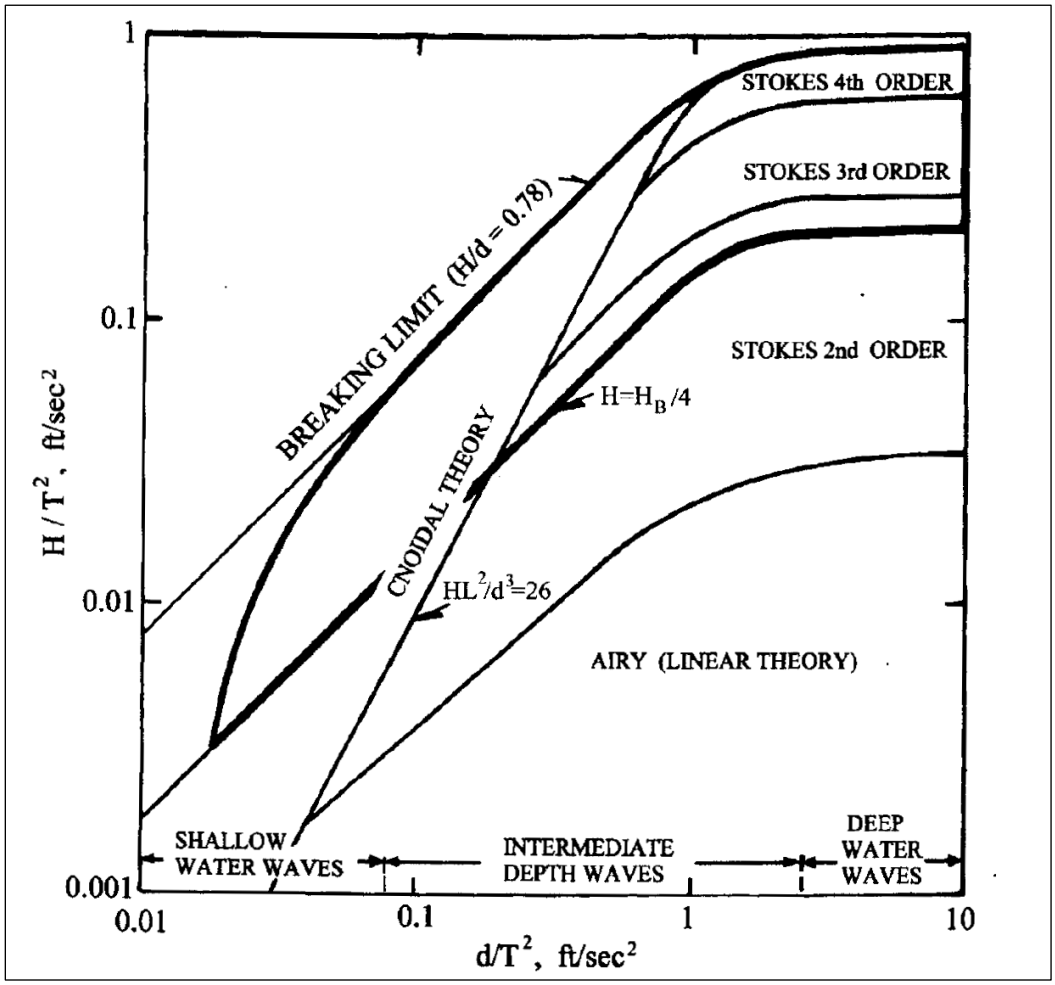

Figure 3-3: Limits of Wave Theory Validity. Adapted from (Wilson, 2003).

Regarding the nature of swells, the thesis shall be limited to deep water wave conditions where h > 1/2λ. Notable, as proposed in the formative aspect of Airy wave theory, the seabed is fixed and impermeable. Hence, the definition of a wave as either deep, intermediate, or shallow water wave depends on the wave amplitude (2λ). So, following this notion, the dispersion relation for swells will take the form of that for deep water conditions expressed in equation 31.

$$\omega^2 = gk \qquad \text{Equ. 3233}$$

By restricting the wave regime to deep water, the velocity potential (ø) is then expressed as a cosine function of the wave frequency w and the wave number k, as shown in equation 32 (Equ. 32).

$$ø = \frac{ag}{\omega} e^{kz} \cos(\omega t - kx) \qquad \text{Equ. 3435}$$

$$u = \omega a e^{kz} \sin(\omega t - kx) \qquad \text{Equ. 3637}$$

$$w = \omega a e^{kz} \cos(\omega t - kx) \qquad \text{Equ. 3839}$$

$$\dot{u} = \omega^2 a e^{kz} \cos(\omega t - kx) \qquad \text{Equ. 4041}$$

$$\dot{w} = -\omega^2 a e^{kz} \sin(\omega t - kx) \qquad \text{Equ. 4243}$$

With the solution to the velocity potential obtained, while disregarding lateral water particle motion, the velocities (Equ. 33 & 34) of a regular wave for both vertical and longitudinal direction can then be obtained by performing respective differentiation of equation 32 and subsequent differentiation of the velocities to obtain the wave-particle acceleration (Equ. 35 & 36). In equations 34 and 36, "w" must be taken to mean the wave angular frequency. Instead, it is wave velocity in the j vectorial direction.

Concerning figure 3-2, these equations express a single regular plane progressive wave. Under the Airy wave assumption, swells are groups of regular waves travelling together away from their source of disturbance. This brings the concept of group velocity (C_g) and phase velocity (C_p) as a property of the idealised wave train to bear. For the wave arriving in Southern Nigeria, if the earlier deep-water assumption holds, the group velocity and the phase velocity are related by "n" and described according to equation 37.

$$n = \frac{C_g}{C_p} = 0.5\left(1 + \frac{2kh}{sinh2kh}\right) \qquad \text{Equ. 3744}$$

Equation 37, according to (Krogstad & Arntsen, 2000a), only applies to intermediate water conditions. However, according to (Barber & Ursell, 1948), for swells in deep waters, the group

velocity reduces to half of the phase velocity, as shown in equation 38. T represents the wave period.

$$\frac{C_g}{C_p} = 0.5; C_p = \left(\frac{g}{4\pi}\right)T \qquad \text{Equ. 3845}$$

For a given set of swell trains, those with significantly higher energy would arrive at the Southern Nigerian waters before those with less energy. According to (Ardhuin et al., 2009), swells with less energy are likely to damp, decay and eventually dissipate. This explains why the swell significant height and energy not far from the storm's proximity could be much higher than those arriving in Southern Nigeria waters. As posited by (Ardhuin et al., 2009; Barber & Ursell, 1948), swell dissipation and decay can be attributed to shear stress modulation as induced by swell orbital velocities, modifications of the swell regime due to swell-swell interactions, swell interaction with the wind (wind), and other prevailing ocean conditions.

Next on the build-up and conceptualisation of the relevant wave theories and principles is wave superimposition, whose resultant effect is the irregular wave.

3.2 Swells as Irregular Ocean Waves

Ocean waves are irregular, according to (Newman, 2018). This qualifies swells in all senses to be termed irregular waves. An irregular sea state can be viewed as a composition of different Airy wave trains that can be fitted into a specific spectra description such as the P-M spectrum, the JONSWAP, etc. (Haritos, 2007) while according to (Newman, 2018), an accurate description of ocean waves must be that of the probabilistic event in due to their stochasticity.

From both positions (Haritos, 2007; Newman, 2018), swells can be generalised as fully developed, long-crested, long-travelling irregular ocean waves with a probabilistic distribution, whose wave model is a composition of different Airy wave trains. This follows that the sea state in Southern Nigeria, being swell dominated according to (Forristall et al., 2013; Olugbenga et al., 2017), can be modelled using combinatorics of different Airy wave trains.

(Newman, 2018, p. 311) presented quite a holistic approach which included traditional assumptions in naval architecture and ocean engineering on deriving the equation for an ocean spectrum; hence a reinvention of the wheel is irrelevant. Therefore, the semi-empirical model expressive of an ocean spectrum in the frequency domain is presented in equation 39 (Equ. 39). Further reference can be made to section 2.3 to review the modelling of ocean surface waves.

$$S(\omega) = \frac{ag^2}{\omega^5} ex[-\beta(g/u\omega)^4] \qquad \text{Equ. 46}$$

3.3 Flow Around Fixed-Floating Objects

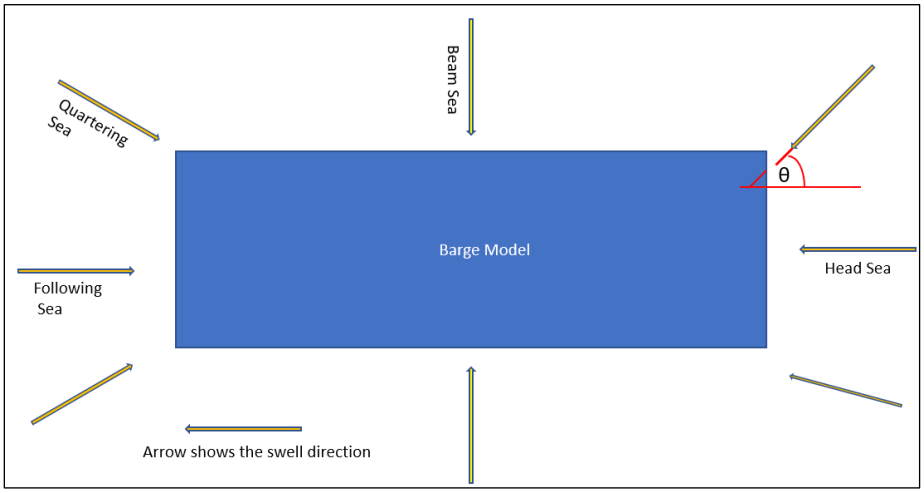

Figure 3-4: Depiction of Barge in a Typical Flow Field

So far, a description of the nature and modelling of ocean surface waves have been presented in the respective leading chapters of this thesis. Given attempting to understand the response of an offshore structure, it is considered essential to grasp the nature of the flow around a fixed-floating object offshore. The term "fixed" is used intentionally as the semi-submersible barge considered for this analysis is non-self-propelled, and offshore installation operations happen mostly when the vessel is required to keep the station. This is significant because there is no forward speed during the swell encounter.

In general terms, flow theory explains the characteristic of the motion of a fluid in space and time. Sometimes, the flow may be laminar, turbulent, viscous, non-viscous, rotational, irrational, uniform, non-uniform, free vortex etc. With each classification and assumption, a lead is provided mathematically, and subsequently, relevant equations are used to model, and compute required flow characteristics and properties.

As figure 3-3 shows, customarily, the assumption is that it swells from multiple directions. If each arrow signifies a specific swell train (swell group), it should therefore follow that the description of each swell particle motion is generalised for all within the same wave train.

In fluid mechanics, flows around the externals of an object (see figure 3-3 and figure cite figure) can be described as a frictionless flow; this translate to the absence of viscosity (inviscid is mostly relevant between the boundary layer) and irrotational (the fluid particle is not rotating about its centre of mass). Summarily, external flows are based on the following:

I. Flow is inviscid.
II. Flow is irrotational.
III. There is no vorticity.
IV. Flow is incompressible.

If condition I, II, II, & IV holds mathematically, the following can be formulated.

$$\mathbf{V} = \nabla \emptyset \qquad \text{Equ. 40}$$

According to equation 40, the curl of the velocity vector field is equal to zero. If a vectorial cross product is performed on the said equation (Equ. 40), then it can be said that;

$$\nabla \times \mathbf{V} = \nabla \times \nabla \emptyset \qquad \text{Equ. 41}$$

But recall from the principle of incompressibility, which holds that the cross product of the velocity vector by the gradient, which equals the vorticity, must be zero on the grounds of zero vorticity in the flow regime.

$$\omega = \nabla \times \mathbf{V} = 0 \qquad \text{Equ. 47}$$

It is consistent following from equation 42 that equation 41 reduces to zero. Hence written as equation 43, which is also called the Laplace equation.

$$0 = \nabla^2 \emptyset \qquad \text{Equ. 48}$$

In a 3D flow, equation 43 will take the form of equation 18 (Equ. 18) in all possible three translational degrees of freedom (cartesian coordinate).

These equations (Equ. 40 to Equ. 43) are the basic equations governing potential flow theory, whether applied to source flow, sink, uniform, or free vortex. If this thesis argues that swells that originate from a source (storm) gradually acquire momentum and progressively radiate outward from the storm, one can allude, based on the context, that swells are source flows. When swell combinations (swell groups with joint velocity) propagate outwards, the total swell potential becomes the summation of the full swell potential contained within a particular swell train.

$$\emptyset_{totalswell} = \emptyset_{swell_1} + \emptyset_{swell_2} + \cdots + \emptyset_{swell_n} \qquad \text{Equ. 44}$$

If equation 44 (Equ. 44) is rearranged, it can be simplified as;

$$\emptyset_{total} = \sum_{i=1}^{i=n} \frac{q_i}{2\pi} \log_e r \qquad \text{Equ. 45}$$

Where q is the source energy and r is an arbitrary radial position taken away from the storm's centre. From equation 40 to equation 45, the primary flow characteristic around a floating object (external flow) has been derived. This explains the modelling approach and assumptions needed to proffer a mathematical solution to external flows. However, as the streamlines encounter the external object, the fluid-structural interaction's mechanics must be understood if the response of the offshore structure is to be computed.

In the following subsection, the thesis explores how the response of an offshore structure under wave influence can be derived.

3.4 Vessel Response in Waves

The motion of floating, submerged, or moored objects is of great interest to the practitioners of naval architecture and ocean engineers as it provides the needed insight into the oscillatory motion of such objects during wave interactions (Newman, 2018). In the customary nature of moving from the least complex scenario with simplifications and assumptions, (Newman, 2018, p. 285) argues that the motion can be conceived as simple plane progressive waves of small amplitude having a harmonic time dependence.

If the above assumption holds, the far-reaching implication is that the response from an ocean wave (ideally irregular) becomes constricted as a standard wave response. But, by recollecting, among other things, one of the basic assumptions of ocean waves as being a combination of a multiplicity of regular waves during the derivation of the mathematics of irregular ocean waves, one sees a leeway that eventually prevents the apparent pitfall of oversimplification and non-compliant assumptions. There is a need to introduce the idea of a frame of reference or a coordinate system since the dealing is now about displacement and motions.

3.4.1 Ship Frame of Reference & Degrees of Freedom

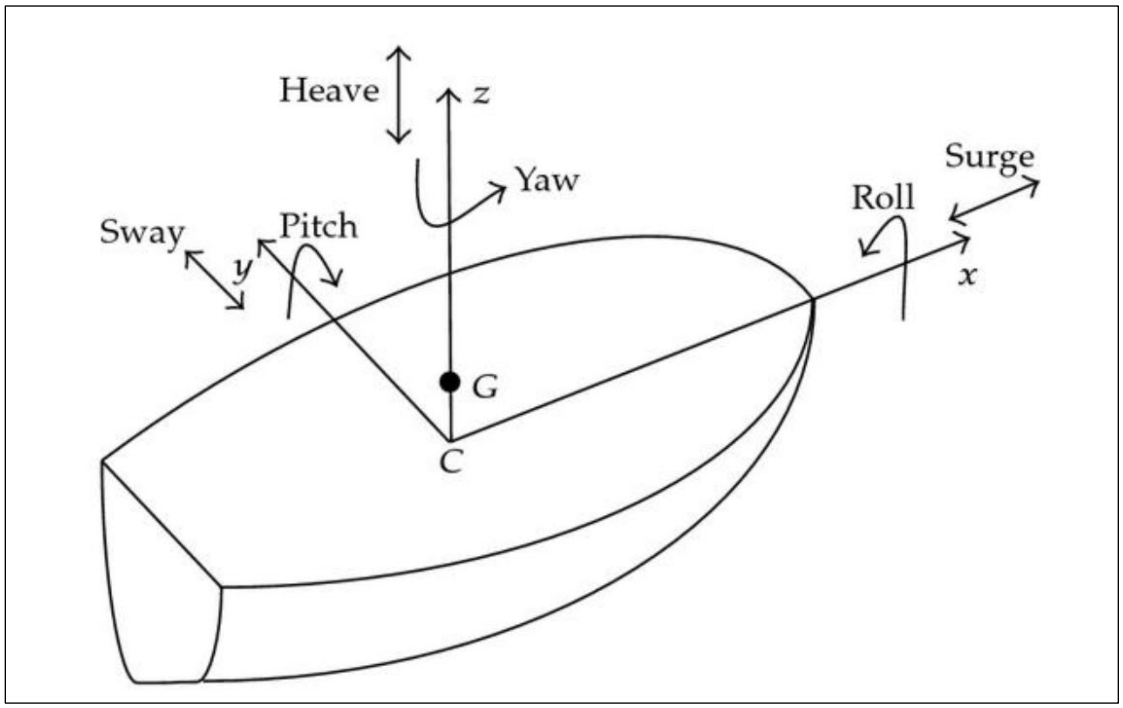

Figure 3-5: Schematic of Ship's Degrees of Freedom

Figure 3-5 shows a ship's or offshore structure's axis of freedom when excited. Six degrees of space exist, three translations and three rotations. From a reference standpoint, the three axes include longitudinal (x-axis), transversal (y-axis), and vertical (z-axis). The Origo may be located at the ship's midship or taken from the transom. An explicit explanation of the reference point will be presented case by case.

3.4.2 Motion & Excitation Forces

The study of motion and excitation of bodies when acted by an external force can be traced back to Newtonian physics and the accompanying laws of motion. Equation 46 (Eq. 46) shows the relationship between excitation force, the excited body's mass, and the body's acceleration (response).

$$\bar{F} = M\vec{a} \qquad \text{Equ. 49}$$

However, the wave excitation problems and a body's response are much more complex than that provided by Newtonian physics. However, the wave excitation problems and the body's response provide an excellent foundational understanding of the relationship between external force and body excitation, which will be built upon.

From figure 3-5, three translation and three rotational motions of a floating object in a seaway can be written ascribed as surge (ξ_1), roll (ξ_4), heave (ξ_3), yaw (ξ_5), sway (ξ_3), and pitch (ξ_6). Previously, an assumption of waves with small amplitude was made—similarly, an assumption of the response from waves with small amplitude as small amplitude response is made. The response amplitude is also assumed to be equal to the wave amplitude. With this, it is consistent to write that at zero forward speed, the response velocity (Equ. 47) is the same as the wave velocity related to the encounter frequency.

$$U_j = Re\left(\omega\xi_j e^{i\omega t}\right), \text{ j = 1, 2 ...6} \qquad \text{Equ. 50}$$

In equation 47, there is also an imaginary side which has been deliberately omitted. For a unit amplitude wave/response, the general velocity potential can be written as a sum of all the potentials. This is shown in Equations 48 & 49.

$$\emptyset_t = \emptyset_1 + \emptyset_2 + \cdots + \emptyset_6 \qquad \text{Equ. 51}$$

Alternatively,

$$\emptyset = (x, y, z, t) = Re\left\{\left(\sum_{j=1}^{6} \xi_j \emptyset_j(x, y, z) + A\emptyset_A(x, y, z)e^{i\omega t}\right)\right\} \quad \text{Equ. 52}$$

The second term $\emptyset_A$ on the RHS in equation 49, according to (Newman, 2018), is the diffracted component of the response. It can further be discretised into the diffracted potential ($\emptyset_{diff}$) and another term called the Froude-Krylov force ($\emptyset_{fk}$) opposite to the diffracted potential. The letter "A" represents the amplitude of the diffracted wave. This has been exemplified in figure 3-6.

If n designates a unit vector on the body surface directed inward the body, and r represents a position vector in the cartesian coordinate, the normal derivative of velocity potential in equation 49 (Equ. 49) to the normal component of the body velocity under the condition that their respective amplitudes are independent of each other (Newman, 2018).

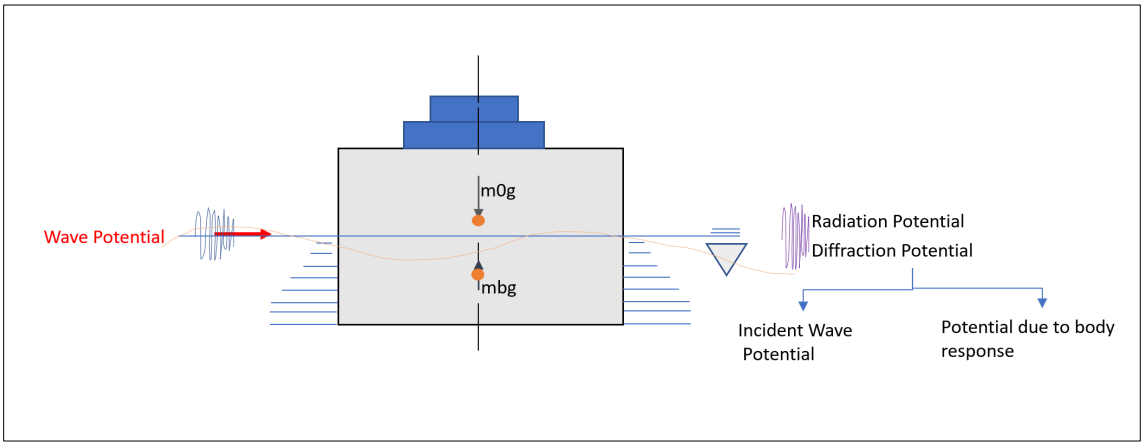

Figure 3-6: Decomposition of body motion in a seaway

Imposing the necessary boundary conditions at the semi-submersible side shell includes.

- The partial derivative of the potential function w.r.t the normal direction must be equal to the normal velocity of the vessel.

$$\frac{\partial \emptyset_j}{\partial n} = V_{n_{body}} = \left(\frac{\partial \emptyset}{\partial n}\right) V_J \quad \text{Equ. 53}$$

- The differential of the diffracted wave potential with respect to the normal direction must be equated to zero on the vessel's side shell, otherwise called the body surface.

$$\frac{\partial \emptyset_{jrad}}{\partial n} = 0 \quad \text{Equ. 54}$$

- The partial derivative of the potential generated because of the disturbance of the body on the incident wave concerning the normal direction must be the opposite of the result of incident wave potential relative to the normal direction.

$$\frac{\partial \emptyset_{jfk}}{\partial n} = -\frac{\partial \emptyset_{jdiff}}{\partial n} \qquad \text{Equ. 55}$$

The terms $\emptyset_{fk}$ represents the Froude-Krylov component of the response potential, $\emptyset_{diff}$ represents the diffracted potential of the response, and $\emptyset_{rad}$ is the radiation potential of the response respectively.

These three conditions are in addition to the pre-imposed conditions on Airy wave theory; hence the problem, as decomposed in the figure and shown in equation 53, is that of a boundary-value problem. The implication is that solutions to the sets of differential equations formulated so far are only possible if all the boundary conditions and their governing equations are actual.

$$p = \rho\left(\frac{\partial \emptyset}{\partial t} + gz\right) = -\rho\left(Re\left\{\left(\sum_{j=1}^{6} \xi_j \emptyset_j + A(\emptyset_{diff} + \emptyset_{fk})\omega\, e^{wt}\right)\right\} - gz\right) \qquad \text{Equ. 56}$$

If the total response potential (equation 49) is substituted into Bernoulli's equation giving rise to equation 53, which is then integrated over the surface of the vessel below the mean sea level (MSL), the response (force ad moment) acting on the body can then be obtained. Applying Green's theorem, the resulting force and moment can be expressed as shown in equation 54.

$$\begin{pmatrix} F_j \\ M_j \end{pmatrix} = -\rho g \iint \begin{pmatrix} n \\ r \times n \end{pmatrix} y dS - \rho Re \sum_{j=1}^{6} \omega \xi_j e^{\omega t} \rho g \iint \begin{pmatrix} n \\ r \times n \end{pmatrix} \emptyset_j dS - \rho Re \omega A e^{\omega t} \iint \begin{pmatrix} n \\ r \times n \end{pmatrix} (\emptyset_{diff} + \emptyset_{fk}) dS \qquad \text{Equ. 57}$$

In equation 54, the first integral represents the hydrostatic component, the second represents the added mass, and the third integral indicates the contribution from the excitation force. This shows that the total force casing body motion can be expressed according to equation 54. Further treatment and discussion of these constituent forces and moments have been done by (BASO et al. 2013; Haritos, 2007; Newman, 2018; R. Adrezin et al., 1996).

Recalling equation 46, Newton's law of motion can be re-written in its dynamic form as;

$$F_e(t) = \sum_{j=1}^{6} M_j \dot{u}_j \qquad \text{Equ. 58}$$

Where M_j represents the mass matrix. If the symmetry assumption is made and the vessel's centre of gravity is located at x = $L_{pp}/2$, y = B/2, and Z_g = vertical CoG. The mass matrix can be written as;

$$M = \begin{matrix} M & 0 & 0 & 0 & Mz_g & 0 \\ 0 & M & 0 & -Mz_g & 0 & 0 \\ 0 & 0 & M & 0 & 0 & 0 \\ 0 & -Mz_g & 0 & I_4 & 0 & I_{64} \\ Mz_g & 0 & 0 & 0 & I_5 & 0 \\ 0 & 0 & 0 & I_{64} & 0 & I_6 \end{matrix} \qquad \text{Equ. 59}$$

Where I_{xx} is the moment of inertia defined in chapter four, M is the body's mass, and Mz_G is the mass moment about the vertical axis, a generalised equation of motion in six-coupled, linear, and harmonic motion of a body may be expressed according to equation 57. However, the added mass computation of a ship is seen as a great deal of subject. Sen & Vinh (2016) presented some historicity on added mass, a simplified definition termed a virtual increase in the inertia and moment of a vessel in a seaway due to a unit acceleration of water particle. The added mass is analogous to the mass matrix of equation 56. Comparing methods for evaluating a ship's added mass has been discussed (Yang, 1990).

$$F_j exp.^{i\omega t} = \sum_{j=1}^{6} \left(M_{kj} + A(\omega)_{kj}\right)\ddot{\xi}_j + B(\omega)_{kj}\dot{\xi}_j + C_{kj}\xi \qquad \text{Equ. 60}$$

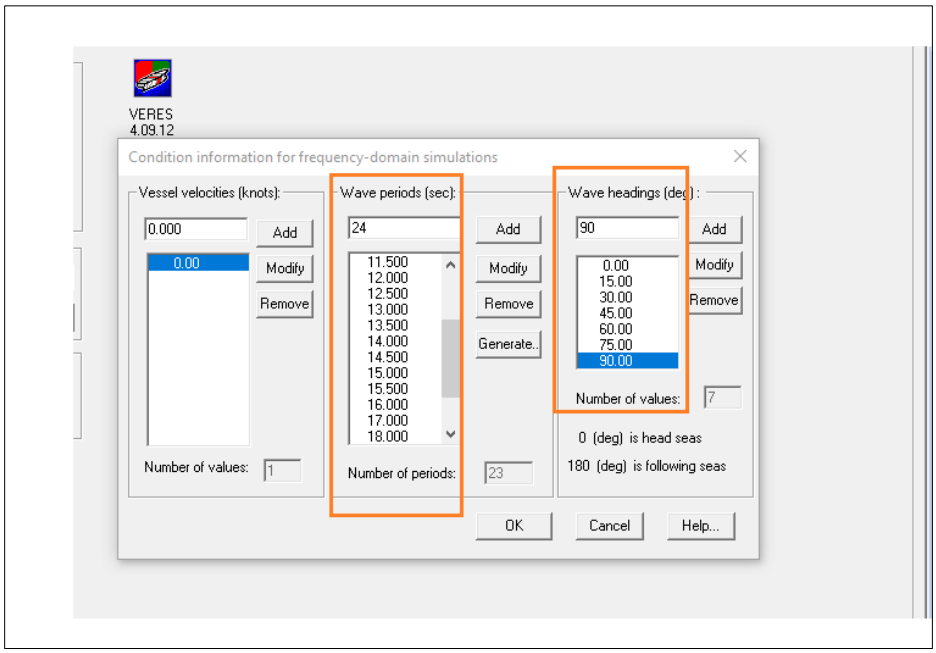

Figure 3-7: VERES Wave Period & Heading Dialogue Box

In equation 57, higher order terms have been neglected; j can take up values from 1 – 6, designating surge, heave, roll, etc. The real part of the same equation, F_1, F_2 and F_3, represents the amplitude of the surge, sway, and heave excitation forces, while F_4, F_5 and F_6 are the amplitude of the roll, pitch, and yaw.

The added mass and damping force resulting from the forced motion of the body earlier highlighted in j degrees of freedom may be written as;

$$F_j = -A(\omega)_{jk}\ddot{\xi} - B(\omega)_{jk}\xi \qquad \text{Equ. 61}$$

While the restoring coefficient may be expressed as equation 59.

$$F_j = -C_j k\xi \qquad \text{Equ. 62}$$

With added mass A_{jk}, damping (B_{jk}) and restoring (C_{jk}) coefficients, solutions to equation 57 provide the forces acting on a floating body. The software ShipX (Fathi & Hoff, 2004) it's the ability to solve the motion equations that require the wave period and headings as user input, as shown in figure 3-7. The response in terms of the amplitude can be written in the form expressed in equation 60.

$$\xi_j = \tilde{\xi}_j e^{i\omega t} = \xi_a \cos(\omega t + \Theta_j) \qquad \text{Equ. 60}$$

The added mass coefficient, damping and restoring coefficients in equations 57 – 59 are equally in the form of a matrix. The strip theory formulation by (Salvesen et al., 1970), the work on the assessment of forward speed effect on sway, roll and yaw coefficients (Troesch, 1978), and other

similar works such as (Ogilvie & Tuck, 1969) provides for extensive mathematical background and formulation for the determination of added mass, damping and restoring coefficients of a floating body in a seaway.

Without going into the lengthy and rigorous route of the derivation, according to (Salvesen et al., 1970), the added mass or the damping coefficient may be written as;

$$A_{jk}\ or\ B_{jk} = \begin{matrix} A_{11} & 0 & A_{13} & 0 & A_{15} & 0 \\ 0 & A_{22} & 0 & A_{24} & 0 & A_{26} \\ A_{31} & 0 & A_{33} & 0 & A_{35} & 0 \\ 0 & A_{42} & 0 & A_{44} & 0 & A_{46} \\ A_{51} & 0 & A_{55} & 0 & A_{55} & 0 \\ 0 & A_{62} & 0 & A_{64} & 0 & A_{66} \end{matrix} \qquad \text{Equ. 61}$$

The subscripts in the elements of the added mass matrix indicate the coupling of the added mass regarding motion direction. Furthermore, according to (Salvesen et al., 1970), if the ship is assumed to be located at the free surface, most of the restoring coefficients vanish to zero while the remaining elements can be expressed as;

$$C_{33}, C_{44}, C_{55}, \& \ C_{35} = C_{53} \qquad \text{Equ. 62}$$

With all the constants in the general equation of motion determined, it is now possible to write the equations for all the linear translatory motion, the moments, and their coupled form.

So far, it is plausible to state that the characteristics and behaviour of a body in a regular wave train have been known through the series of equations discussed in this chapter. But the goal is to use the regular wave response to obtain a body's response in an irregular wave. If the relation between a wave potential and a response potential is described using cause and effect (causality). In that case, mathematically, one can say that a random sea state will produce a random body motion made possible through the transfer of impulse or energy. This analogy can be represented using a linear time-invariant mathematical model called a transfer function $T_f(\omega, \Theta)$.

$$\xi_j(t) = Re \iint \mathrm{T}_{f_j}(\omega, \Theta) e^{i\omega t} dA(\omega, \Theta) \qquad \text{Equ. 63}$$

3.4.3 Response Amplitude Operators (RAOs)

The response amplitude operator of a vessel is a transfer function H(w) that relates the magnitude of the wave potential (amplitude) to the response potential (amplitude).

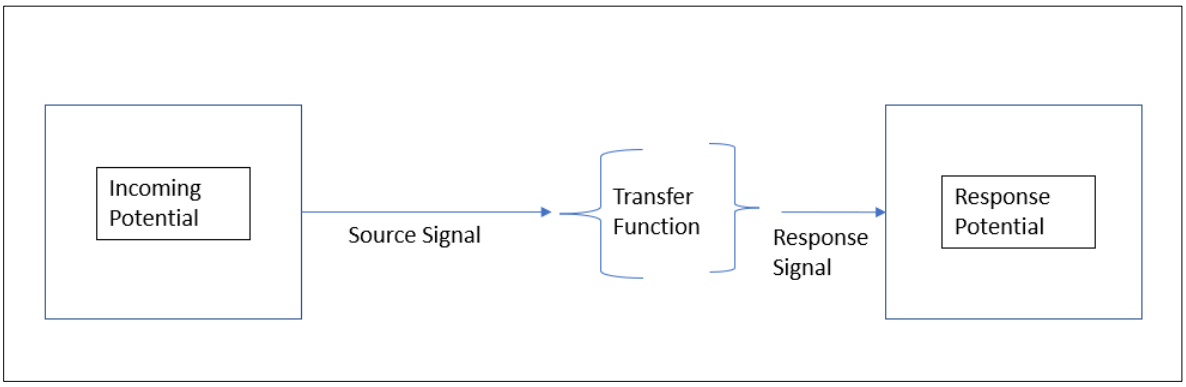

Figure 3-8: Transfer Function H(w) Connecting Source Signal & Response

Recalling the dynamic equation of motion (equation 57), the real part of the LHS represents the force and momentum component of the wave excitation force. If the excitation force is expressed as a linear equation of the response amplitude, the transfer function (figure 3-8) can be expressed as equation 64.

$$F_j exp.^{i\omega t} = \xi_a X_j(\omega, \Theta) exp.^{i\omega t} \quad \text{Equ. 64}$$

Furthermore, the concept of the body's complex notation is introduced according to equation 65.

$$\xi_k = \xi_{ka} exp.^{i\omega t} \quad \text{Equ. 65}$$

By substituting equation 65 into equation 57 and using standard matrix inversion techniques (Newman, 2018), solutions to the equation of motion can be obtained for a body's distinctive and simultaneous six degrees of motion.

$$\sum_{i=1}^{6} \xi_{jka} \left[-\omega^2 \left(M_{kj} + A_{jk}\right) + i\omega B_{jk} + C_{jk}\right] = \xi_a X_j(\omega, \Theta) \quad \text{Equ. 66}$$

If both sides of equation 63 are divided by ξ_a, the transfers function for the motion amplitude and phase of a body motion can be written as;

$$\boldsymbol{H}_j(\omega, \Theta) = \frac{\xi_a}{\xi_j} = \left(\frac{X_j(\omega, \Theta)}{-\omega^2 \left(M_j + A_j\right) + i\omega B_j + C}\right) \quad \text{Equ. 67}$$

So, from equation 65, by multiplying the ROA (*Re* LHS) by the denominator, the motion of a body can quickly be deciphered. Thus, RAO is a key performance indicator of the hydrodynamic assessments of offshore structures.

4 Chapter Four – Analysis Set-Up

Chapter four discusses and presents the installation vessel model used for the analysis, the computer software ShipX, and a description of the simulation setup.

4.1 Analysis Set-Up

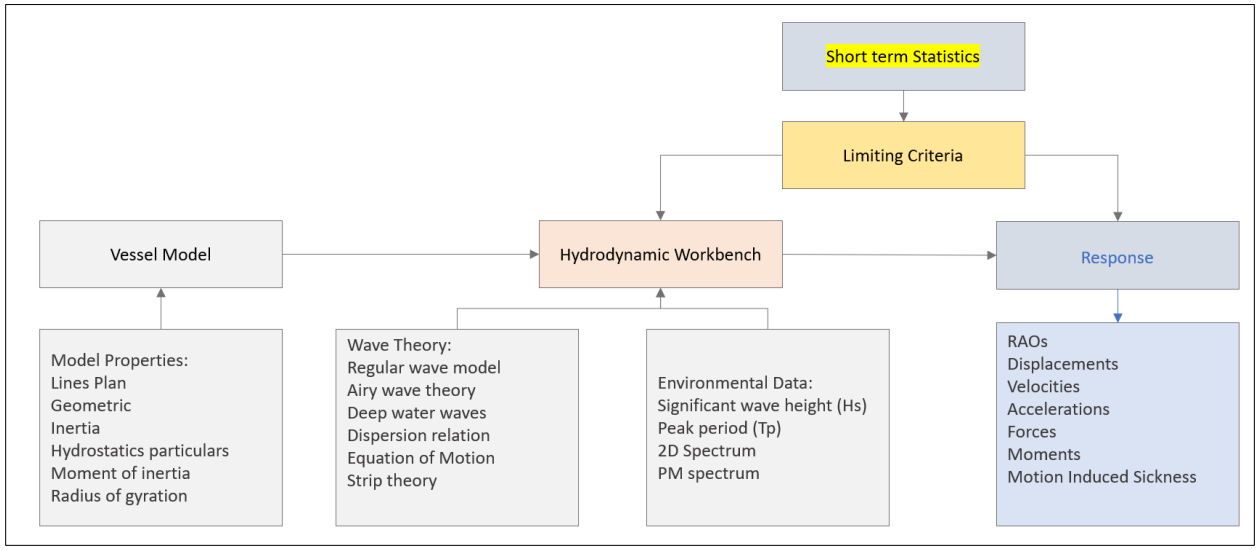

Figure 4-1: Analysis Set-Up

Figure 4-1 illustrates the setup of the simulation. From the algorithm, a semisubmersible barge model was designed using ShipShape[1]. Next is the definition of the ballast condition for a typical installation operation and the calculation of the vessel properties at the loading condition.

The lines plan is imported into the workbench and designed for the wave theories discussed in the section; environmental conditions and limiting states are further defined, and the input data is checked for errors. If zero error is returned as feedback, the analysis runs, and the response is extracted.

4.2 Vessel Modelling

The vessel used for the analysis is a semi-submersible, heavy-lift, heavy-deck cargo barge. Within the offshore market, semi-submersible heavy lift vessels are centric on the success of most installation operations. This may be due to its large deck area, which allows for the transportation of large structures, its ability to be used as a work platform, and its variable displacement and buoyancy, which makes it possible for the execution of float-off operations.

[1] Shipshape is a ship design software approved by the Norwegian Maritime Authority (NMA) for tonnage, hydrostatics, and global strength calculations.

Using publicly available information from the DNV vessel register and interpolating between similar vessels on the same vessel register, a semi-submersible barge (figure 4-2) with principal dimensions as per table 4-1 is used for the analysis.

Table 4-1: Vessel Geometric Properties (Ref. /Appendix 1/)

Vessel Property	Value
L_{pp}	110.00 [m]
Breath	28.00 [m]
Depth	8.00 [m]
Design T	5.20 [m]
Displacement	14182.6 [tonnes]
TPC	31.227 [tonnes/cm]
Initial GM	9.387 [m]

The hydrostatic model of the vessel and particulars were derived using the ship design software Shipshape.

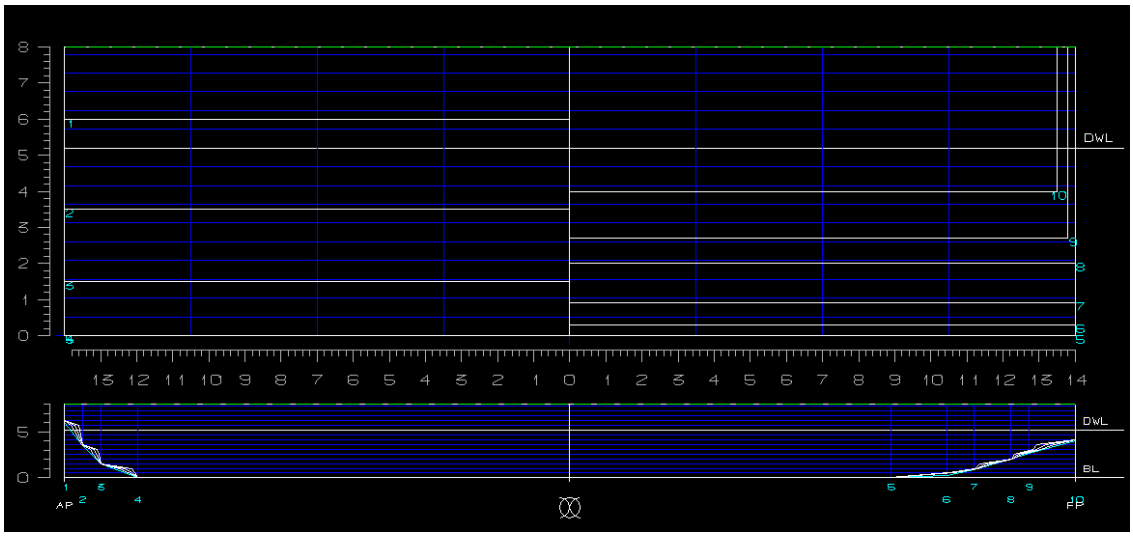

Figure 4-2: Semi-Submersible Hull Lines Generated with ShipShape

4.2.1 Installation Ballast Condition

A hydrodynamic analysis using ShipX requires the vessel loading condition as input. ShipX directly integrates the dynamic hull pressure below the waterline (wl) or subdivides the below-waterline hull into strips and applies the ordinary theory. An exact vessel displacement is also relevant for determining the mass, the moment of inertia and the radii of gyration of the vessel, which collectively form part of the input into ShipX.

The summary of the vessel a typical installation load case is presented in figure 4-3, while table 4-2 contains the barge hydrostatic particulars at the installation load case.

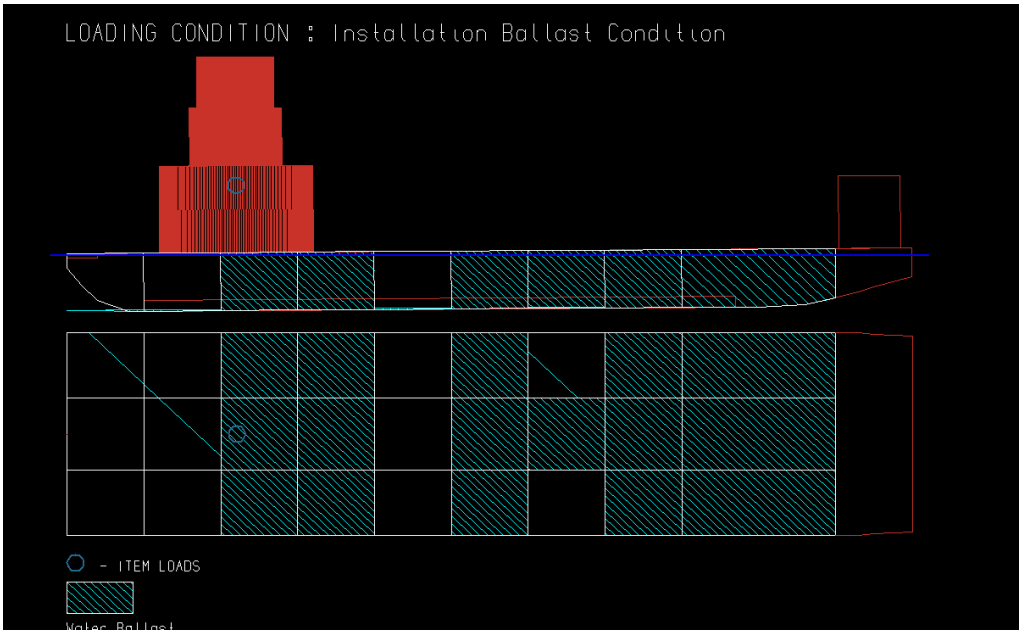

Figure 4-3: Typical Installation Ballast Condition with Cargo on Deck

Table 4-2: Summary of Vessel Properties for Installation Ballast Condition

Properties	Value
Light Ship Weight [T]	5200.00
Mass of Turbine Foundation [T]	3500.00
Ballast [T]	14015
Total Mass [T]	22714.8
Draft [m]	7.39
Trim [m]	0.827
GM [m]	5.624
Vertical Centre Gravity (Z_g) [m]	6.610

4.2.2 Mass Model

The hydrodynamic workbench automatically calculates the ship mass matrix. It is possible to plug the mass and respective centre of gravity into equation (56) and compare it to the ShipX-derived matrix (Fathi & Hoff, 2004). In this case, the ShipX-derived mass matrix is deemed fit for use as it shows little to no deviation from a manually computed mass model using the total mass in the table, a moment arm of 6.610m – D/2, and the I_{xx} determined using the relation between the radius of gyration and the body mass (equ. 72-74).

ShipX calculates the added mass, damping and restoring coefficients based on the works of (Salvesen et al., 1970). The computer algorithm can be found in (Fathi & Hoff, 2004). For this

analysis, both the values obtained for the added mass, damping, and restoring coefficients have been used as computed by VERES.

4.2.3 Radius of Gyration

Table 4-3: Radii of Gyration for a Typical Mono-hull (Ref. /Appendix 1/)

Radii of Gyration	Description	Range of Values [m]
r_{44}	Roll radius of gyration	0.30B – 0.45B
r_{55}	Pitch radius of gyration	$0.20L_{pp}$ – $0.30L_{pp}$
r_{66}	Yaw radius of gyration	$0.25L_{pp}$ – $0.30L_{pp}$
r_{64}	The coupled radius of gyration	≈0.00

For the analysis, ShipX accepts the mass-radius of gyration in roll (r_{66}), pitch (r_{55}), yaw (r_{66}), and the coupled radius of gyration (r_{64}) of the vessel as impute. The software manual (Appendix 1) provides a rule of the thump, which can be used to obtain the values of these radii of gyrations in table 4-3.

Alternatively, the following equations 72-74 can be used to calculate the radii of gyrations for the different degrees of freedom.

$$r_{44} = \frac{\sqrt{\sum(y^2 + z^2)\Delta M}}{M} \quad \text{Equ. 68}$$

$$r_{55} = \frac{\sqrt{\sum(x^2 + z^2)\Delta M}}{M} \quad \text{Equ. 69}$$

$$r_{66} = \frac{\sqrt{\sum(x^2 + z^2)\Delta M}}{M} \quad \text{Equ. 70}$$

$$r_{64} = \begin{cases} \sqrt{\frac{I}{M}}\ If\ I \geq 0 \\ -\sqrt{\frac{I}{M}}\ If\ < 0 \end{cases} \quad \text{Where } I = -\sum x.z.\Delta M, \quad \text{Equ. 71}$$

According to the documentation provided by (Fathi & Hoff, 2004), the radii of gyration in VERES 1.0 is taken relative to the motion coordinate system, while for recent versions, it is taken about the centre of gravity of the vessel. While x, y, and z are coordinates relative to the vessel' CoG, M represents the body's total mass, Δand M is the weight of an item in space within the ship's boundary.

From table 4-3, the following radii of gyration have been derived:

Table 4-4: Derived Radius of Gyration (Ref. /Table 4-3/)

Radii of Gyration	Basis of Estimation	Values [m]
r_{44}	0.40×Breadth	11.20
r_{55}	0.28×L_{pp}	30.80
r_{66}	0.26×L_{pp}	28.60
r_{64}	Null	≈0.00

4.2.4 Moment of Inertia

DNV in (Det Norske Veritas, 2010) provided a functional equation (72-74) relating the radius of gyration to the body's moment of inertia which is part of the elements of the mass matrix. The terms r_{xx} and I_{xx} retain their usual meaning, while m_T is the total system mass.

$$I_{44} = {r_{44}}^2 . m_T \quad \text{Equ. 72}$$

$$I_{55} = r_{55}^2 . m_T \quad \text{Equ. 73}$$

$$I_{66} = r_{66}^2 . m_T \quad \text{Equ. 70}$$

4.2.5 Natural Frequency & Period

The natural period is the period of oscillation of a body under excitation from the mean to its equilibrium positions. Mathematically, the natural frequency of a body can be expressed as;

$$\omega_n = \sqrt{\frac{c}{m}} \quad \text{Equ. 71}$$

Where m is the body's mass, and c is the hydrostatic restoring coefficient of the body.

Following equation 75, the natural period in heave ($\omega_{na33}/\omega_{nheave}$) and in roll ($\omega_{nroll}$) can be expressed with respect according to equation 76, while the natural roll period is indicated in equation 81.

$$\omega_{na33} = \sqrt{\frac{\rho g A_{wp}}{m + A_{33}}} \quad \text{Equ. 72}$$

If A_{33} is the added mass in heave, and A_{wp} is the area of the waterplane corresponding to the installation load case, then A_{wp} can be expressed in terms of the length of the waterline (L_{wl}) and the submerged volume as;

$$A_{wp} = L_{wl} \times B_{submerged} \quad \text{Equ. 73}$$

If the added mass is simplified and expressed in terms of the coefficient of the added mass;

$$A_{33} = (1 + C_a) \quad \text{Equ. 74}$$

$$\omega_{na33} = \sqrt{\frac{\rho g L_{wl} \times B \times C_{wp}}{(1 + c_a) \times \rho L_{wl} B T C_B}} \qquad \text{Equ. 75}$$

The equation above shows that the natural heave period depends on the draft at any given loading.

$$\omega_{n_{a33}} = \sqrt{\frac{g}{(1 + c_a)} \left(\frac{c_{wp}}{C_B}\right) \left(\frac{1}{T}\right)} \qquad \text{Equ. 80}$$

In the roll motion axis, the natural period depends on the volumetric displacement, the transverse metacenter (GM_T), and the roll moment of inertia.

$$\omega_{n_{roll}} = \sqrt{\frac{\rho g \nabla G M_T}{I_{zz} + (1 + k_i)}} \qquad \text{Equ. 81}$$

K_i is the coefficient in roll. Something worth mentioning is that natural roll frequency directly correlates with metacentric height. From a hydrostatic perspective, a high GM can be interpreted as a very stable ship. Still, under wave action, in practice, it translates to a more extended period for the vessel to return to equilibrium. It must then follow that a low GM should produce the reverse effect.

4.2.6 Forward Speed

The vessel is considered to have zero forward speed. This is relevant because the encounter frequency will equal the wave frequency.

4.3 Analysis software – ShipX

ShipX, according to the description provided by the vendor (Fathi & Hoff, 2004), is a hydrodynamic workbench that is built using the strip theory approach developed by (Salvesen et al., 1970) as the primary approach for the calculation of ship motion and response. The main engine responsible for the numerical analysis is a plug-in called VEssel RESponse (VERES). Initially intended for the early ship design stage, ShipX can also be used for varying hydrodynamic calculations (Fathi & Hoff, 2004).

With ShipX's VERES plug-in, the body's motion in six degrees of freedom, relative motion transfer function, motion transfer function at a specific location, and global wave-induced loads can be calculated (Fathi & Hoff, 2004). Short- and long-term statistical and operability analyses can also be performed using the software. For more information on ShipX, including limitations, reference is made to both (Fathi & Hoff, 2004) and Appendix 1.

4.4 Environmental Wave Data

Wave data from some offshore locations in Southern Nigeria has been sourced and subsequently used for the analysis. The author did not receive these pieces of data directly from the source. Instead, it was extrapolated from some studies conducted using shell-provided data.

4.4.1 Location 1 – Asabo Oil and Gas Field, Offshore Nigeria

Figure 4-4: Asabo Field Location Source: Google Maps 2023

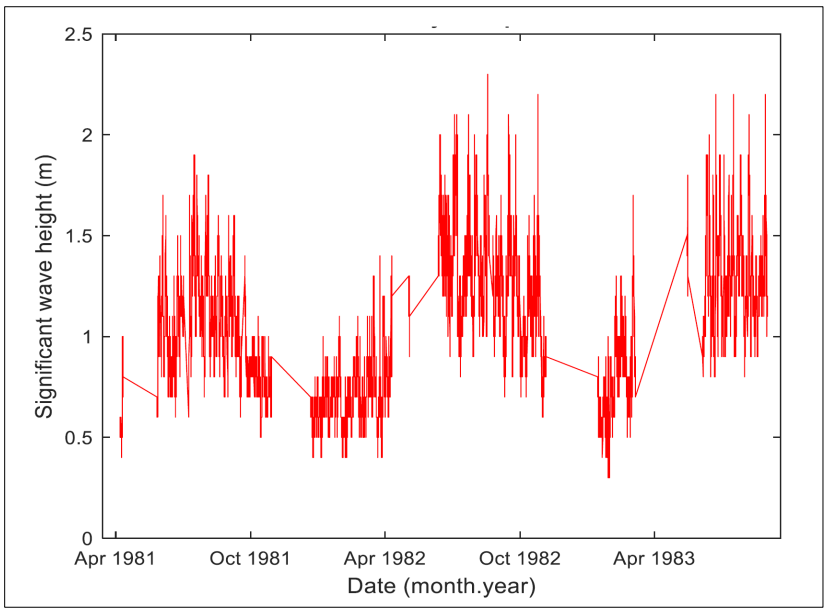

Figure 4-5: 3-Year Time History Plot of Significant Wave Height at Asabo Field. Source: (Agbakwuru et al., 2020)

Asabo field is an oil and gas field located in offshore Akwa-Ibom state in Southern Nigeria, or in a global sense, it is a field in the Gulf of Guinea. It has the following coordinates: 4°05'45.6"N 7°46'19.2" E (figure 4-4). According to (Agbakwuru et al., 2020), from 1981 through 1983, a Baylor Wave staff was deployed at the oil and gas field to record the time-dependent water-wave surface elevation, spectra peak periods and corresponding spectra directions.

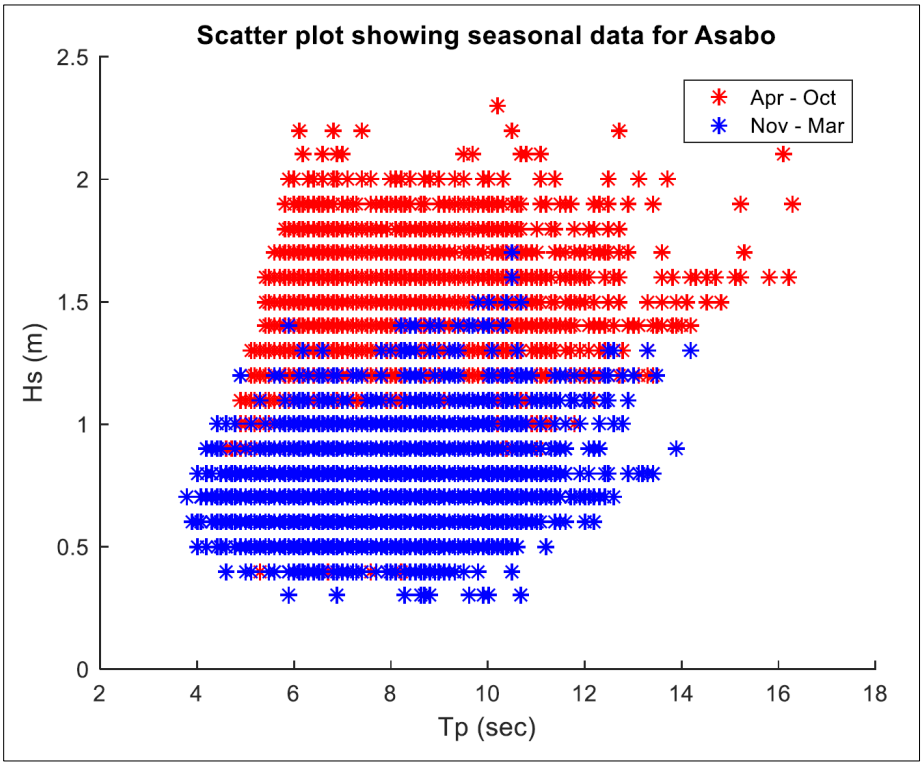

Figure 4-6: Scatter Plot of Hs(m) Vs Tp (S) for Asabo 1981-1983 Source: (Agbakwuru et al., 2020)

Table 4-5: 0.5-2.5m H_s & 6s-17s T_p for Asabo Field Offshore Nigeria. Adapted from (Agbakwuru et al., 2020)

H_s (m)	0.5 – 2.25	0.5-2.0	0.5-2.0	0.5-2.3	0.58-1.9	1.4-2.0	1.6-2.2	1.52-2.1
T_p (s)	6	8	10	10.2	12	14	16	16.1

Figure 4-6 shows the H_s and T_p distribution of the wave data collated in Asabo from 1981 to 1983. The range of the wave peak period is from ≈3.8 secs to ≈16.4 secs. From the available swell properties as a long-period wave, it is uncertain whether the high-frequency waves with 3.8 secs to around 6.0 secs are typical swells or a contribution from wind-generated seas.

To avoid any unintended error from using out-of-range data, the range of peak periods considered would be from 6.00 sec to 16.1 secs and Hs from 0.5m to 2.1m. These are directly read from figure 4-6.

4.4.2 Location 2 – Forcados Field, Delta State, Offshore Nigeria

Forcados is described (Agbakwuru & Bernard, 2019) as a shallow water offshore facility in Burutu local government of Delta State, Southern Nigeria. It has a latitude of 5.1722 and a longitude of 5.1792. The in-situ data for the Forcados field was collected using a directional wave-rider to record the sea state every 30 minutes under a 3-hour interval from September 1980 to May 1982 (Agbakwuru & Bernard, 2019).

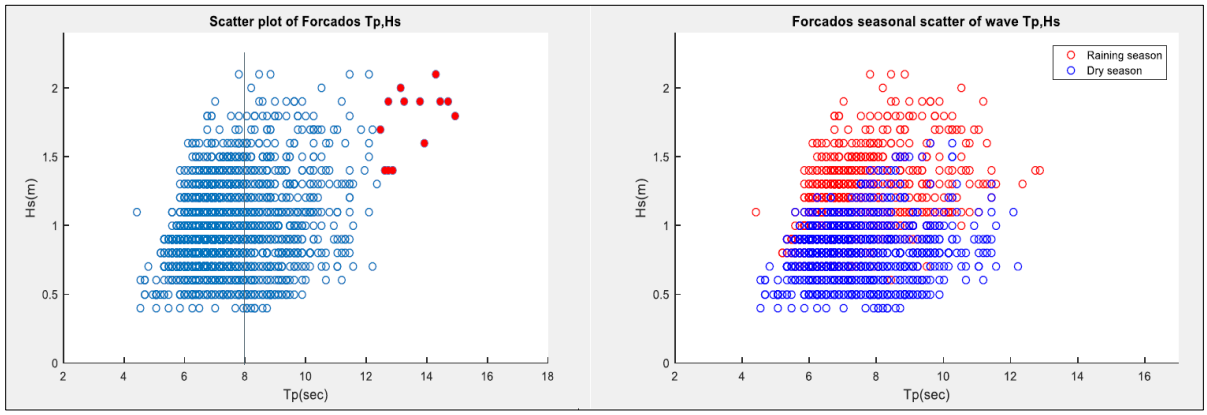

Figure 4-7: Scatter Plot of Hs & Tp for Forcados Offshore Delta State, Nigeria. Source:(Agbakwuru & Bernard, 2019)

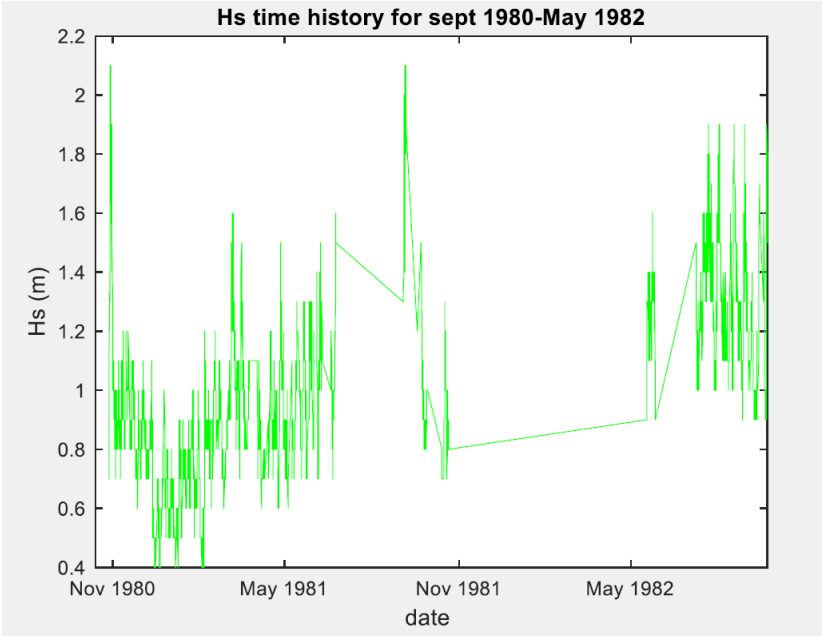

Figure 4-8: Time History of Hs between Sept. 1980-May 1982
Forcados Offshore Delta State, Nigeria. Source:(Agbakwuru & Bernard, 2019)

According to (Agbakwuru & Bernard, 2019), the spectra peak periods were obtained by multiplying the zero-up crossing period by 1.3. Figure 4-7 shows the distribution of the significant

wave height and the spectra peak periods, while the figure shows a historical plot of the significant wave heights from September 1980 to MAY 1982.

The distribution obtained a range of significant wave heights and peak periods for Forcados-specific response analysis.

Table 4-6: 0.5-2.2m H_s & 6s-14.4s T_p for Asabo Field Offshore Nigeria. Adapted from (Agbakwuru et al., 2020)

H_s (m)	0.5 – 1.52	0.5-2.0	0.5-2.0	0.5-1.8	0.54-2.2	1.7-1.8	1.8-2.2	1.7-1.8
T_p (s)	6	8	10	10.2	12	14	14.1	14.4

4.4.3 Location 3 – Bonga Field, Offshore Nigeria

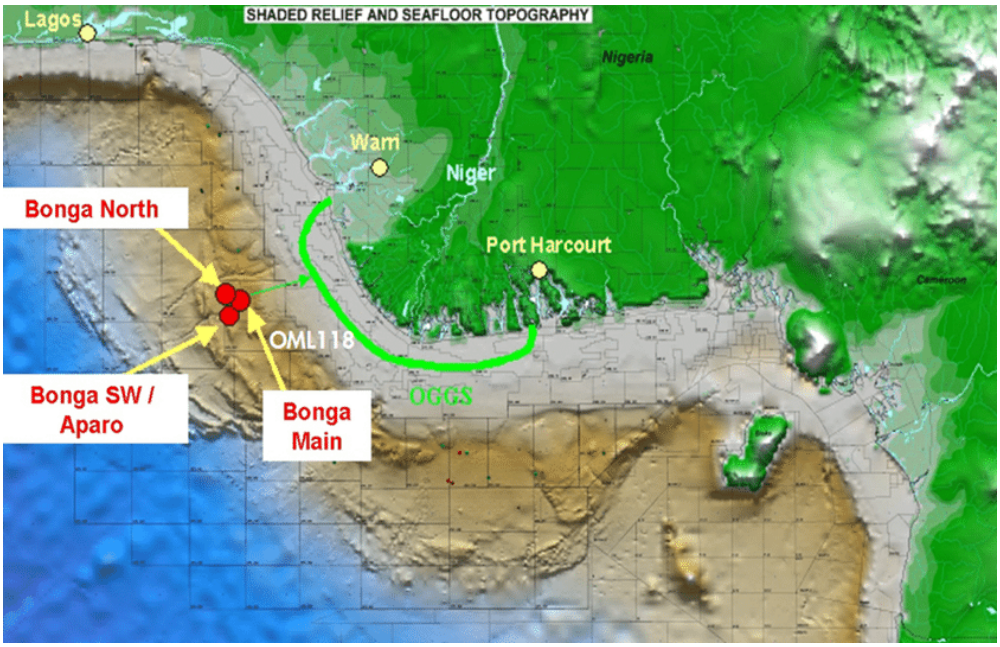

Figure 4-9: Location of Bonga Field, Offshore Nigeria. Source: (Xiao et al., 2016)

Bonga Field is a deep-water hydrocarbon field in Southern Nigeria's Oil Mining License (OML) 118 (Xiao et al., 2016). Previous studies such as WASP (Forristall et al., 2013), the West Swell Spectra Shapes (Olagnon et al., 2013), and (Olugbenga et al., 2017) have relied on the in-situ data recorded using a wave-rider deployed at the Bonga field. This study follows in the same fashion, with specific reference to (Olugbenga et al., 2017), where the actual significant height and peak periods of the spectra used for the ShipX simulation were taken.

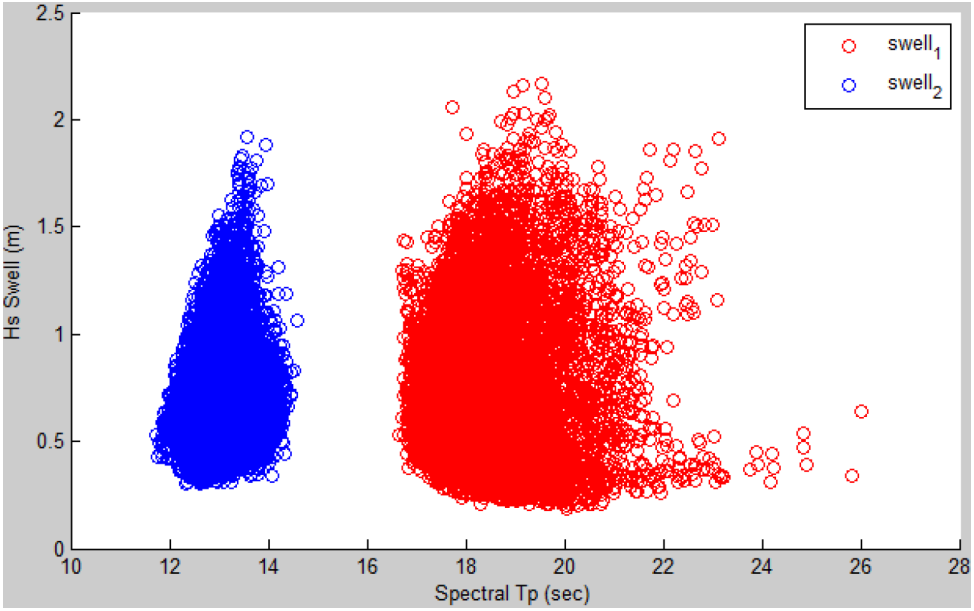

Figure 4-10: Scatter Plot for Bonga Field July 1998 - Sept. 1999. Source: (Olugbenga et al., 2017)

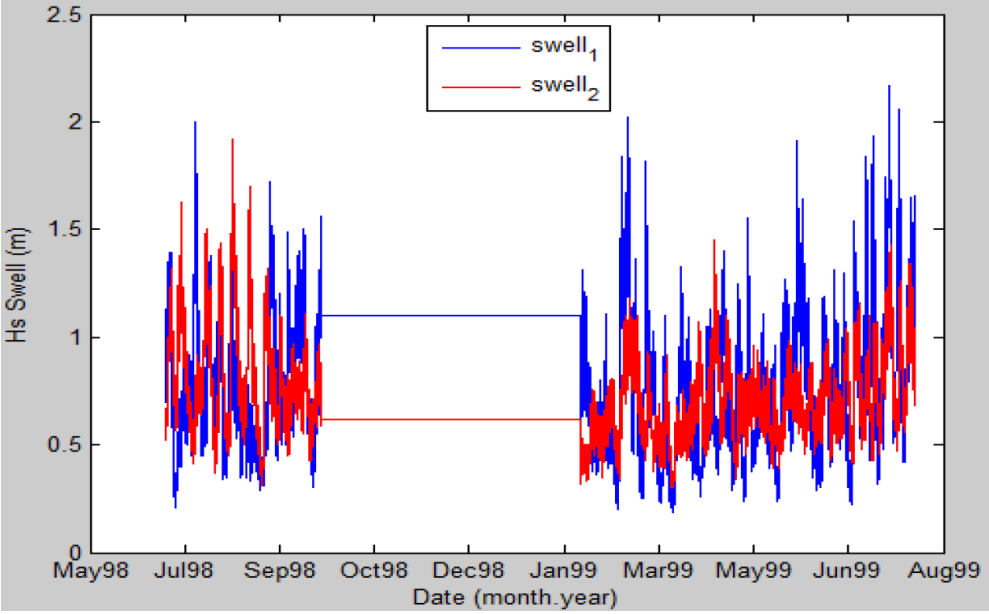

Figure 4-11: Time History of Swells for Bonga Field July 1998 - Sept. 1999. Source: (Olugbenga et al., 2017)

Figure 4-10 shows two types of swell: swell type 2 ($swell_2$) and swell type 1 ($swell_1$), amongst recorded spectra from July 1998 – July/September 1999. $Swell_2$ seems primarily concentrated within 11.8 secs to 14.2 secs with H_s of around 0.25m – 1.9m, while $swell_1$ is densely concentrated around 17.0 secs to 22.0 secs and sparsely about 22.0 to 26 secs. See figure 4-10 for context.

The gap between the two categories of swell is from September 1998 – January 1999, as shown in figure 4-10, where probably no record was captured. This was discussed by (Olugbenga et al., 2017). Significant heights and peak periods have been derived as per Table 4-7.

Table 4-7: 0.5-2.2m H_s & 6s-14.4s T_p for Bonga Field Offshore Nigeria. Adapted from (Olugbenga et al., 2017)

H_s (m)	0.5 – 0.75	0.5-1.5	0.5-1.9	0.5-1.8	0.5-2.0	0.5-2.25	0.5-2.0	0.5-1.8
T_p (s)	12	13	14	17	18	19	20	21
H_s (m)	0.5-1.9	1- 1.8	0.25-0.5	0.4-0.5	0.4-0.6			
T_p (s)	22	23	24	25	26			

4.4.4 Swell – Barge Interaction & Natural Periods: Analysing Implications

From the ranges of the swell periods for the Asabo field, waves with peak periods of about 4 secs were recorded; for Forcados, waves from 4.8 secs, while the Bonga field has much higher peaks than the first two fields. In the context of installation operation, where good seakeeping is required, barges may become susceptible to massive motion amplification due to these high-frequency ends of the spectrum and, even so, within the median frequencies. This is because barges have their natural periods between 5-7 secs in roll (El-Reedy, 2012), while according to (Mehn-Andersen, 2018), most ship-shaped objects have a natural roll period of 12 – 18 secs.

For an installation operation in Southern Nigeria waters, the probability that a semi-submersible barge encounters a sea state with frequencies within its natural frequency becomes almost unity, at least considering the range of wave periods presented in section 4.4.1 to section 4.4.3. The implication is that both resonance and resonance-induced response will give new sets of challenges structurally for the barge, the module/cargo on deck, motion-induced interruption of the operation, or motion-induced sickness.

Barges are generally well-known to have small roll damping (Mehn-Andersen, 2018). However, the design of modern heavy-lift semisubmersible barges has incorporated roll dampers such as bilge keels and roll-reduction tanks; equally, the large beam may contribute to roll reduction, but pertinently, as earlier stated, large beams may increase the roll response period. Viscosity and viscous effects earlier disregarded in the derivation of potential flow may also aid the roll damping in seaways close to the barge's natural roll period, but as (Jung et al., 2006) put it; outside the natural roll period, viscous effects resulting from flow separation amplifies the roll motion of barges.

In heave degree of freedom, however, heavy-lift semisubmersibles have more leeway for heave response compensation through variable displacement. But, in cases where installation operations become draft-restricted, barges are also not immune from motion amplification in the heave degree of freedom.

Heave amplification compensation may be unattainable for smaller barges due to inadequate ballast systems. In general, these scenarios have consequences for the safety of the operation, time/schedule, and cost overruns since planning must consider favourable weather.

Interestingly as heave and roll are coupled, one motion may induce the other. An amplified role also creates a pressure differential relative to the centerline (CL) as flow separations between

the port and starboard side of the barge are produced, thereby rendering the concept of integrating the pressure below the waterline on the starboard side and equating to the portside inadmissible. For the non-linear effects earlier disregarded, a more scientific question of the validity of such assumptions now emerges.

With these, some degrees of evidence that support the notion that although the swells in Southern Nigerian waters do have a relatively low significant height (fairly < 4m) when compared to other ocean spaces of the world, its long periods could present some amount of risk and criticality not just for installation and other marine operation, but also the safety of navigation.

4.5 Idealized Wave Spectrum

The spectrum choice for this analysis is limited by the spectrum allowable and available in ShipX. According to the theory manual, only the standard spectrum like the PM/ Brettschneider, JONSWAP, and Torsethaugen spectra are available. A user-defined spectrum with limitations for post-processing of the response is also available.

Due to this limitation, a modified JONSWAP spectrum is selected. As (Olagnon et al., 2013) noted, a lognormal distribution provided a better fit than others for the sea states in West Africa; however, it does not mean that other models cannot be applied with rational assumptions.

It is, therefore, necessary to re-introduce the spectrum peak parameter (γ) and Philips constant (α), the only modifiable variables of the JOSNWAP. But ShipX does not provide the incentive to modify Philips's constant, only the peak parameter.

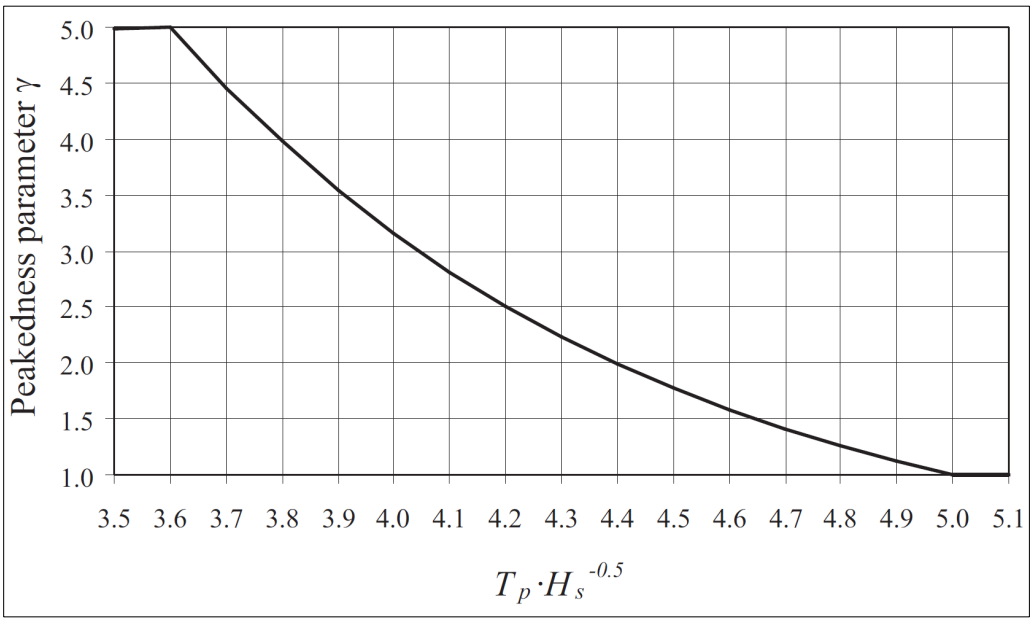

Figure 4-12: Graph of the Relationship Between γ, T_p & H_s. Source: (Fathi & Hoff, 2004)

Therefore, using figure 4-12, or Equation 82, different wave peak parameters can be derived for different Hs and Tp combinations.

$$\gamma = \begin{cases} 5 & for \quad Tp/\sqrt{Hs} \leq 3.6 \\ e^{5.75-1.15T_p/\sqrt{H_s}} & for \quad 3.6 \leq Tp/\sqrt{Hs} \leq 5 \\ 1 & for \quad 5 \leq Tp/\sqrt{Hs} \end{cases} \qquad \text{Equ. 82}$$

4.5.1 Short-Term Statistical Model

For the statistical model, a short-term wave statistical model is deemed fit enough for the analysis. In wave statistics, short-term models are used to express the statistical properties such as root-mean-square (RMS), significant value and behaviour of a vessel in a seaway while allowing for comparison with operational demands (Fathi & Hoff, 2004). From a theoretical validity assessment, a short-term statistical analysis of deep-water waves must assume that the sea surface elevation is stationary at any time, the wave height is twice the wave amplitude, and the resulting Gaussian process with a Rayleigh distribution (Casas-Prat & Holthuijsen, 2010; Longuet-Higgins, 1952).

These descriptions provided by (Casas-Prat & Holthuijsen, 2010; Longuet-Higgins, 1952) for the qualifiers of short-term statistics aligns with the previous assumptions made during the modelling process of ocean surface waves in the last chapter. Justifiably so, the interest of this research is to understand and establish vessel response in long-period swells (say 6-26secs). A short-term statistical approach is thus considered sufficient.

4.6 Simulation Run

The vessel properties defined in this chapter are replicated in ShipX to run the simulation. Regular waves with a wide range of periods are defined to create a high for the RAOs as recommended by (ABS, 2016; Fathi & Hoff, 2004). A successful data check and calculation then provide the basis for using the Veres Response Postprocessor to analyse the body's motion in an irregular sea state.

5 Chapter Five – Results

The findings presented in this chapter are derived from the numerical simulation conducted in the frequency domain using ShipX software, as discussed in section 4.3. Reflecting on the research question in section 1.2 is essential to ensure coherence and logical order.

The thesis embarked on addressing three primary research questions. Firstly, it aimed to understand how the sea state in Southern Nigeria can be effectively modelled, as highlighted in Research Question 1. Secondly, it explored the dynamic nature of loads experienced by installation vessels in long-period swells which prevail in Southern Nigeria. Lastly, it investigated the impact of the sea state and its associated loads on the designs, planning and execution of installation operations in this region.

Chapter two, an extensive literature survey, was conducted to establish a solid knowledge base on swells in general and specifically in Southern Nigeria waters. In Chapter three, a theoretical framework for modelling ocean waves was presented. Chapter four delved into the modelling of a typical installation vessel, the utilisation of computer software ShipX, the characterisation of the spectra in 2D, the adoption of a statistical model for simulating irregular swells, and the execution of the simulation to obtain the vessel response.

The results and subsequent discussions, coupled with the now-established understanding of the sea states in Southern Nigeria, aim to address the research questions and offer valuable insight for other related enquiries.

5.1 RAOs in Regular Wave

The response amplitude operators associated with barge motion in regular waves relate the response amplitude with the amplitude of the incoming wave potential. This has been discussed in section 3.4.3, and consideration of different wave headings will be assessed and presented.

5.1.1 RAOs – Heave Displacements

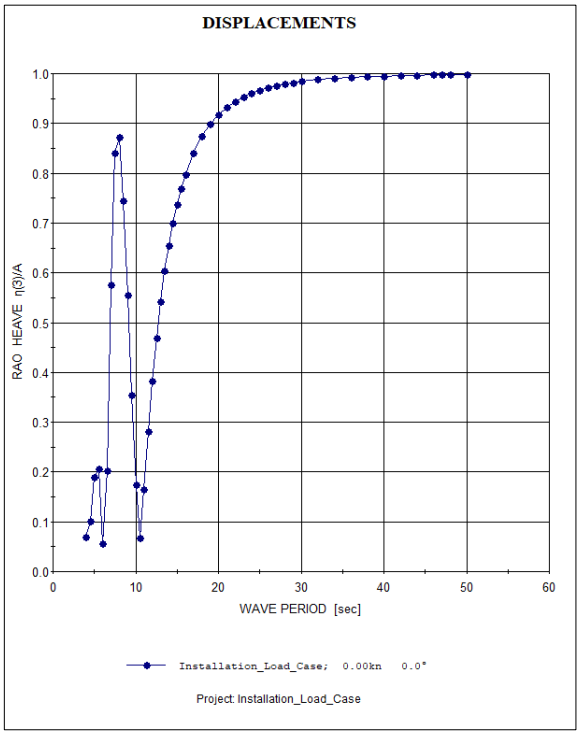

Figure 5-1: RAO in Heave - 0^0 Wave Direction

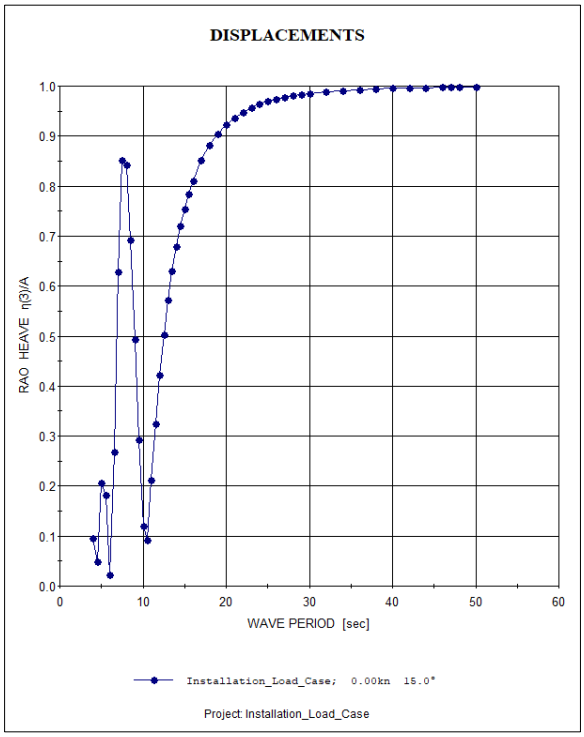

Figure 5-2: RAO in Heave - 15^0 Wave Direction

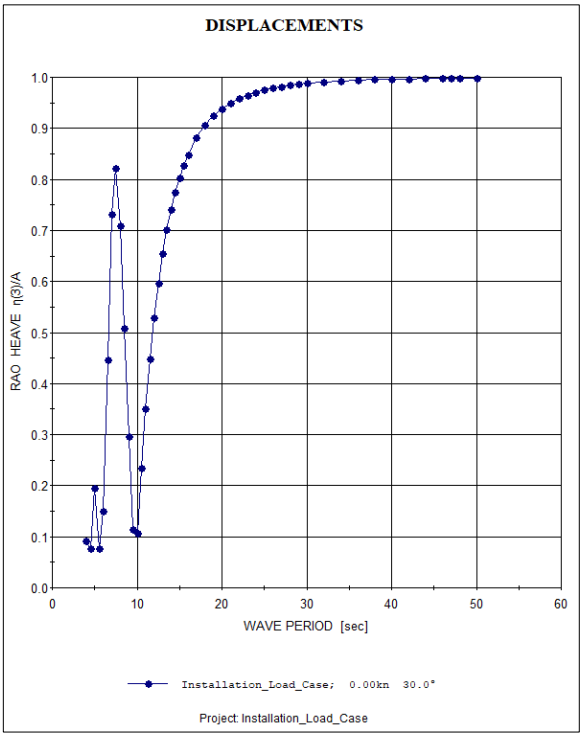

Figure 5-3: RAO in Heave - 30^0 Wave Direction

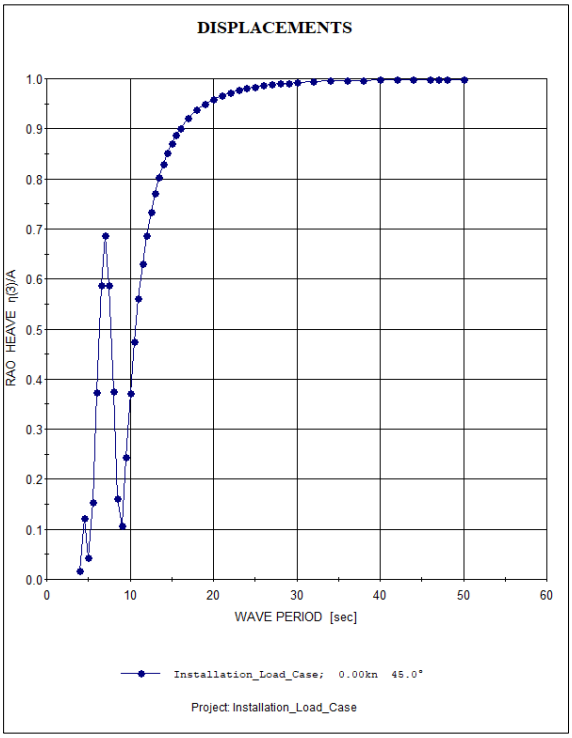

Figure 5-4: RAO in Heave - 45^0 Wave Direction

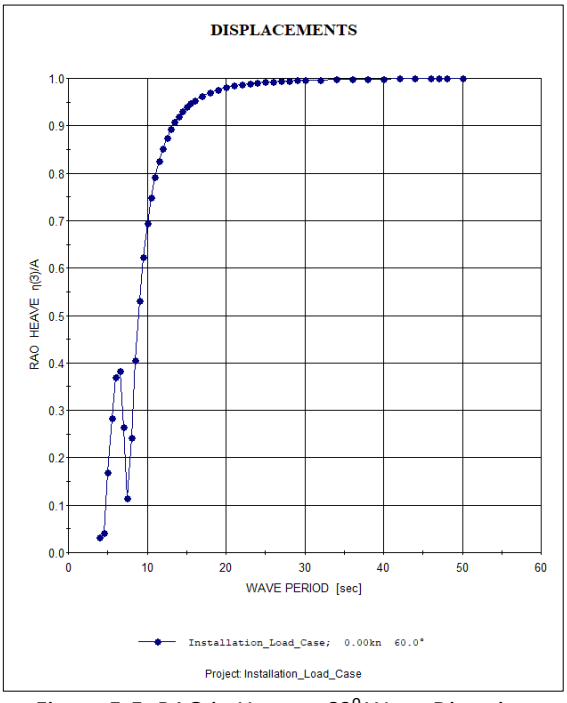

Figure 5-5: RAO in Heave - 60^0 Wave Direction

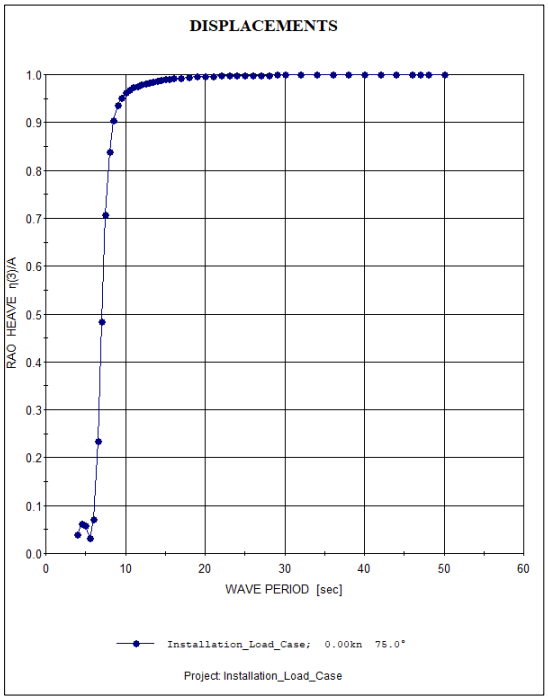

Figure 5-6: RAO in Heave - 75^0 Wave Direction

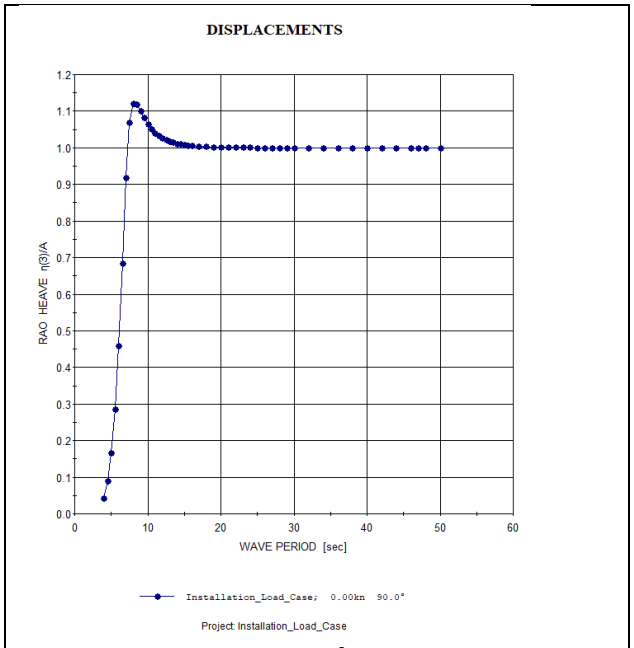

Figure 5-7: RAO in Heave - 90^0 Wave Direction

5.1.2 RAOs – Roll Displacement

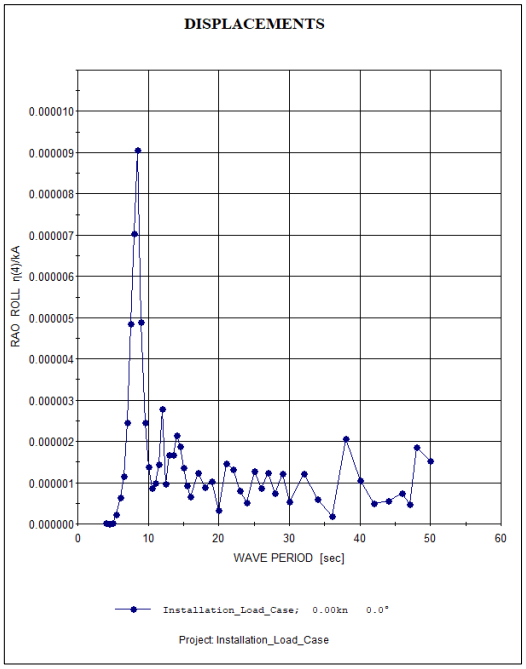

Figure 5-8: RAO in Roll - 0^0 Wave Direction

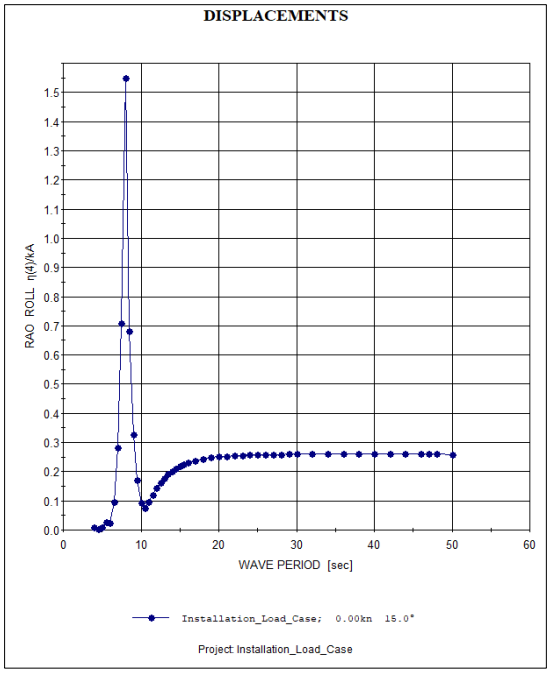

Figure 5-9: RAO in Roll - 15^0 Wave Direction

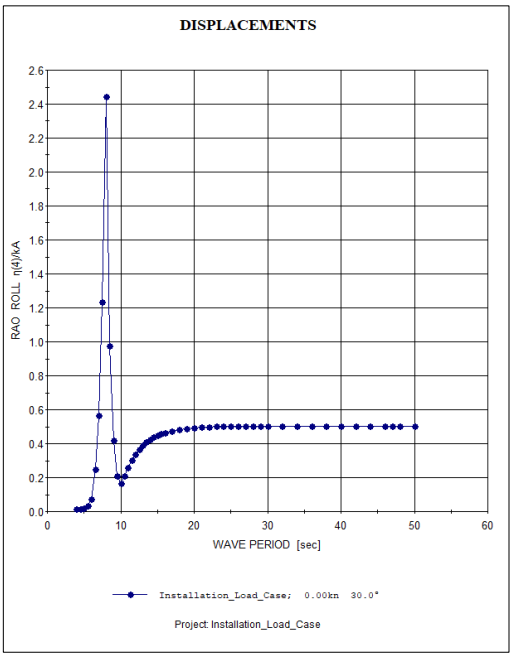

Figure 5-10: RAO in Roll - 30^0 Wave Direction

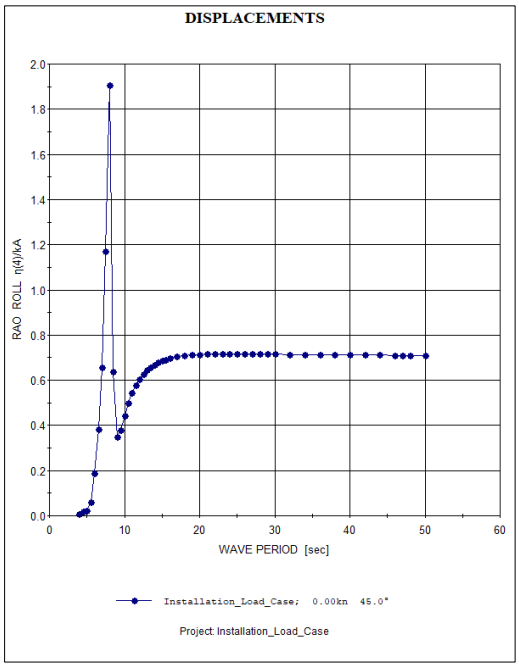

Figure 5-11: RAO in Roll - 45^0 Wave Direction

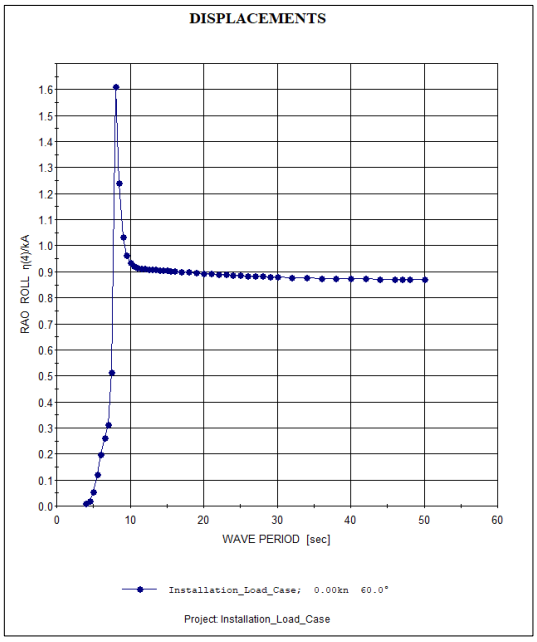

Figure 5-12: RAO in Roll - 60^0 Wave Direction

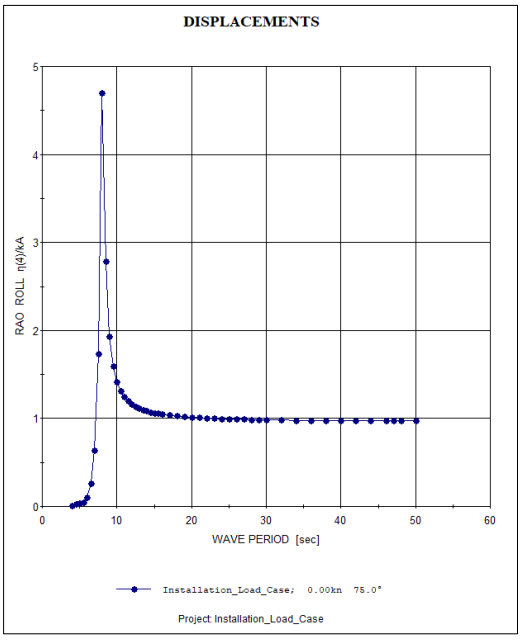

Figure 5-13: RAO in Roll - 75^0 Wave Direction

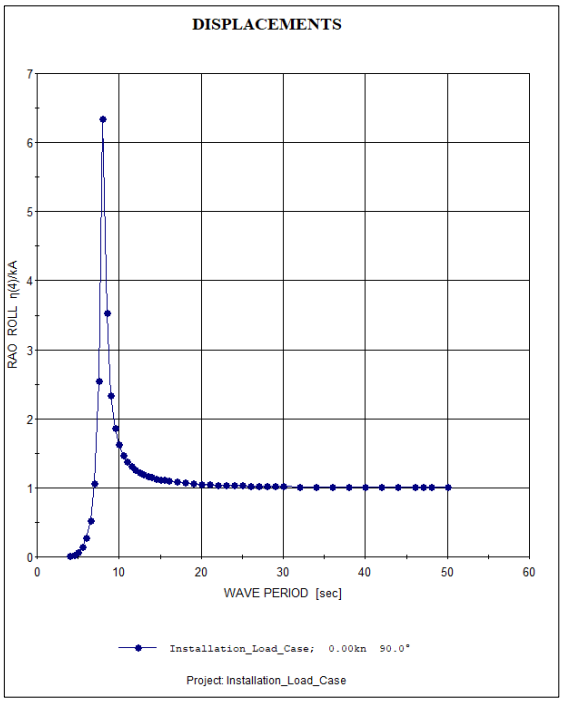

Figure 5-14: RAO in Roll - 90^0 Wave Direction

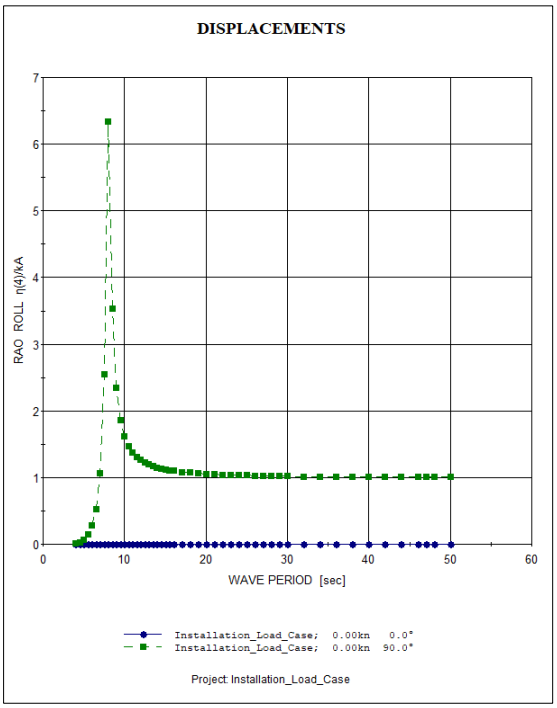

Figure 5-15: RAO in Roll - 0^0 & 90^0 Wave Direction

5.1.3 RAOs – Heave Velocity

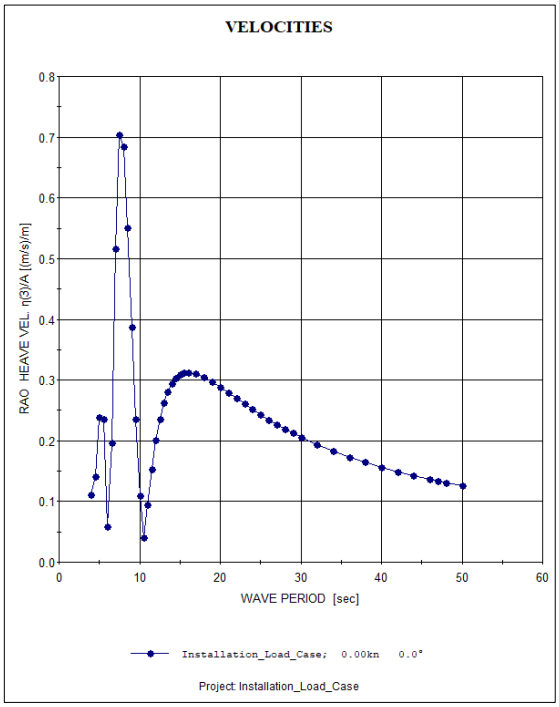

Figure 5-16: RAO Heave Vel. - 0^0 Wave Direction

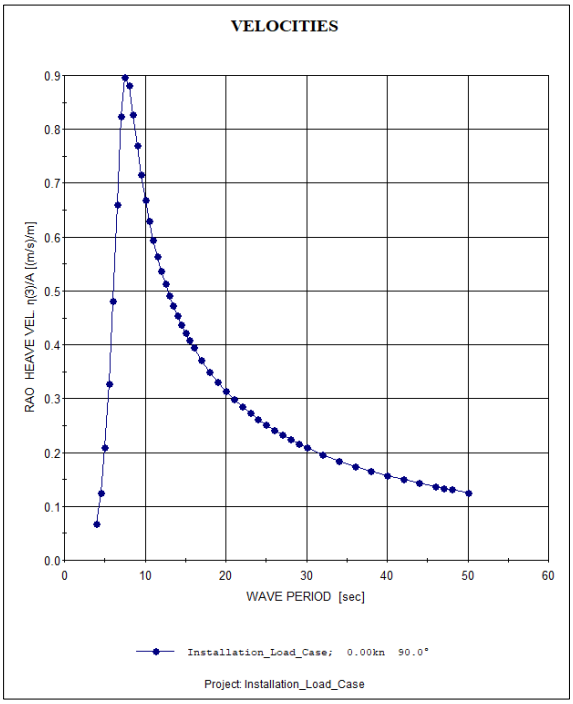

Figure 5-17: RAO Heave Vel. - 90^0 Wave Direction

5.1.4 RAOs – Roll Velocity

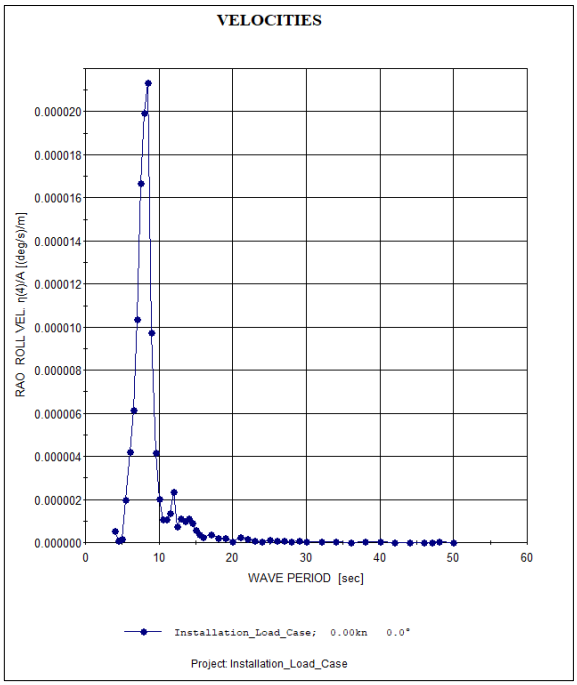

Figure 5-18: RAO Roll Vel. - 0^0 Wave Direction

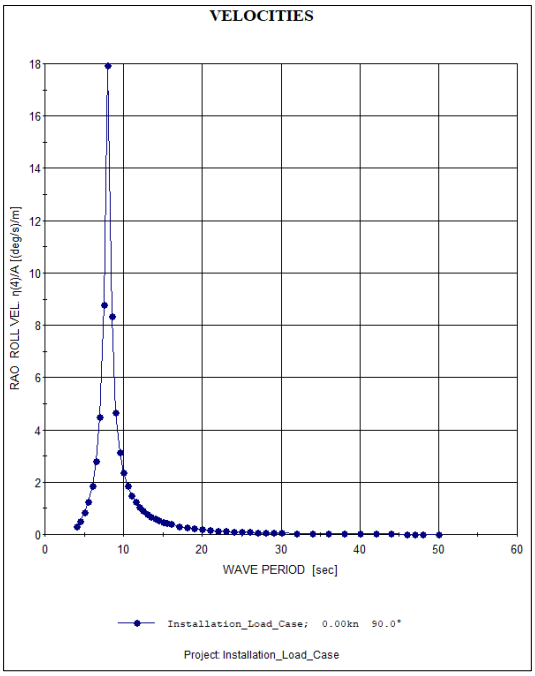

Figure 5-19: RAO Roll Vel. - 90^0 Wave Direction

5.1.5 RAOs – Heave Acceleration

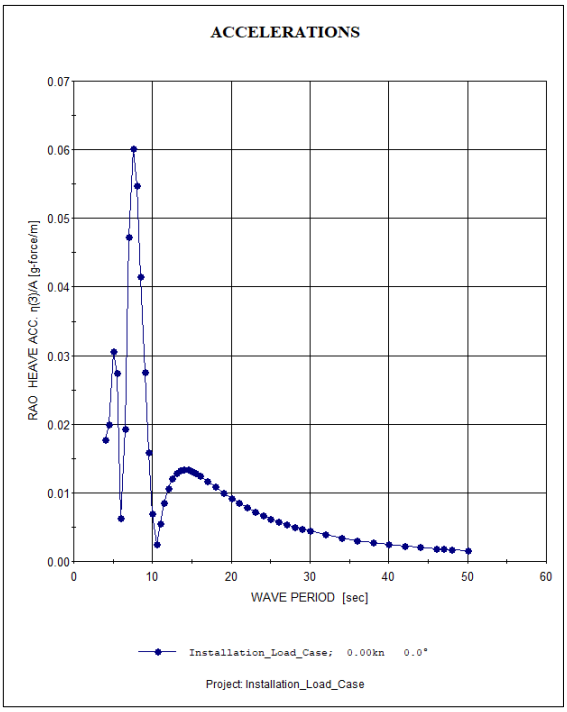

Figure 5-20: RAO Heave Acc. - 0^0 Wave Direction

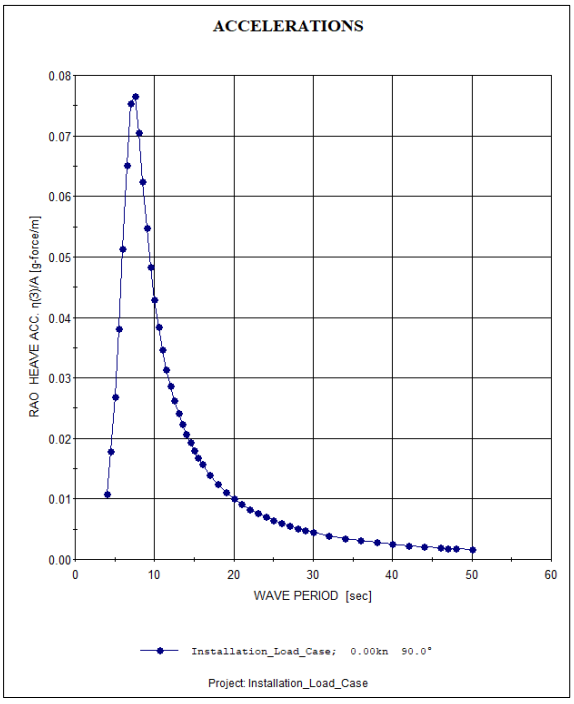

Figure 5-21: RAO Heave Acc. - 90^0 Wave Direction

5.1.6 RAOs – Roll Acceleration

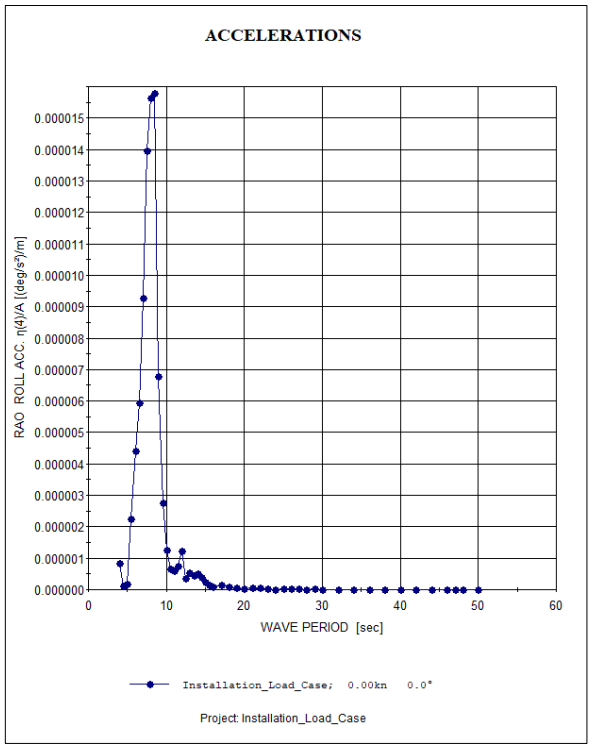

Figure 5-22: RAO Roll Acc. - 0^0 Wave Direction

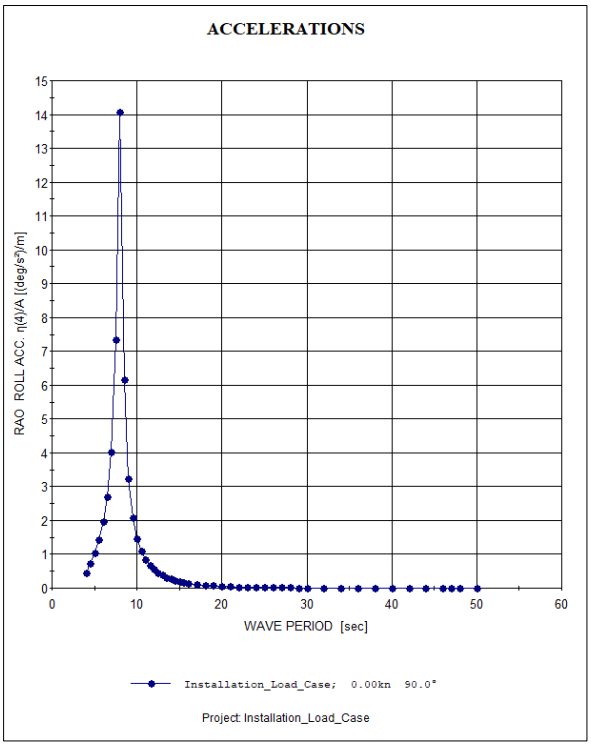

Figure 5-23: RAO Roll Acc. - 90^0 Wave Direction

5.2 Response Spectrum – Asabo Field

To analyse the hydrodynamic response in irregular waves for Asabo Field, the relevant wave peak periods and significant wave heights are obtained from table 4-5. Initially, a generalised modified JONSWAP spectrum was considered the spectrum of choice, as mentioned in section 4.5. However, this is only attainable for a few H_s and T_p combinations. This is due to further examination of the practicality of the parameterisation of the sea states in greater offshore West Africa. As formulated by (Olagnon et al., 2013, pp. 8–9), the spectra offshore West Africa are dependent on the wave peak period (Tp), the significant wave height (Hs), and the location parameter (p).

Regrettably, the ShipX hydrodynamic workbench has limitations in the combinatorics of spectra parameters. While it allows for the combination of T_p, H_s, and $\gamma(\text{gamma})$ for a JONSWAP spectrum, it does not include a location parameter in the spectrum definition. Appendix 2 shows that the wave conditions at Asabo predominantly follow the Pierson-Moskowitz (PM) distribution with a gamma value of 1 as $Tp/\sqrt{H_s}$ ratio exceeds 5 in most cases. This aligns with the nature of long-crested, fully developed sea states, where a gamma value of 1 is expected and used to designate a fully developed sea state. Consequently, the results for Asabo Field are computed using a PM spectrum with a unit peak parameter.

Furthermore, due to the extensive frequency range, the assessment will be selective to ensure a concise and focused analysis. This approach is adopted to maintain robustness and prevent overwhelming the results with excessive data.

5.2.1 Heave Response Spectrum – Asabo Field

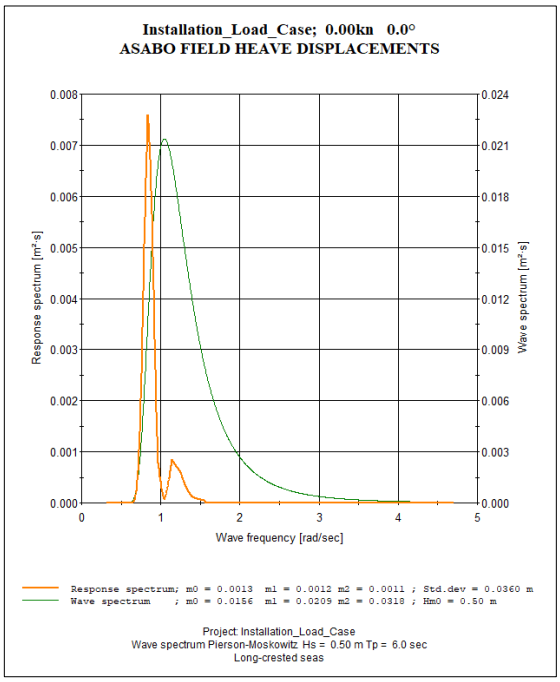

Figure 5-24: Heave Response Spectrum. - 0^0 Wave Direction HS: 0.5m / Tp: 6 sec

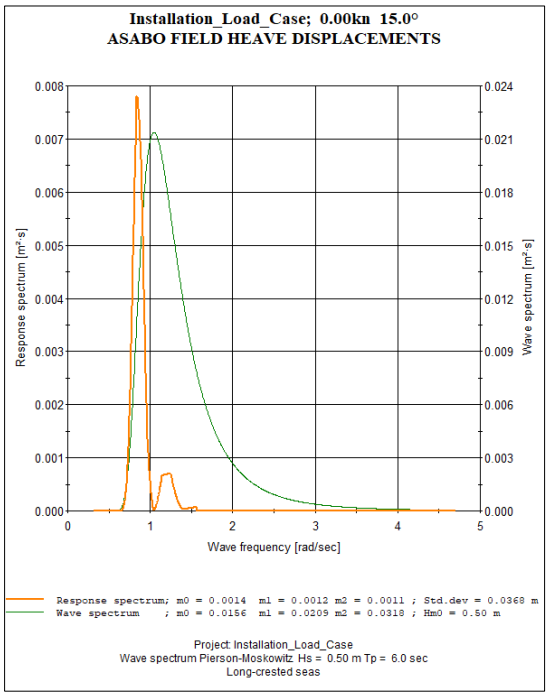

Figure 5-25: Heave Response Spectrum. - 15^0 Wave Direction HS: 0.5m / Tp: 6 sec

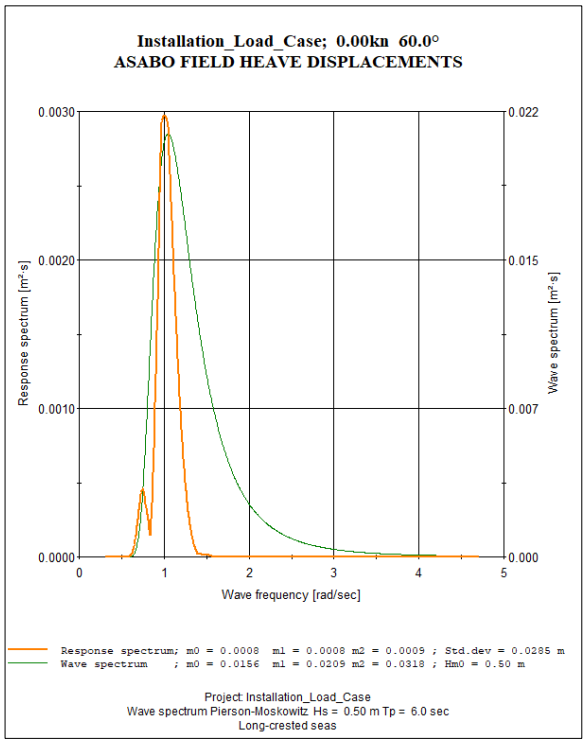

Figure 5-26: Heave Response Spectrum. - 0^0 Wave Direction HS: 0.5m / Tp: 6 sec

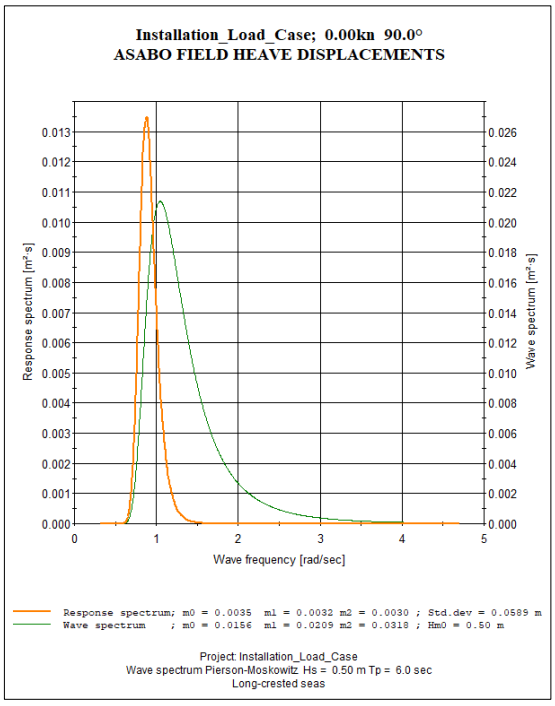

Figure 5-27: Heave Response Spectrum. - 90^0 Wave Direction HS: 0.5m / Tp: 6 sec

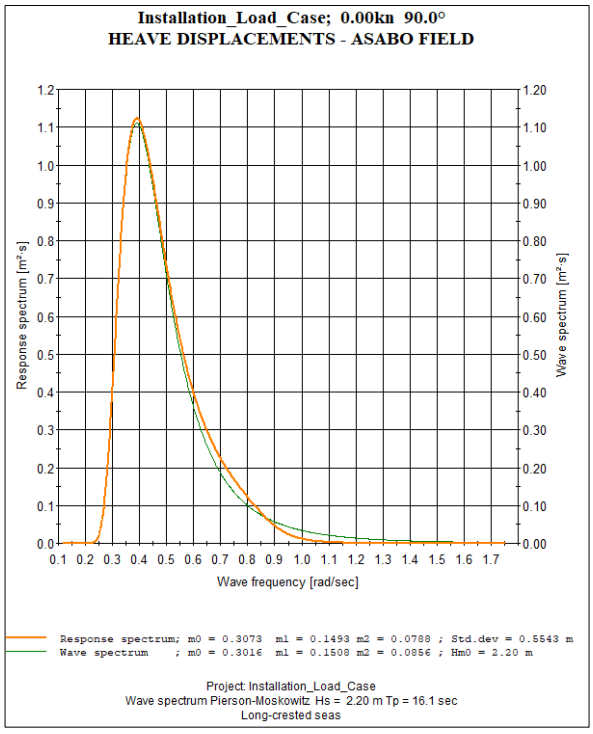

Figure 5-28: Heave Response Spectrum. -9 0^0 Wave Direction HS: 2.2 / Tp: 16.2 sec

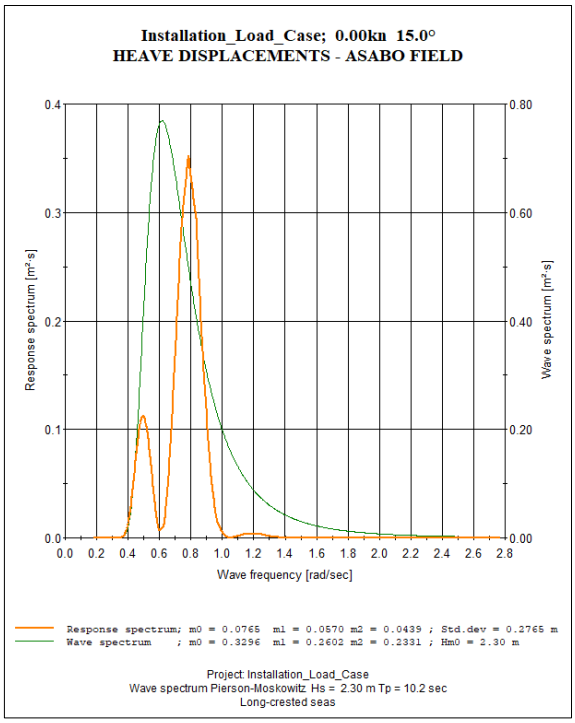

Figure 5-29: Heave Response Spectrum. - 15^0 Wave Direction HS: 2.3m / Tp: 10.2 sec

5.2.2 Roll Response Spectrum – Asabo Field

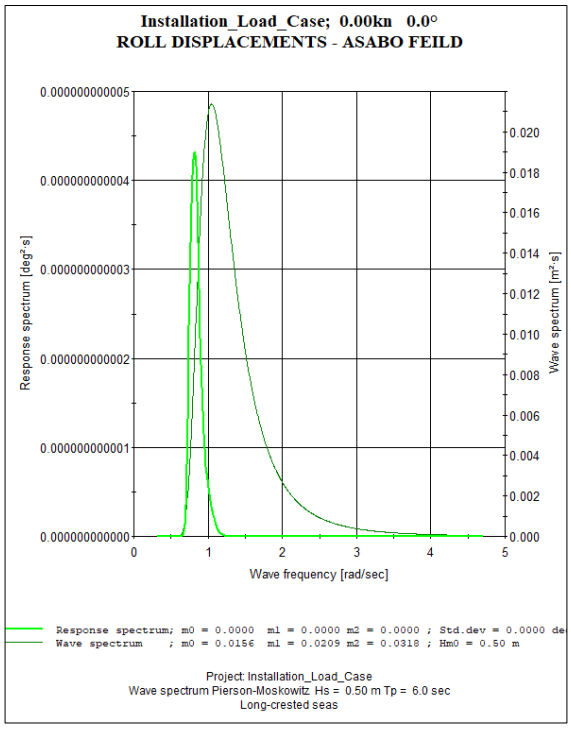

Figure 5-30: Roll Response Spectrum. - 0^0 Wave Direction H_S: 0.5m / T_p: 6 sec

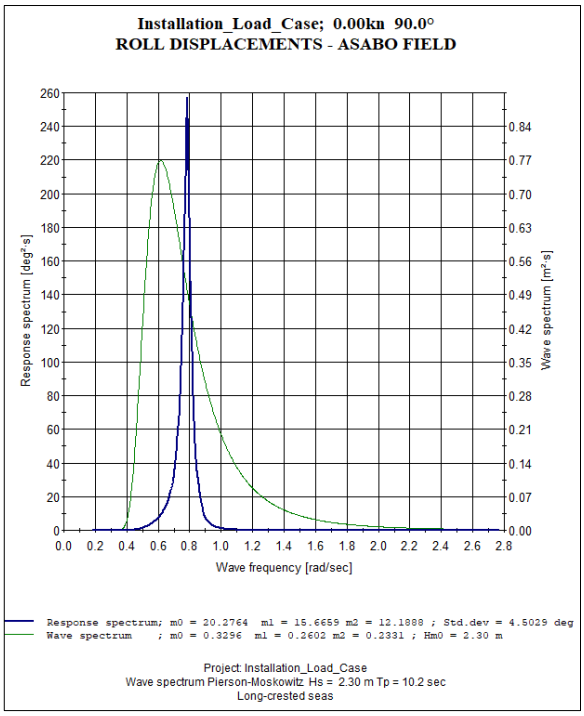

Figure 5-31: Roll Response Spectrum. - 90^0 Wave Direction H_S: 2.3 m / T_p: 10.2 sec

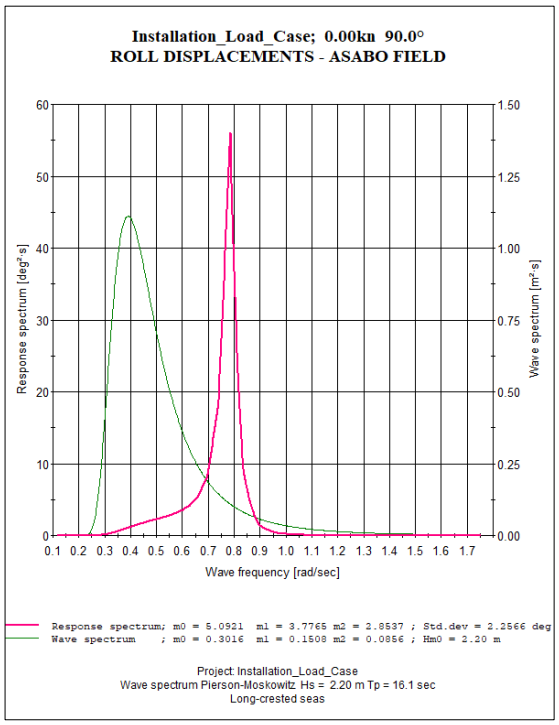

Figure 5-32: Roll Response Spectrum. - 90^0 Wave Direction HS: 2.2m / Tp: 16.1 sec

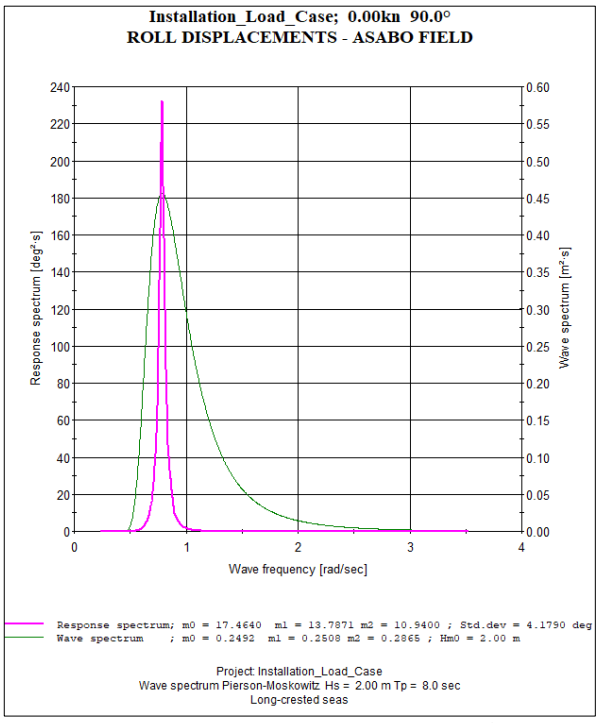

Figure 5-33: Roll Response Spectrum. - 90^0 Wave Direction HS: 2.0m / Tp: 8 sec

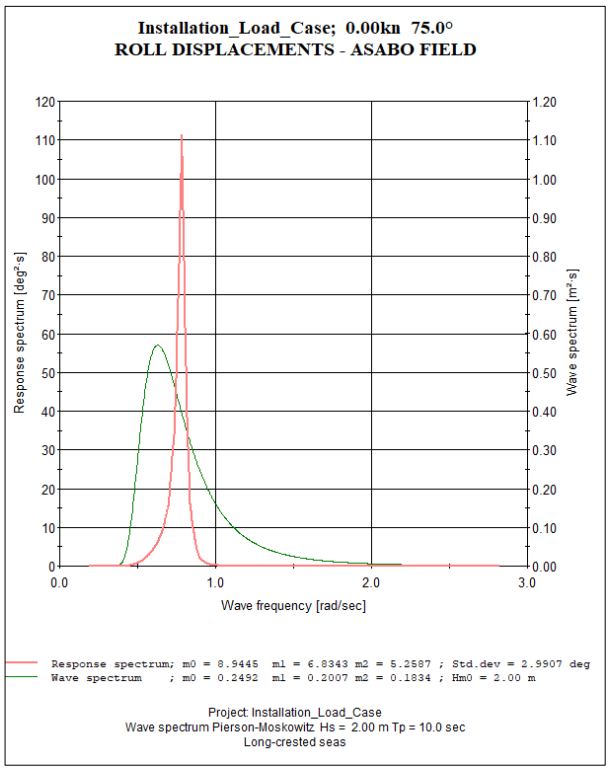

Figure 5-34: Roll Response Spectrum. - 75^0 Wave Direction HS: 2.0m / Tp: 10.0 sec

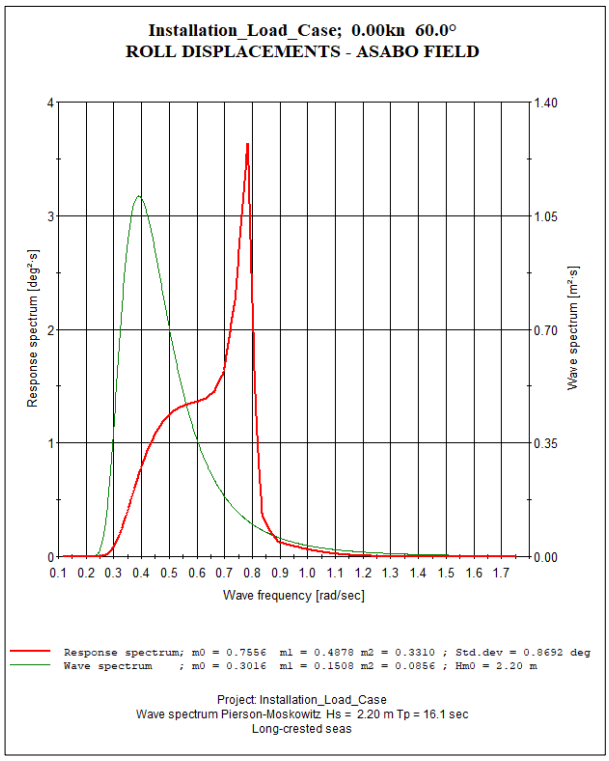

Figure 5-35: Roll Response Spectrum. - 75^0 Wave Direction HS: 2.2m / Tp: 16.1 sec

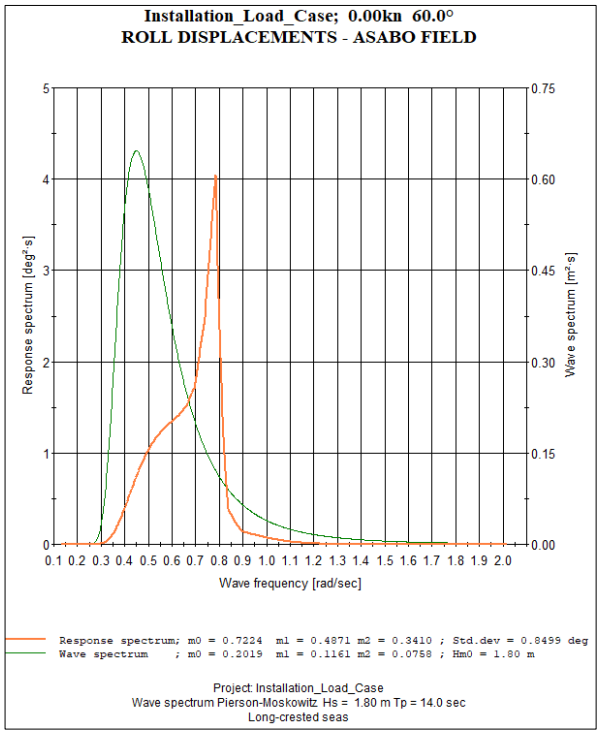

Figure 5-36: Roll Response Spectrum. - 75^0 Wave Direction HS: 2.0m / Tp: 10.0 sec

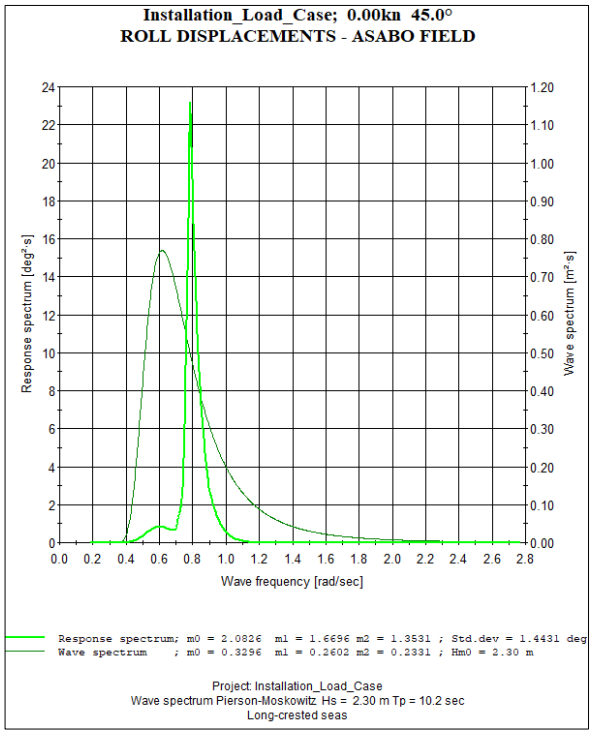

Figure 5-37: Roll Response Spectrum. - 45^0 Wave Direction HS: 2.3m / Tp: 10.2 sec

5.3 Response Spectrum – Forcados Field

The spectra analysis for the Forcados Field was performed using the significant wave height and spectra peak period presented in table 4-6. The modelling of the wave spectra considered the gamma value of the individual combinations of significant wave height and peak periods. As Appendix 2 shows, waves with a gamma value of 1 dominate. As earlier discussed, this is symbolic of a fully developed sea state, therefor a JONSWAP with a gamma value of 1 was used to model the sea state. Invariably, this is also equivalent to using a Pierson-Moskowitz spectrum.

Below are the results for both heave and roll displacements for different spectra properties (Hs & Tp) for different wave headings.

5.3.1 Heave Response Spectrum – Forcados Field

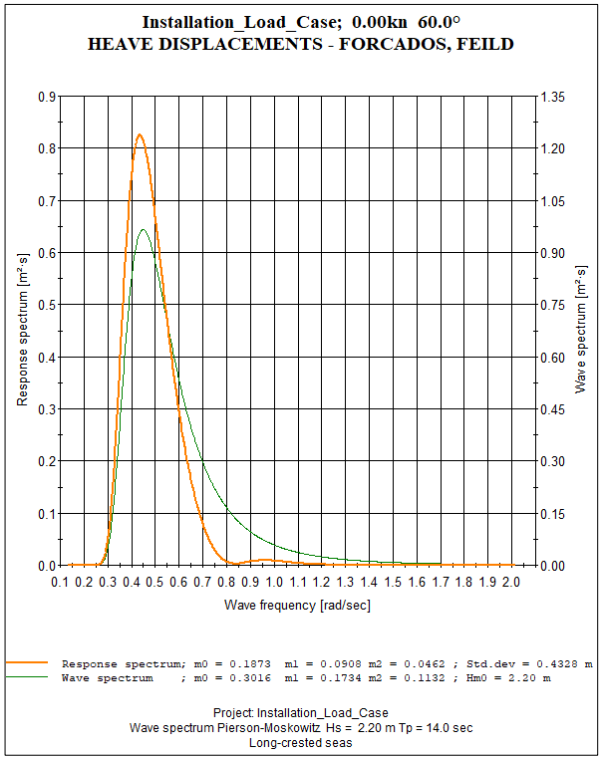

Figure 5-38: Heave Response Spectrum 60^0 Wave Direction HS: 2.2m / Tp: 14 sec

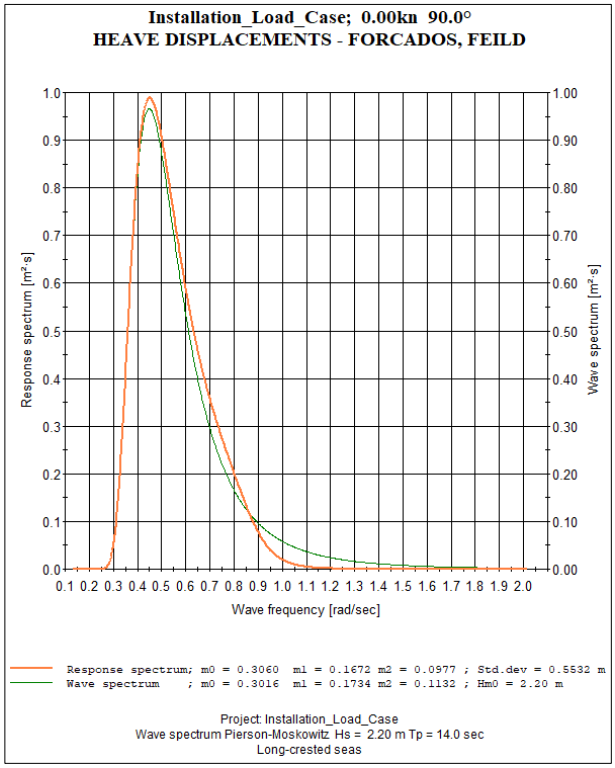

Figure 5-39: Heave Response Spectrum 90^0 Wave Direction HS: 2.2m / Tp: 14 sec

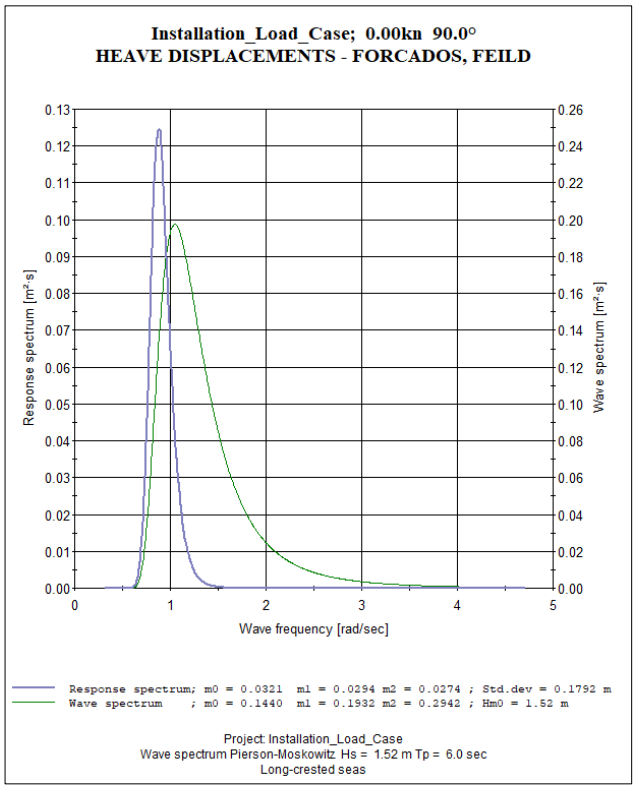

Figure 5-40: Heave Response Spectrum 90^0 Wave Direction HS: 1.52m / Tp: 6 sec

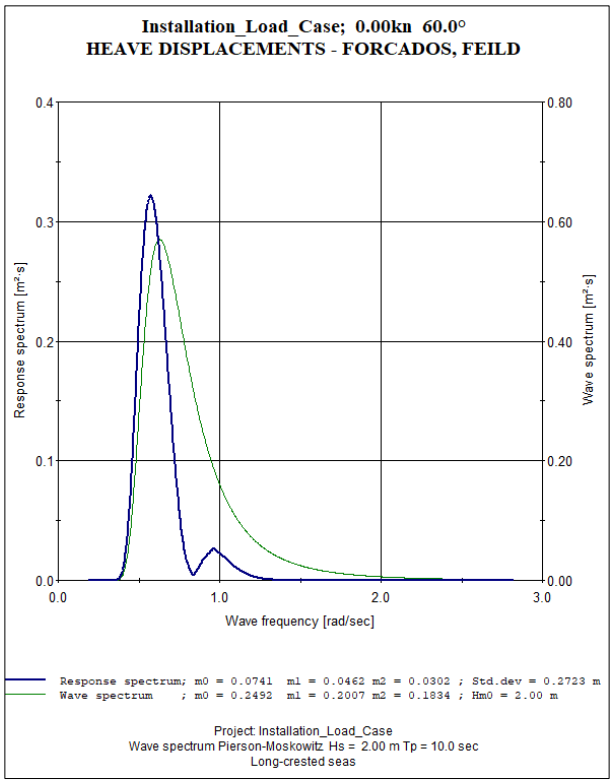

Figure 5-41: Heave Response Spectrum 60^0 Wave Direction HS: 2.0m / Tp: 10 sec

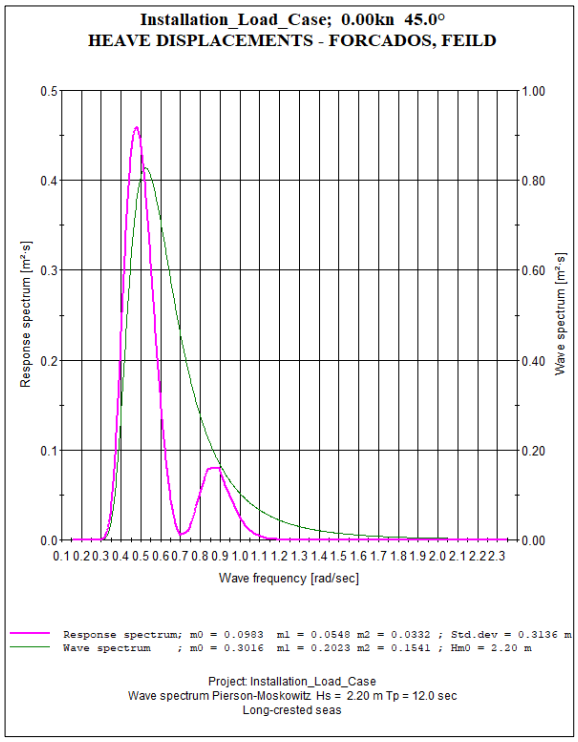

Figure 5-42: Heave Response Spectrum 45^0 Wave Direction HS: 2.20m / Tp:12.0 sec

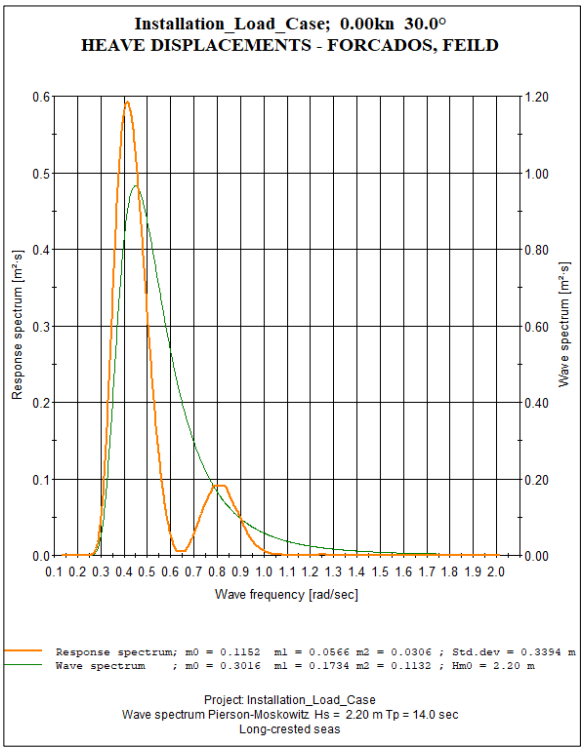

Figure 5-43: Heave Response Spectrum 30^0 Wave Direction HS: 2.20m / Tp:14.0 sec

5.3.2 Roll Response Spectrum – Forcados Field

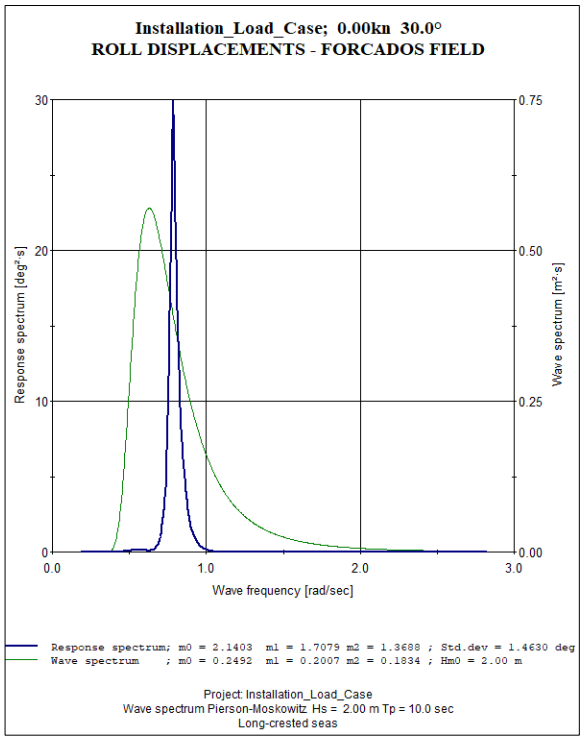

Figure 5-44: Roll Response Spectrum - 30^0 Wave Direction HS: 2.0m / Tp: 10.0 sec.

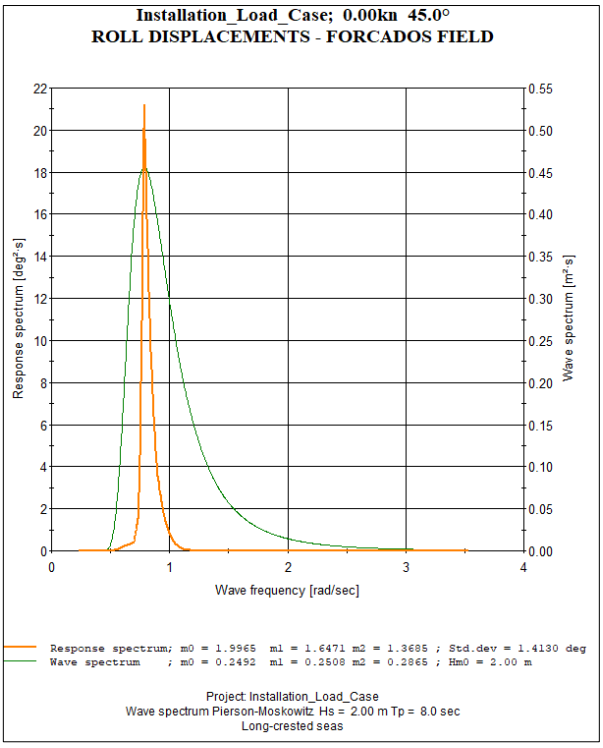

Figure 5-45: Roll Response Spectrum - 45^0 Wave Direction HS: 2.0m / Tp: 8.0 sec

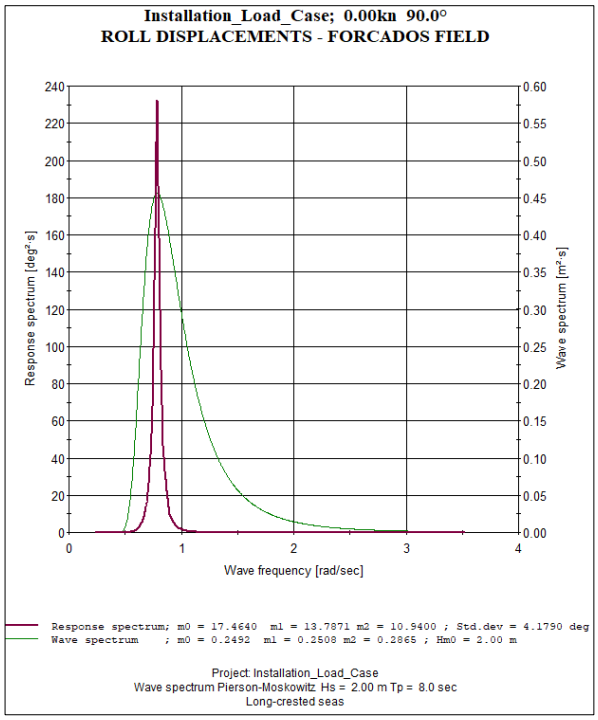

Figure 5-46: Roll Response Spectrum - 90^0 Wave Direction HS: 2.0m / Tp: 8.0 sec.

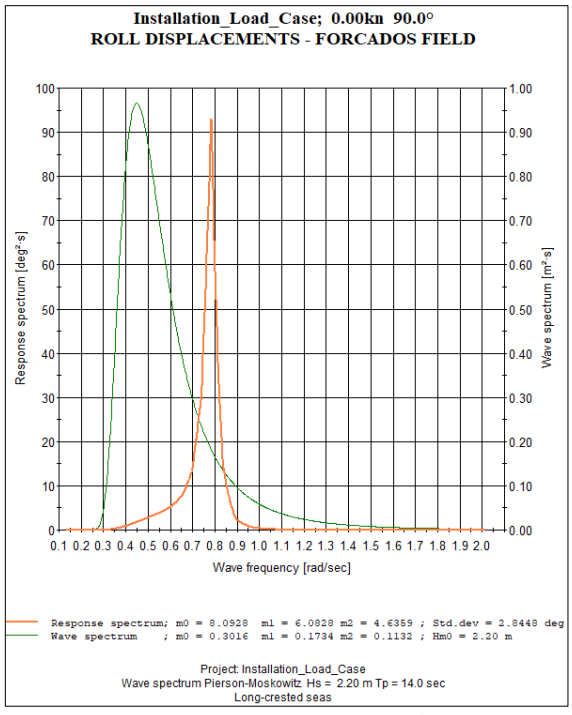

Figure 5-47: Roll Response Spectrum - 90^0 Wave Direction HS: 2.2m / Tp: 14.0 sec.

5.4 Response Spectrum – Bonga Field

The Bonga field spectra analysis has been conducted in the same manner as the Asabo and Forcados filed, still with spectra properties per the table. Like the earlier two fields analysed, the waves at the Bonga field also have a peak parameter of 1, leading to a PM spectra model. The results for heave and roll displacements are present in the following sections.

5.4.1 Heave Response Spectrum – Bonga Field

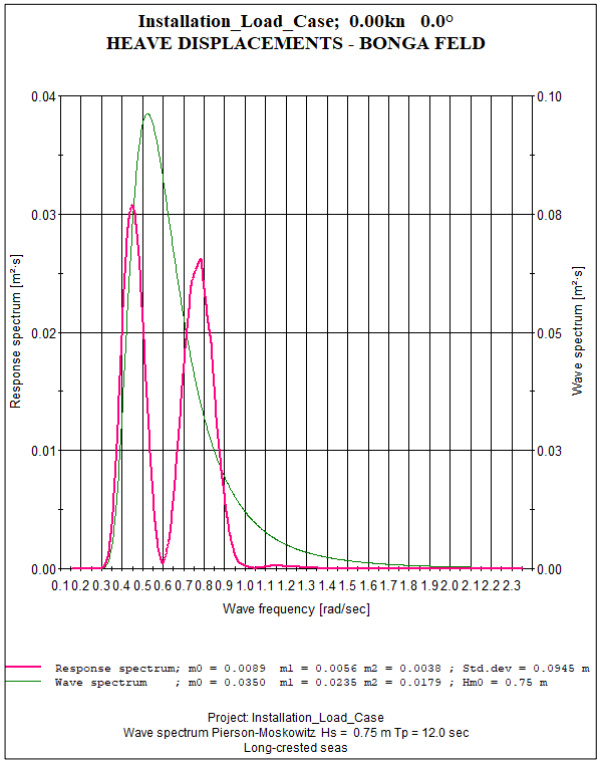

Figure 5-48: Heave Response Spectrum 0^0 Wave Direction HS: 0.75m / Tp: 12 sec

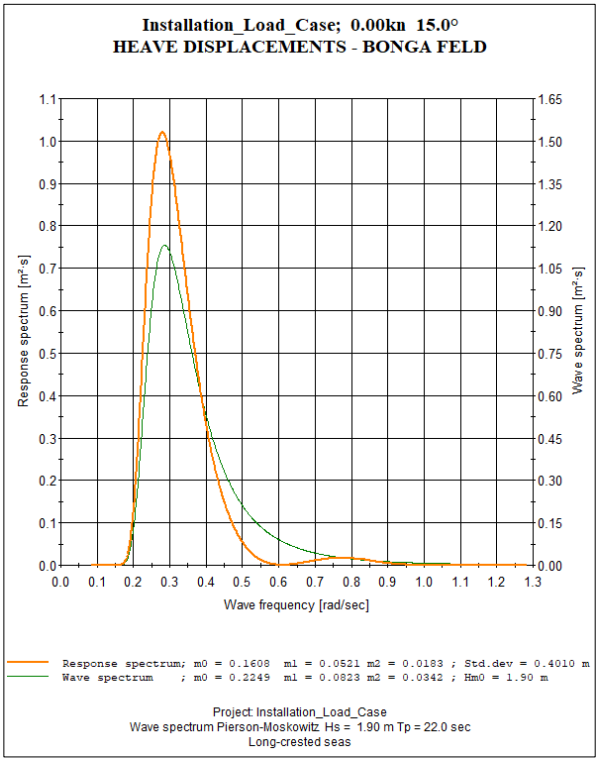

Figure 5-49: Heave Response Spectrum 15^0 Wave Direction HS: 1.9m / Tp: 22 sec

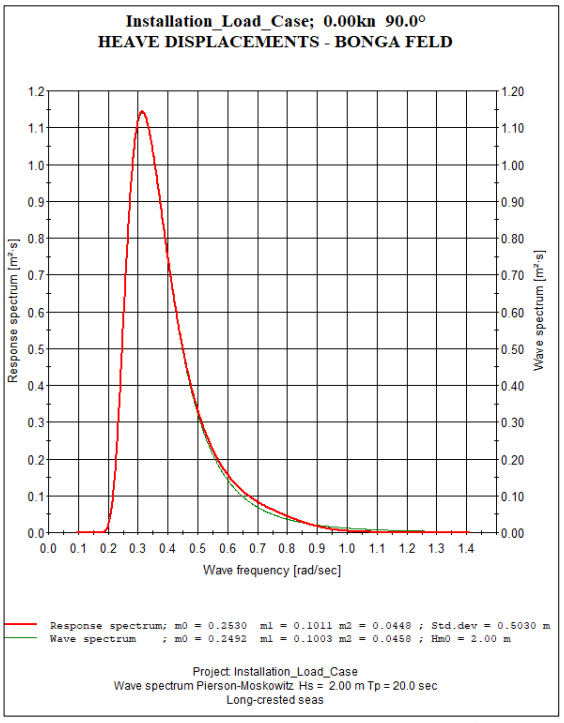

Figure 5-50: Heave Response Spectrum 90^0 Wave Direction HS: 2.0m / Tp: 20 sec

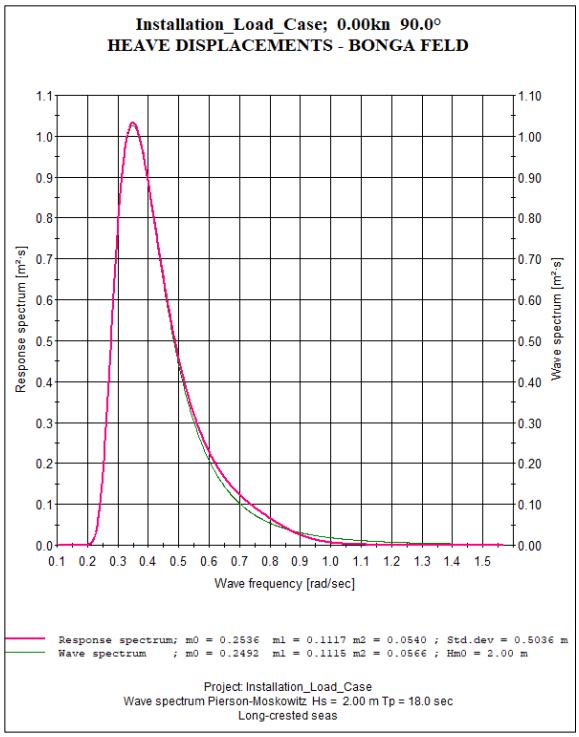

Figure 5-51: Heave Response Spectrum 90^0 Wave Direction HS: 2.0m / Tp: 18 sec

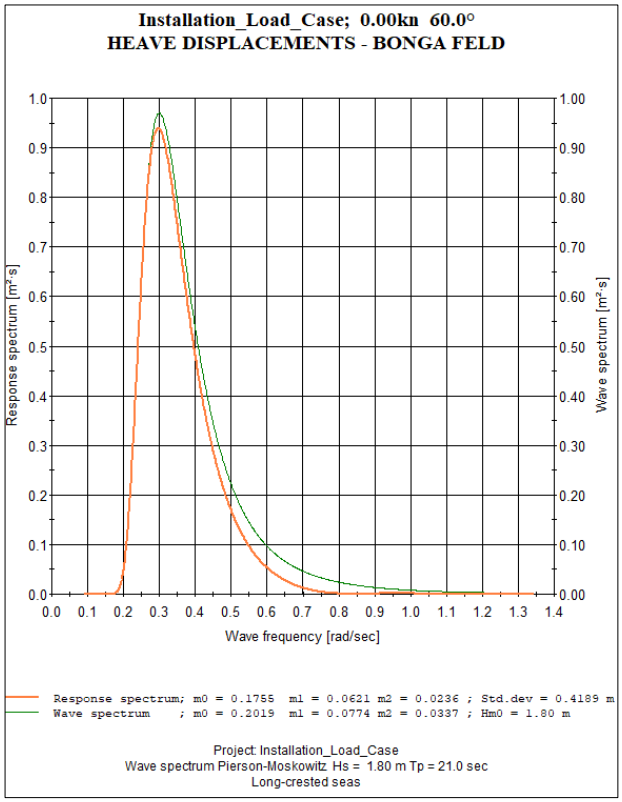

Figure 5-52: Heave Response Spectrum 60^0 Wave Direction HS: 1.8m / Tp: 21 sec

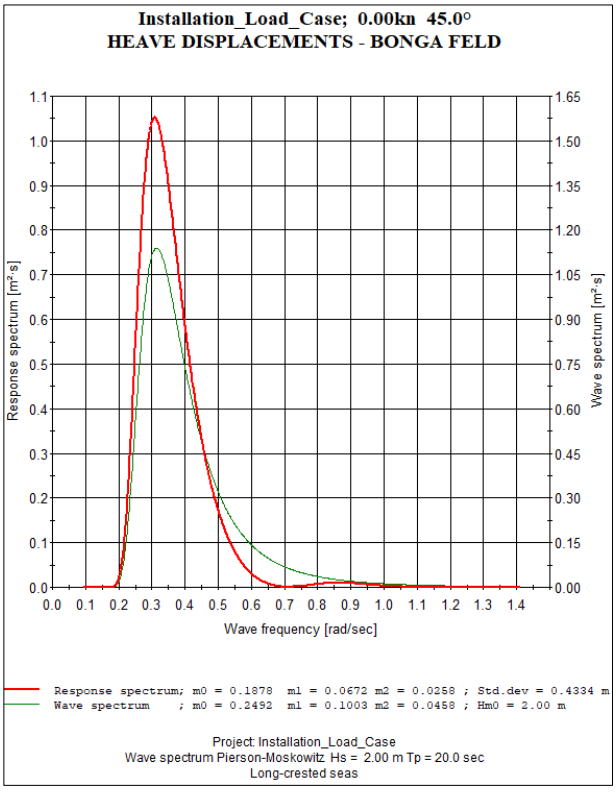

Figure 5-53: Heave Response Spectrum 45^0 Wave Direction HS: 2.0m / Tp: 20 sec

5.4.2 Roll Response Spectrum – Bonga Field

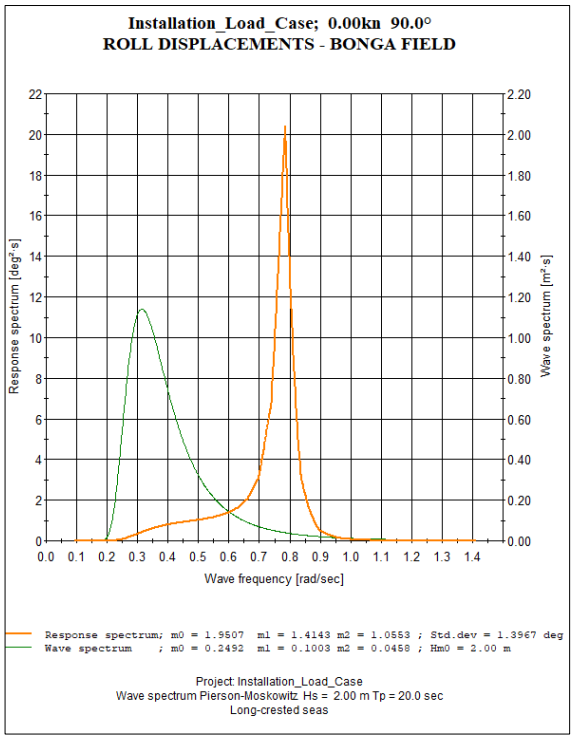

Figure 5-54: Roll Response Spectrum - 90^0 Wave Direction HS: 2.0m / Tp: 20.0 sec.

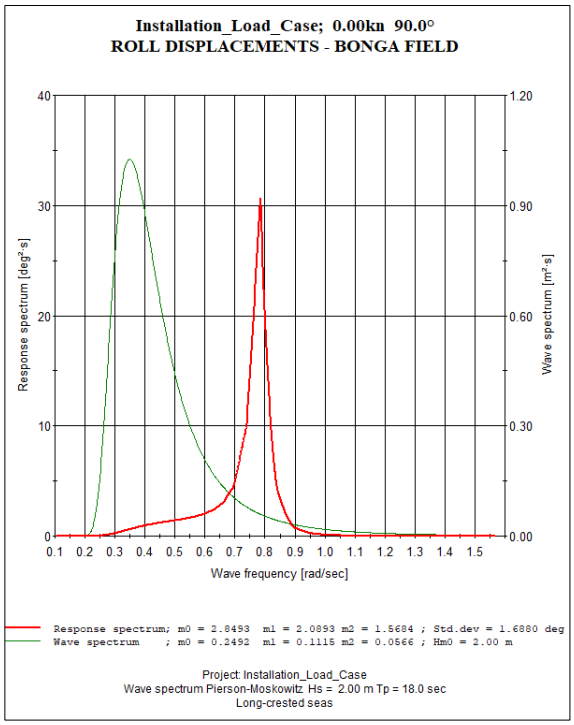

Figure 5-55: Roll Response Spectrum - 90^0 Wave Direction HS: 2.0m / Tp: 18.0 sec.

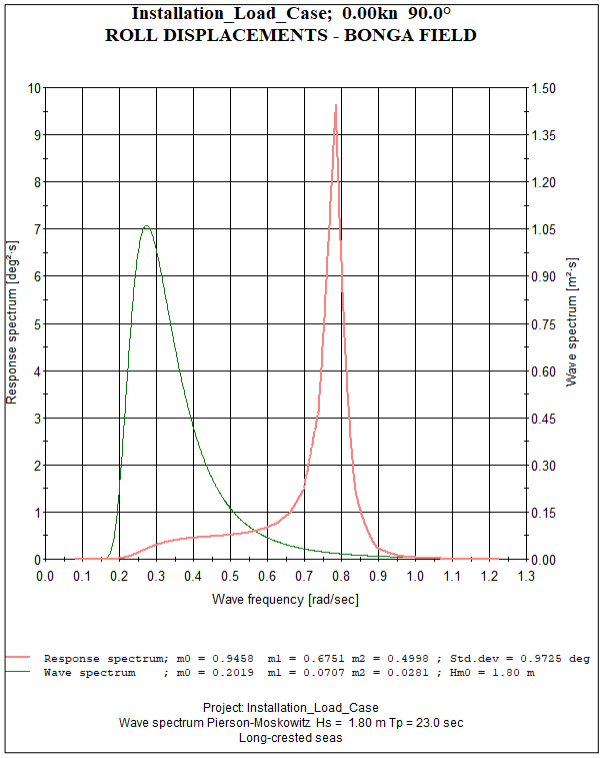

Figure 5-56: Roll Response Spectrum - 90^0 Wave Direction HS: 1.8m / Tp: 23.0 sec

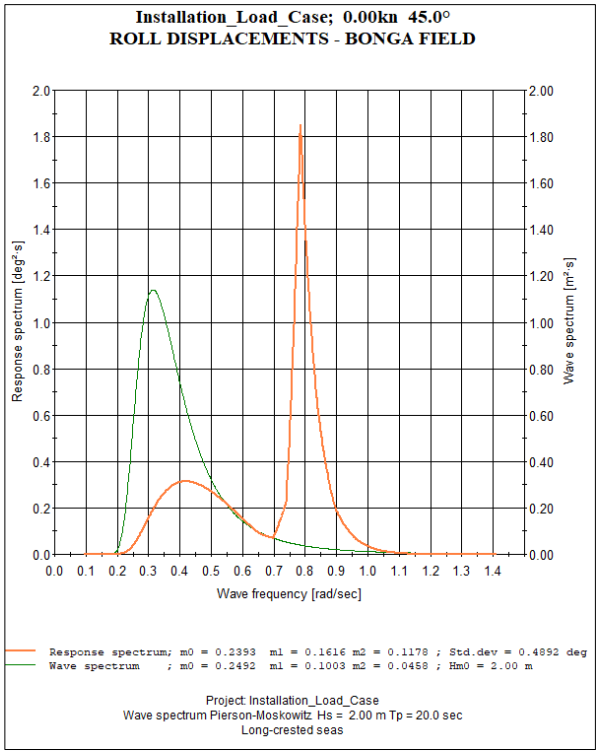

Figure 5-57: Roll Response Spectrum - 45^0 Wave Direction HS: 2.0m / Tp: 20.0 sec

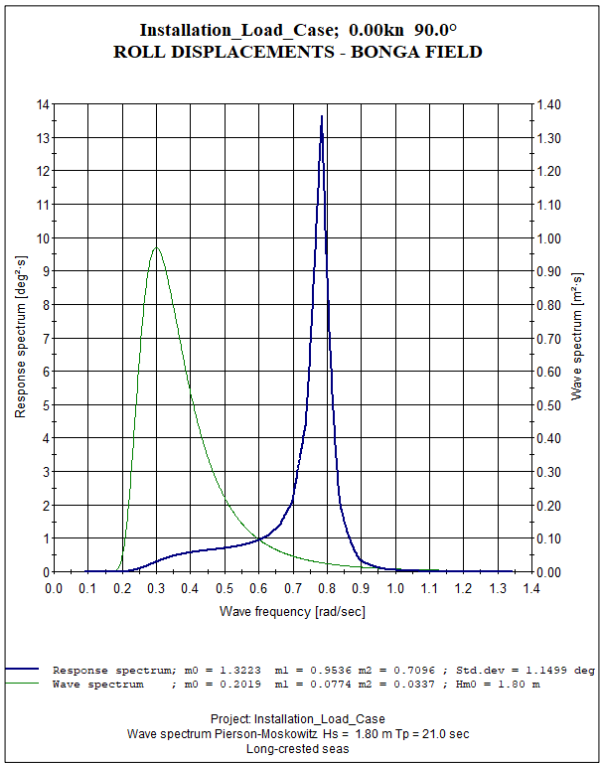

Figure 5-58: Roll Response Spectrum - 90^0 Wave Direction HS: 2.0m / Tp: 20.0 sec

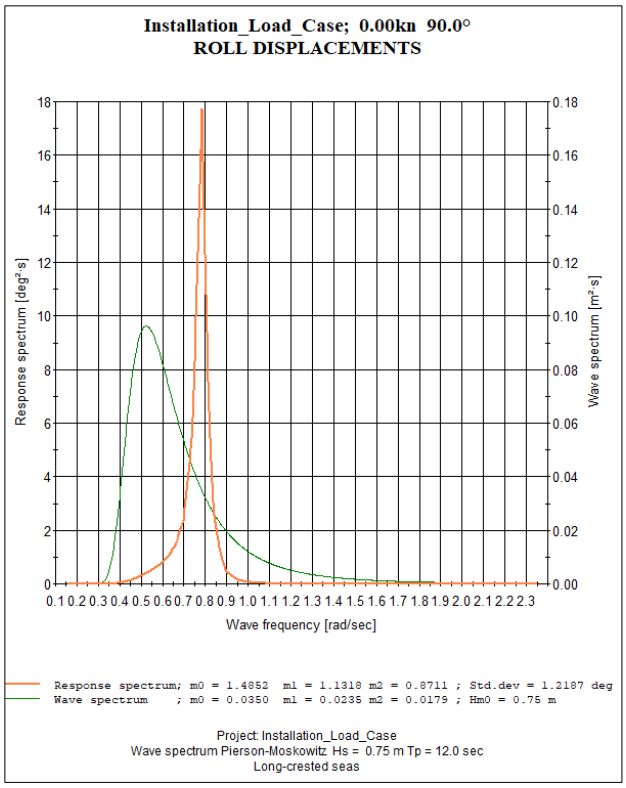

Figure 5-59: Roll Response Spectrum - 90^0 Wave Direction HS: 0.75m / Tp: 12.0 sec

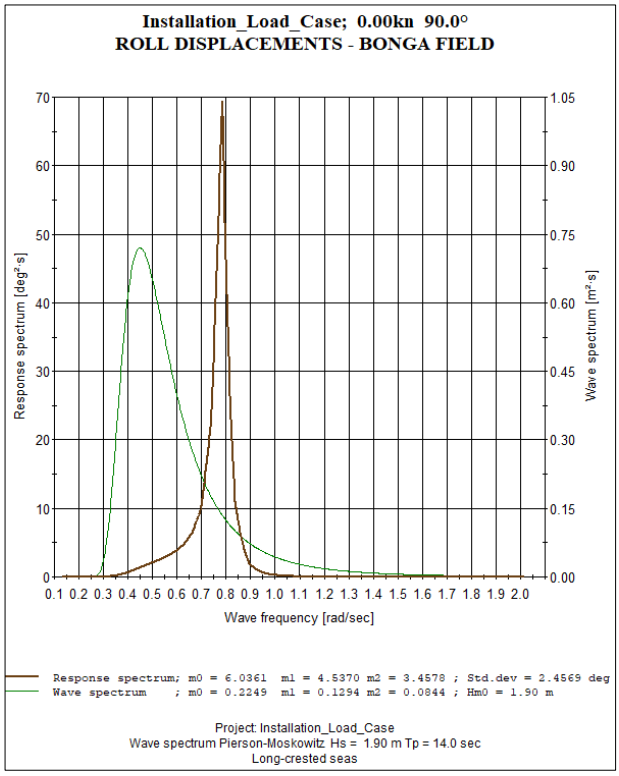

Figure 5-60: Roll Response Spectrum - 90^0 Wave Direction HS:1.9m / Tp: 14.0 sec

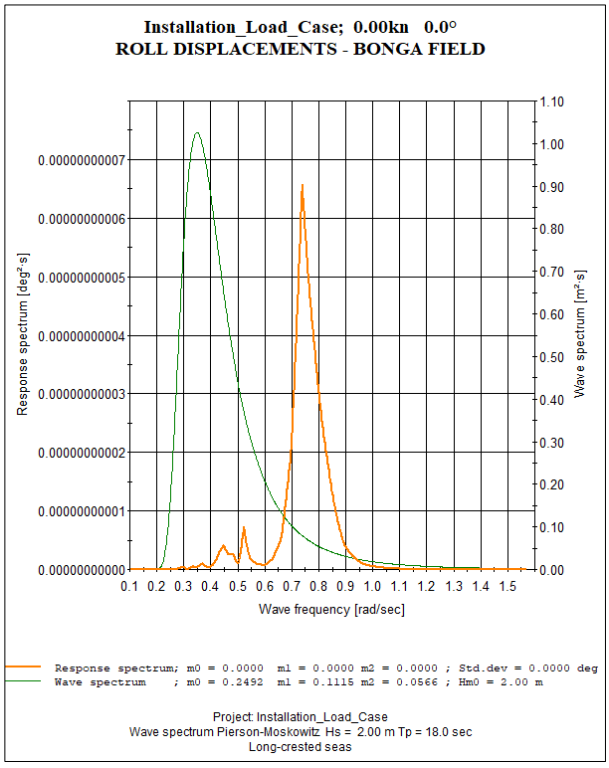

Figure 5-61: Roll Response Spectrum - 0^0 Wave Direction HS:2.0m / Tp: 18.0 sec

6 Chapter Six – Results Discussion

To discuss the results shared in Chapter 5, a due reference and reflection on the objective of this study is needed. The goals, which can be found in section 1.3, include exploring relevant ways of modelling the sea states in Southern Nigeria, investigating the response of offshore installation or structures in Southern Nigerian waters, understanding the nature and types of loads experienced by these structures under the influence of swell sea states which previous studies noted as the dominant spectra in Southern Nigeria, and using the knowledge to discuss the implications for the design of offshore structures, the planning and execution of marine operations in this ocean space of the world.

The nature, properties, and swell characteristics in Southern Nigeria were uncovered through extensive literature studies. This thesis affirms consistent knowledge of swells as a long-crested, long-period wave. But as available data shows, the swells in this area are of low significant wave heights, moderately below 4m, while the wave periods are within 4s – 22s, and some extremes up to 26s, at least for the Bonga field.

In Chapter 3, the thesis explored the modelling of ocean surface waves. As the documentation in that chapter points out, swells are dispersive deep-water waves whose modelling can assume the same classical approach to modelling irregular waves for marine operations. This includes approaching the sea state as a bunch of regular waves, which, through superimposition, form periodic waves (spectrum) that can co-exist in six degrees of freedom. This only explains the route to land, describing a typical swell as a spectrum. As for the question of what type of spectra should provide answers to question number 1 of the research question, the thesis initially attempted to use a modified JONSWAP spectrum.

As (Olagnon et al., 2013) pointed out, generalised spectra for Offshore West Africa are of the form expressed in equation 83. This equation is referred to as the JONSWAP-Glenn spectrum. Applying this notion to the case of Offshore Southern Nigeria implies that the modelling of swells in Southern Nigerian waters is different from 2D spectra, where the parameterisation is purely a function of the significant wave heights and the wave peak period. Including the so-called location parameter that directly correlates with the spectra width does infer that the spectra properties from location to location may differ – hence a generalisation may be deemed erroneous in some regards. This makes absolute scientific sense as a location far from the swell source can affect the swell decay rate and, inevitably, the embedded energy. Sites with shielding and other barriers can also affect flow characteristics and the general swell distribution; in shallow areas where the seabed properties affect spectra propagation, the ensuing results could be the transformation of swells into intermediate or breaking waves. Another feature of the location property concerns the width of the spectrum.

$$G(f) = G(Hs, Tp, p) \qquad \text{Equ. 83}$$

But as this thesis has already been established, a JONSWAP or its hybrid, the JONSWAP-Glenn spectrum, is an extension of the PM spectrum. That means the swells in Southern Nigerian waters are of the PM spectrum, perhaps in an enhanced form. Accordingly, the transformation of PM into JONSWAP is only valid if the peak parameter of the spectra is more significant than 1. As for the spectra properties for the Asabo, Forcados and Bonga fields shows, except for Asabo, where two of the spectra considered for analysis had a peak parameter of about 1.5, the rest had peak parameters of 1. With these, it is therefore practically consistent with modelling swell spectra in Southern Nigerian waters as fully developed, deep water, long-crested, and long-period waves in the form of a PM spectrum if the location parameter is disregarded following the case already made in Chapter 5 on the limitation of the software and the admissibility of adding location parameters to the simulation.

With these, it is believed that the thesis has laid a rational description of how the modelling of the sea state in Southern Nigeria can be approached; thus, an answer to research question 1 is provided.

The following section explores the spectra and the response of an offshore installation vessel modelled as a semi-submersible barge for the Southern Nigerian Sea state. Also, the discussion of the implication is extended to a jack-up barge famous for installation operations in Southern Nigeria.

6.1 Spectra–Response Correlation: Emerging Lessons

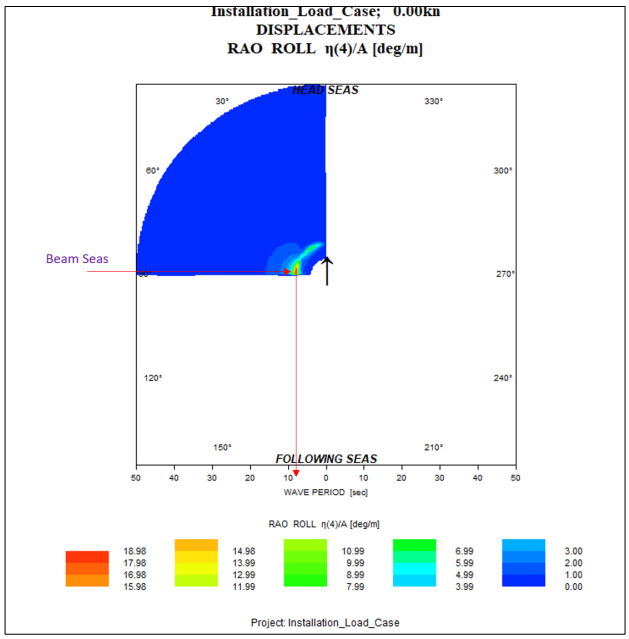

Figure 6-1: Contour Plot of the Roll RAO

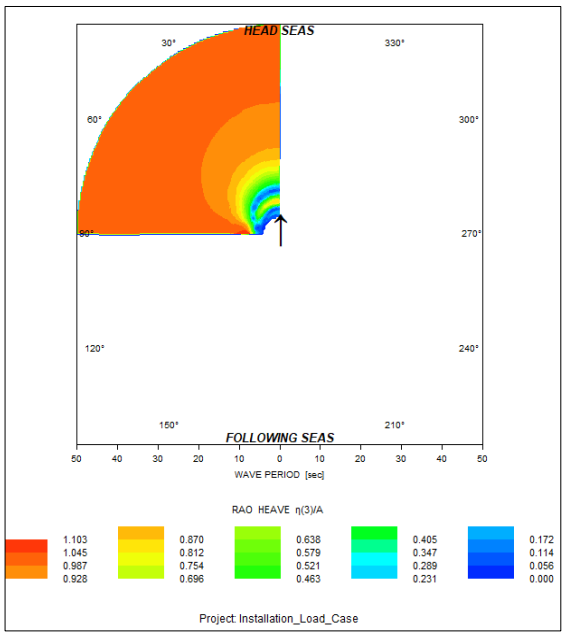

Figure 6-2: Contour Plot of the Heave RAO

By carrying out a spectra analysis with ShipX, an assessment of the behavioral dynamics and the response of a semi-submersible heavy-lift barge in a swell seaway was carried out. The intention

was to relate the simulated motion of the vessel to the spectra properties of significant wave height and peak periods.

In total, 19 spectra were analysed, with wave headings separated in steps of 15^0. The results from the regular wave assessment show consistency in response regarding wave heading. Using figure *6-1*, figure *6-2*, figure *6-3*, and Figure show that beams seas are most critical regarding wave-heading relationship to the response. Also, the RAOs further show a certain peak around 8secs. This could be due to the vessel's natural period coinciding with the wave period of this range. This pattern in the RAO is repeated for all the degrees of freedom. Therefore, for this reason, an amplification of the body's motion is expected to be around 8s.

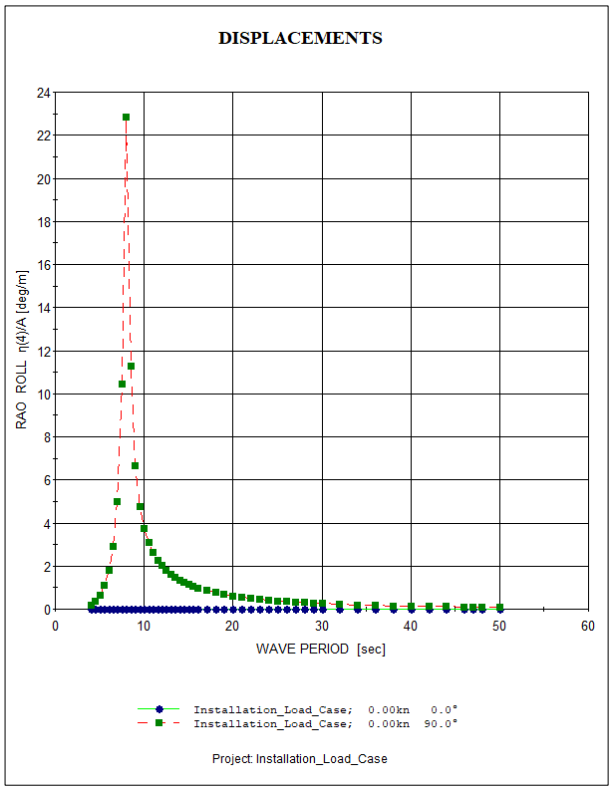

Figure 6-3: Roll RAO for Head & Beam Seas

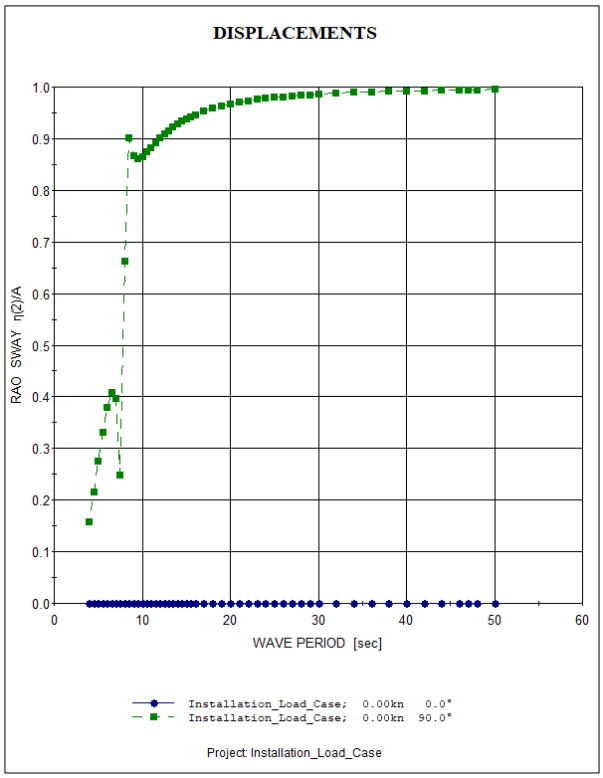

Figure 6-4: Sway RAO for Head & beam Seas

In order of magnitude, though, roll response can be seen to be dominant even for any of the wave headings, and this is more pronounced for beam sea; thus, the response of a body can be summarised as follows:

- The body experiences significant motion amplification around 8s of spectra periods.
- The body's response is pronounced in beam seas.
- Roll motion (j=4) is dominant compared to other degrees of freedom.

With these, the description of the dynamics and nature of loads experienced by installation vessels during long swell periods, with particular attention to Southern Nigeran waters, according

to the findings, can be classified as a roll-dominant motion where beam seas show significant effects when compared to other degrees of freedom. Resonance motion and amplification are at about 8s. In general terms, for most ship-shaped objects, the sea state in Southern Nigeria can be critical since most spectra have peak periods within the ranges of the spectra' peak periods.

6.2 Implications – Design & Planning of Marine Operations

The case considered has shown remarkable motions in roll regarding beams seas. Roll motion and bad seakeeping can induce motion sickness and motion-induced interruptions (MII), increase the probability of green water on deck, increase the risk of capsizing and grossly compromise the safety of the crew, the vessel, and the environment.

To truly grasp the implications of roll amplification, the motion sickness incidence, its dose value, and a few other features like the probability of green water on deck can be used to assess this.

Motion sickness or its dose values, as proposed (McCauley et al., 1976; Nooij 2018), measures comfort regarding ship response for a given exposure period. To McCaulay et al., the dose value of motion sickness is calculated using the equation expressed in equation 84. In equation 84, t is the incidence time, T is the total duration of exposure, and a_ω is the frequency-weighted root mean square (r.m.s) of the acceleration signal.

$$CapMSDV = \left[\int_0^T a_w(t)^2 dt\right]^2 \qquad \text{Equ. 84}$$

Using the ShipX Veres plug-in, the motion sickness incidence (MSI) or its dose value (MSDV) can be evaluated and used as a critical indicator for assessing crew comfort. MSDV has been considered for this case, and it shows a positive correlation with roll motion as the most significant degree of freedom. This is indicated in Figures figure *6-7*, and figure *6-8*.

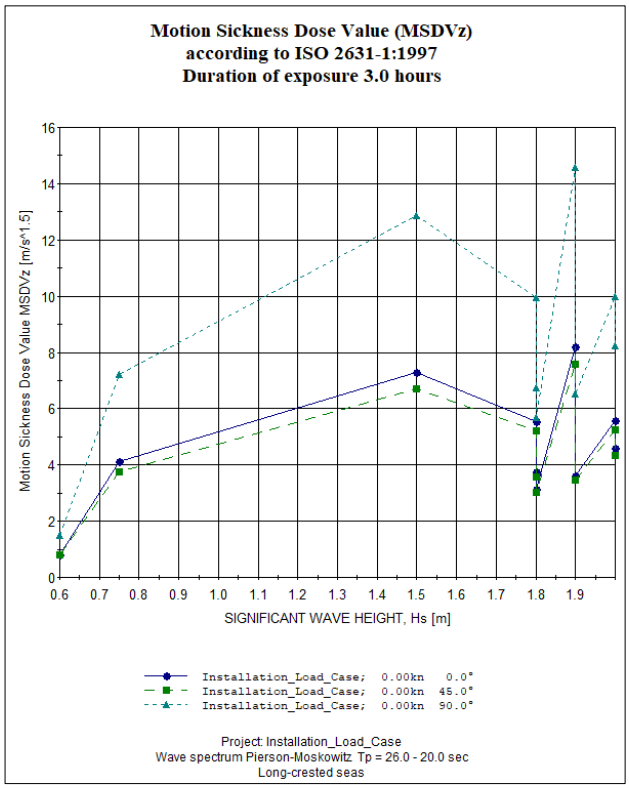

Figure 6-5: MSDV 20-26S Tp

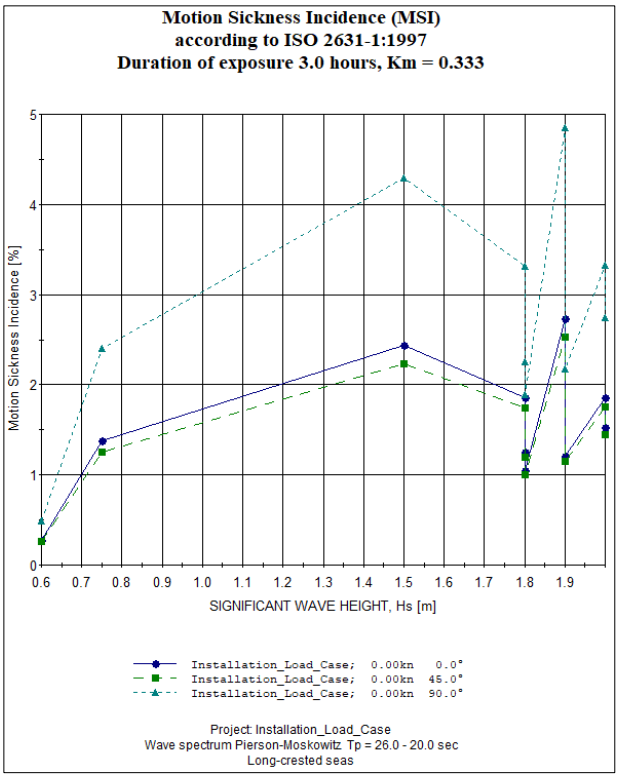

Figure 6-6: MSI 20-26S Tp

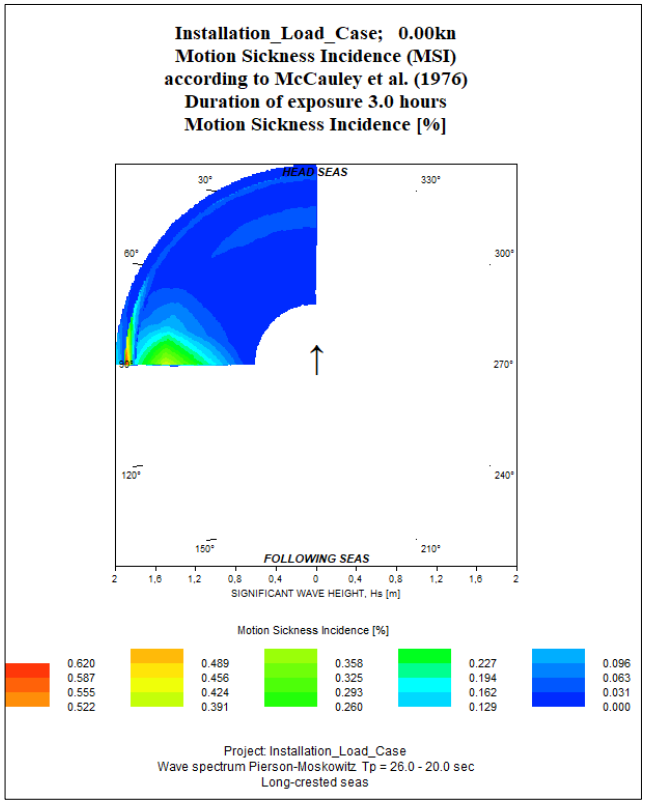

Figure 6-7: MSI Polar Plot 20-26S Tp

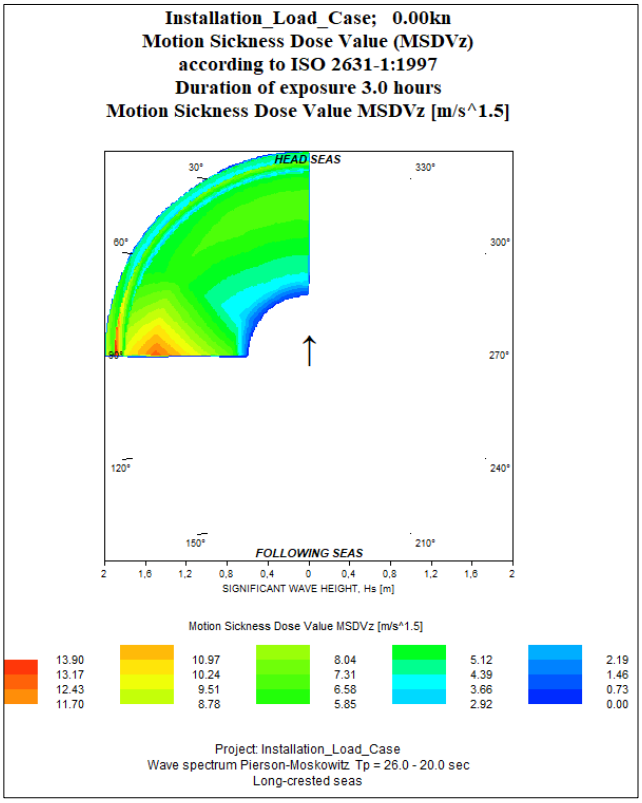

Figure 6-8: MSDV Polar Plot 20-26S Tp

The ensuing implication is that roll in the free-vibrating state is dominant, with the highest potential to cause motion sickness; the support to this notion is the results of the MIS and the MSDV on the previous page. The consequence from the design-planning perspective is that adequate roll damping will be needed to improve the response close to the resonance frequency of the barge.

6.2.1 Roll Motion Control

In general, the motion and response of a semi-submersible barge can be linearised, as shown in Chapter 3. This agrees with the position of (Bangun et al., 2010) on the linearisation of motion of semi-submersibles. Still, as the study noted, including a roll in the linearised form amounts to oversimplifications, according to equation 85. The basic form of the roll response is given. For the roll damping coefficient B, the basic format is provided in equation 86. The equation validates the non-linear structure of the roll response.

$$I\ddot{\xi}_{44} + B\left(\dot{\xi}_{44}\right)\dot{\xi}_{44} + C(\emptyset, t) = MCos(wt) \qquad \text{Equ. 85}$$

In equation 85, M is the angular roll motion, B is the damping coefficient, and C is the restoring coefficient given in the polynomial form. The damping coefficient can also be expressed as;

$$B\left(\dot{\xi}_{44}\right) = B_1\dot{\xi}_{44} + B_2|\dot{\varphi}|\dot{\varphi} + B_3\dot{\xi}_{44}^3 \qquad \text{Equ. 76}$$

Where φ is the roll angle, this affirms the need to include an adequate roll-damping mechanism for barges and attempt to capture the viscous effects around the hull as the vessel rolls from starboard to portside.

According to (Bangun et al., 2010), there are five types of roll damping, namely:

1. Roll damping resulting from skin friction / Viscous damping.
2. Roll damping using bilge keels.
3. Roll damping resulting from eddies.
4. Lift damping
5. Wave damping

The type of roll damping to apply must then consider the case at hand, the applicability and validity. For barges, damping using bilge keels seemingly aligns since, in most cases, barges are designed with skegs which can act as bilge keels. Also, the viscous effect should be accounted for. The most applicable and valid damping mechanisms in roll for barges are bilge keel and viscous damping products.

The computer software ShipX can simulate roll response with bilge keel and viscous effects. A bilge keel can be manually generated in ShipX, or it can be auto-generated. An auto-generated

bilge keel is used to simulate the impact of the bilge keel on roll motion. The effects of viscous damping have also been included.

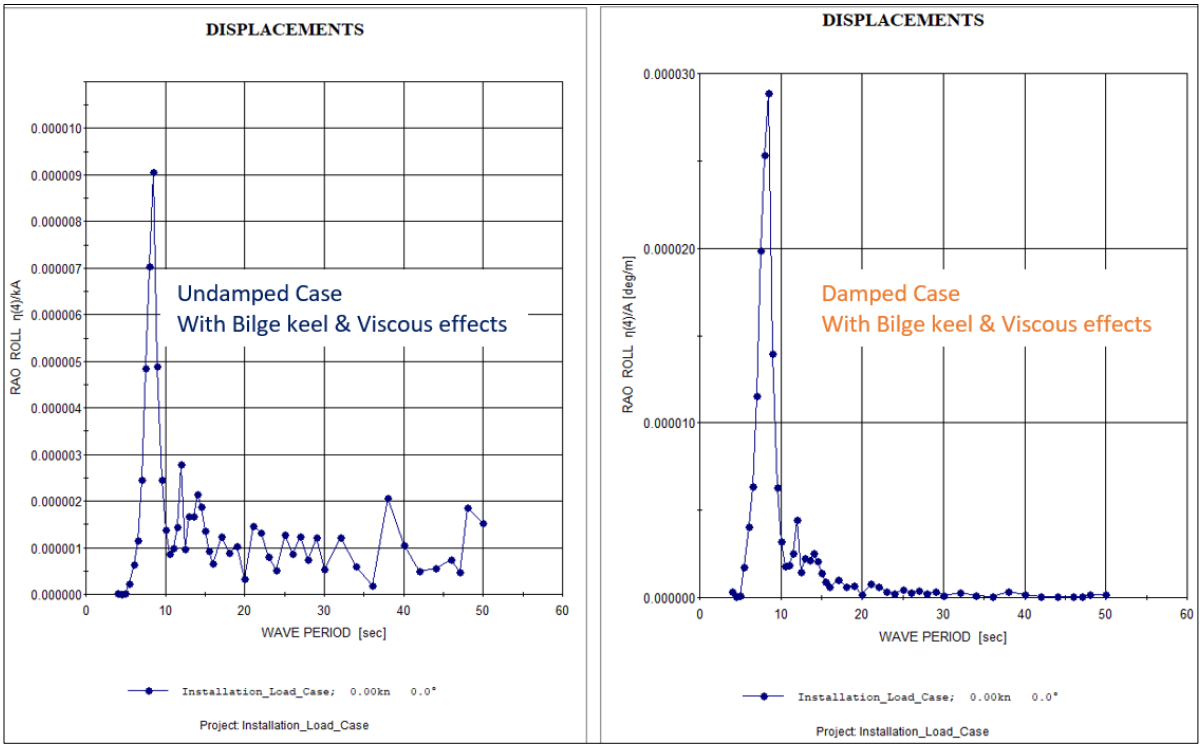

Figure 6-9: Plot of damped & and undamped Roll Displacement RAO at Head Seas

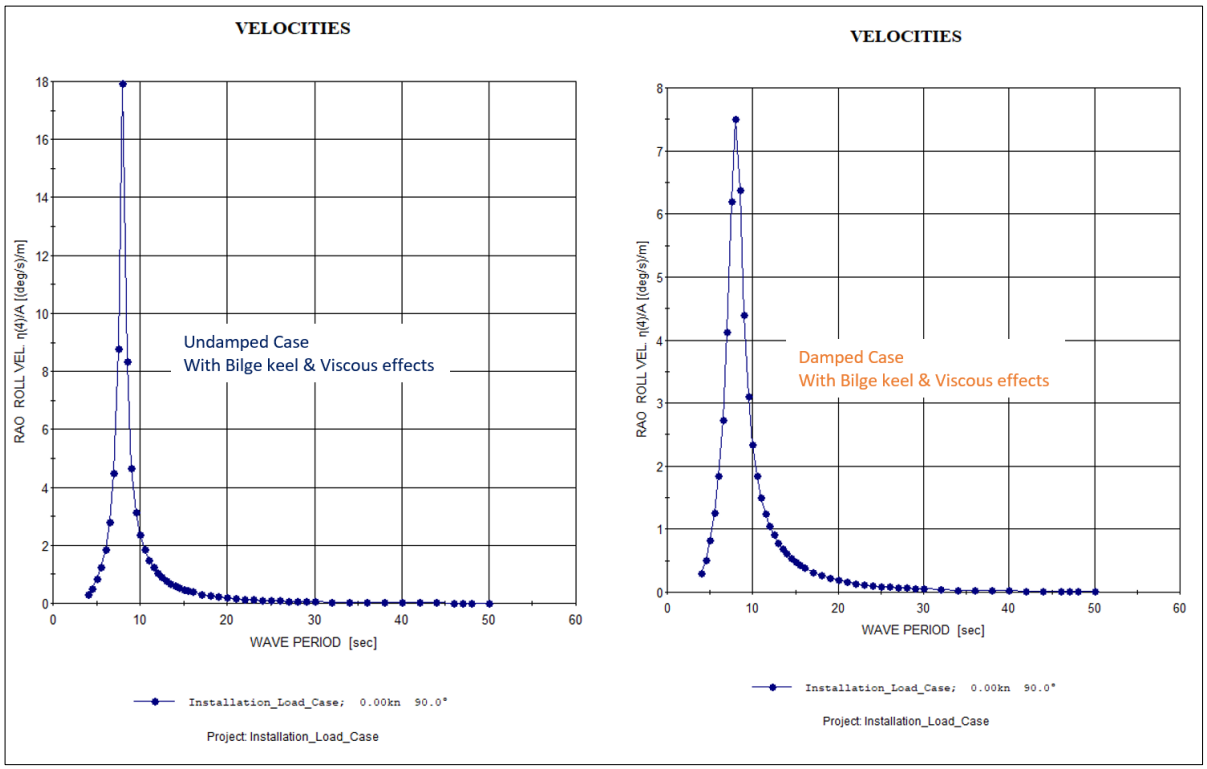

Figure 6-10: Plot of damped & and undamped Roll Velocities RAO in Beam Seas

As figure and figure show, adding roll damping benefits roll response reduction. The figure further shows that the maximum velocity amplification at the same wave heading around the vessel's natural frequency was reduced by more than 50%. This makes a case for properly including a damping mechanism in the design of semi-submersible barges intended for operations.

6.3 Extending Lessons to Jack-Ups

This analysis has been centred on semi-submersible barges in general; however, the results can provide valuable insights for other application areas. Jack-up vessels are famous for installation, drilling, and similar operations in Southern Nigeria, as this region serves as the base for most energy-related offshore activities. While a Jack-up may differ from a semi-submersible barge in terms of geometric properties and, in some cases, shape, for in most part, a jack-up can be moderately modelled as a ponton with extendable spuds. As opined (Sawiji, 2020), a jacket is a combination of self-elevating units called spuds and floating platforms in the form of a barge.

If that is the case, during normal floating conditions and a jack-up's towage, a barge's motion-response analysis can be extended to jack-ups. Such extension can only be valid with the spuds elevated above the mean sea level (MSL). As the spuds start lowering below the mean sea level, the contribution to motion damping must be accounted for. Reference can be made to the thesis work of (Kumar P. Lalith, 2016) for more information on the contribution of jack-up spuds to motion damping at different spud drafts. But the spuds are only lowered during drilling while freely floating during installation (Sawiji, 2020). From this paradigm, it is plausible to state that jack-ups are most likely to be susceptible to the wave's dominant in Southern Nigerian waters in the same pattern shown by the semi-submersible barge considered in this analysis.

So, with this, it can be seen and said that jack-ups and installation operations could show sensitivity to the swell spectra dominating Southern Nigeria. From a planning perspective, offshore installation operations can become weather dependent. This has implications for time, cost, and profitability.

7 Chapter Seven – Conclusion

7.1 Conclusion

This research began modelling and describing the sea state in Southern Nigeria using hybrid modelling techniques, incorporating reviews of scholarly articles, theoretical modelling of irregular waves, and numerical simulations of both regular and irregular waves in the frequency domain. The study learnt that Southern Nigerian waters are swell-dominated, with spectra peak periods spread between 4s – 26s while the significant wave heights can be about 3m.

For the modeling of the sea state, a true reflection of the application/use of spectra in a marine operation needed. If due attention is paid to the spectra peak parameter as an important distinguishing factor, a Pierson-Moskowitz spectrum representing a fully developed, long-crested sea is suitable since the wave peak parameter in most parts was not greater than 1. Therefore, the description and modelling of sea state in Southern Nigeria, explored using Research Question 1 is therefor addressed.

From the perspective of motion amplification, the simulation results from Veres show that the motion of an offshore structure like a barge or jack-ups can be significantly amplified since the natural frequency of most ship-shaped objects is within the ranges of the spectra peak periods for this region. Furthermore, the response in roll appears to be dominant both in the damped and undamped case, with beam seas appearing to be the most critical. This was further validated using an assessment of crew comfort where a motion-induced sickness, a key performance indicator (KPI) for convenience, further agrees with this correlation where roll motion is the dominant contributor to the response.

As the thesis highlighted in Chapter 6, motion amplification has significant implications for the planning and execution of marine operations. First, it is relevant to ensure that from a design perspective, adequate roll-stabilizing features are included in vessels such as barges which do not have dynamic positioning systems to counter the effects of the sea states.

From the planning and execution of an installation operation, the findings suggest that a reliance on good weather forecasts will be most appropriate as the heavy response can compromise safety and operability.

7.2 Contribution to Knowledge

This thesis work is believed to be an addition to existing knowledge and studies on Offshore West Africa but in a more localised fashion where the specificity to Southern Nigerian waters adds context to the general understanding of waves and response.

Another aspect of the thesis' contribution to knowledge is that it is believed that the research may have extensively covered the recommended future work by (Olugbenga et al., 2017) in their study of the Bonga field spectra.

7.3 Limitation of Study

The frequency domain usage in spectra analysis has pros and cons. For example, the linearisation of most of the mathematical formulations could be more consistent with the true state, for example, the linearisation of roll motion is somewhat an oversimplification. Furthermore, the assumption that the wave must be harmonic, and small amplitude waves, the boundary conditions imposed to arrive at the basic equations are simplifications that adds only to make the process of describing the motion of a body in a seaway easier. Things can be more complicated than what has been assumed.

On generalising the results and findings and their application to the entire expanse of Southern Nigerian waters, caution must be applied. The ocean space in Southern Nigeria is vast. The data used for the analysis are only for three locations; However, the spread of the spectra properties is still significantly large, and this still needs to cover the entirety of Southern Nigeria. There is the possibility that the spectra distribution and properties may not follow the same trend; a spectra-location property is an integral part of the spectra property, but for this analysis, it was ignored on the ground of software limitation.

Lastly, the data used were from publications made by other scholars. While the articles where they have been sourced are both scholarly and peer-reviewed, the prospect that there may have some degrees of discrepancies in both data collection and processing should be entertained.

7.4 Future Work

Based on the findings, the discussion and limitations of the research, the following future work may be considered.

- A time-domain response and spectra assessment of barges, semi-submersible barges, or jack-ups in swell sea states of Southern Nigeria with a particular focus on beam seas.
- Assessment of the Effectiveness of different damping methods to the roll response of barges in swells with a focus on beam seas.

References

ABS. (2016). *Guidance Notes on Selecting Design Wave by Long Term Stochastic Method*. American Bureau of Shipping, www.eagle.org

Abam, T. J., Agbakwuru, J. A., & Adumene, S. (2016). Numerical Modelling Of Wave Drift Load On Ship Shaped Offshore Structures (Case Study-West Africa Offshore). *International Journal of Innovative Research and Advanced Studies (IJIRAS)*, *3*(9). www.ijiras.com

Agbakwuru, J. A., Bernard, A. T. , & Gudmestad O. T. (2020). Sea state description of Asabo offshore in Nigeria. *Ocean Systems Engineering*, *10*(1), 25–47.

Agbakwuru, J. A., & Bernard, A. (2019). Statistical Wave Description of Forcados Offshore in Nigeria. *FUPRE Journal of Scientific and Industrial Research (FJSIR)*, *3*(3), 24–34.

Ajao, E.A., Oyewo, E.O., & Unyimadu, J.P (1996). A Review of the Pollution of Coastal Waters in Nigeria. Technical paper No, 107, Nigerian Institute for Oceanography and Marine Research. https://aquadocs.org/bitstream/handle/1834/2214/NIOMR-TP-107-.pdf;jsessionid=D6CBEDAC22B7B2AACEB4B48956832669?sequence=1

Ardhuin, F., Chapron, B., & Collard, F. (2009). Observation of swell dissipation across oceans. *Geophysical Research Letters*, *36*(6), L06607. https://doi.org/10.1029/2008GL037030

Bangun, E. P., Wang, C. M., & Utsunomiya, T. (2010). Hydrodynamic forces on a rolling barge with bilge keels. *Applied Ocean Research*, *32*(2), 219–232. https://doi.org/10.1016/j.apor.2009.10.008

Barber, N. , & Ursell, F. (1948). The generation and propagation of ocean waves and swell. I. Wave periods and velocities. *Philosophical Transactions of the Royal Society of London. Series A, Mathematical and Physical Sciences*, *240*(824), 527–560. https://doi.org/10.1098/rsta.1948.0005

Baso, S., Asri, S., Bochary, R.L., & Pramata, L. (2013). New strip theory approach to ship motions prediction. *Inovasi Teknologi Kelautan*. https://core.ac.uk/download/pdf/25495956.pdf

Bergdahl, L. (2009). *Wave-induced loads and ship motions.* Report No. 2009-1. Chalmers University of Technology, Göteborg, Sweden.

Bitner-Gregersen, E. M., Dong, S., Fu, T., Ma, N., Maisondieu, C., Miyake, R., & Rychlik, I. (2016). Sea state conditions for marine structures' analysis and model tests. *Ocean Engineering*, *119*, 309–322. https://doi.org/1 0.1016/j.oceaneng.2016.03.024

Bunnik, T., & Buchner, B. (2004, May). Numerical Prediction of Wave Loads On Subsea Structures In the Splash Zone. *Paper Presented at The Fourteenth International Offshore and Polar Engineering Conference, Toulon, France*.

Cao, P., & Zhang, J. (1997). Slow Motion Responses of Compliant Offshore Structures. *The Sixth International Offshore and Polar Engineering Conference, Vol. 7. Issue 02.*

Ceraldi, T. S., Hodgkinson, R., & Backé, G. (2017). The petroleum geology of the West Africa margin: An introduction. *Geological Society Special Publication*, *438*(1), 1–6. https://doi.org/10.1144/SP438.11

Chakrabarti, S. K. (1990). *Nonlinear Methods in Offshore Engineering* (Vol. 5). Chicago Bridge & Iron.

Chircop, A., Dzidzornu, D., & Oguamanam, C. (2016). Ocean law reform: A multi-level comparative law analysis of Nigerian maritime zone legislation. *Marine Policy*, *67*, 60–75. https://doi.org/10.1016/j.marpol.2016.01.012

Churchill, R., Lowe, V., & Sander, A. (2022). *The law of the sea*. Manchester University Press. https://doi.org/10.7765/9781526159038

Dean, R. G., & Dalrymple, R. A. (1991). *Water wave mechanics for engineers and scientists* (Vol. 2). World scientific publishing company.

Dennis, B., & Patil, G. P. (2018). Applications in Ecology. In *Lognormal Distributions* (pp. 303–330). Routledge. https://doi.org/10.1201/9780203748664-12

Det Norske Veritas (2010). Recommended Practice Environmental Conditions and Environmental Loads. DNV-RP-C205. http://www.dnv.com

Det Norske Veritas. (2011). Modelling and Analysis of Marine Operations, DNV-RP-H103. http://www.dnv.com

El-Reedy, M. A. (2012). Fabrication and Installation. In Mohamed A. El-Reedy (Ed.), *Offshore Structures* (pp. 293–381). Gulf Professional Publishing, https://doi.org/10.1016/B978-0-12-385475-9.00005-5

Faltinsen, O. M. (1990). Wave Loads on Offshore Structures. *Annual Review of Fluid Mechanics*, *22*(1), 35–56. https://doi.org/10.1146/annurev.fl.22.010190.000343

Fathi, D., & Hoff, J. R. (2004). *Shipx vessel responses (veres).Theory Manual*.

Federal Department of Forestry. (2019). *The Federal Republic of Nigeria National Forest Reference Emission Level (FREL) for the Federal Republic of Nigeria*. https://redd.unfccc.int/files/2019_submission_frel_nigeria.pdf

Foli, B. A. K., Appeaning Addo, K., Ansong, J. K., & Wiafe, G. (2022). Ocean state projections: A review of the West African marine environment. *Journal of Coastal Conservation*, *26*(6), 61. https://doi.org/10.1007/s11852-022-00908-w

Fonseca, N., & Soares, C. G. (1998). Time-Domain Analysis of Large-Amplitude Vertical Ship Motions and Wave Loads. *Journal of Ship Research*, *42*(02), 139–153. https://doi.org/10.5957/jsr.1998.42.2.139

Forristall, G. Z., Ewans, K., Olagnon, M., & Prevosto, M. (2013, June 9). The West Africa Swell Project (WASP). *Volume 2B: Structures, Safety and Reliability*. https://doi.org/10.1115/OMAE2013-11264

Fu, Y., Zhou, X., Sun, W., & Tang, Q. (2019). Hybrid model combining empirical mode decomposition, singular spectrum analysis, and least squares for satellite-derived sea-level anomaly prediction. *International Journal of Remote Sensing*, *40*(20), 7817–7829. https://doi.org/10.1080/01431161.2019.1606959

Gang, C., Hongtao, Y., Peilin, D., Ji, Z., Jian, Z., & Yuhan, W. (2014, June 8). The Effect on Hydrodynamic Performance of Multi-Point Moored FPSO in Swell Condition of West Africa. *Volume 1A: Offshore Technology*. https://doi.org/10.1115/OMAE2014-23144

Garcia-Gabin, W. (2015). Wave Bimodal Spectrum based on Swell and Wind-sea Components. *IFAC-PapersOnLine*, *48*(16), 223–228. https://doi.org/10.1016/j.ifacol.2015.10.284

Geng, B.-L., Teng, B., & Ning, D.-Z. (2010). A TIME-DOMAIN ANALYSIS OF WAVE FORCE ON SMALL-SCALE CYLINDERS OF OFFSHORE STRUCTURES. *Journal of Marine Science and Technology*, *18*(6). https://doi.org/10.51400/2709-6998.1946

Gjevik, B., Pedersen, G. K., Trulsen, K., Karpen, L., & Jensen, A. (2015). *Lecture Notes Mek 4320 Hydrodynamic Wave theory*. Department of Mathematics, University of Oslo https://www.uio.no/studier/emner/matnat/math/MEK4320/h15/undervisningsmateriale/kompendium.pdf

Goda, Y. (2010). *Random seas and design of maritime structures* (3rd ed., Vol. 33). World Scientific Publishing Company Pte Ltd.

Guanche, R., Losada, I. J., & Lara, J. L. (2009). Numerical analysis of wave loads for coastal structure stability. *Coastal Engineering*, *56*(5–6), 543–558. https://doi.org/10.1016/j.coastaleng.2008.11.003

Haritos, N. (2007). Introduction to the Analysis and Design of Offshore Structures– An Overview. *Electronic Journal of Structural Engineering*, *1*, 55–65. https://doi.org/10.56748/ejse.651

Hasselmann, K., Hasselmann, K., Bouws, E., Carlson, H., Cartwright, D., & Enke, K., et al. (1973). Measurements of wind-wave growth and swell decay during the joint North Sea wave project (JONSWAP). *Deutches Hydrographisches Zeitschr*, *A8*(12), 1–95.

He, N., Zhang, C. and Kang, Z. (2018). Analysis of Coupling Characteristics of the Offloading Buoy System in West Africa Seas. *The 28th International Ocean and Polar Engineering Conference,* Sapporo, Japan.

Heising, C. D., & Grenzebach, W. S. (1989). The Ocean Ranger Oil Rig Disaster: A Risk Analysis. *Risk Analysis*, *9*(1), 55–62. https://doi.org/10.1111/j.1539-6924.1989.tb01219.x

Janssen, P. A. E. M., J.A. Battjes, & S. S. H. Wang. (2003). Hybrid modelling of swell and wind sea states. *Journal of Geophysical Research*, *108*(10), 3357.

Jung, K. H., Chang, K.-A., & Jo, H. J. (2006). Viscous Effect on the Roll Motion of a Rectangular Structure. *Journal of Engineering Mechanics*, *132*(2), 190–200. https://doi.org/10.1061/(ASCE)0733-9399(2006)132:2(190)

Kaminski, M., & Rigo, P. (Editors) (2018). *Proceedings of the 20th International Ship Offshore Structures Congress*. 1 of Progress in Marine Science and Technology, IOS Press.

Krogstad, H. E., & Arntsen, Ø. A. (2000a). *Linear Wave Theory Part A Random waves and wave statistics*. Compendium, NTNU, Trondheim, Norway. https://folk.ntnu.no/oivarn/hercules_ntnu/LWTcourse/lwt_ran_2000_part_a.pdf

Krogstad, H. E., & Arntsen, Ø. B. (2000b). *Linear Wave Theory Part B Random waves and wave statistics*. Compendium, NTNU, Trondheim, Norway. https://folk.ntnu.no/oivarn/hercules_ntnu/LWTcourse/lwt_ran_2000_part_b.pdf

Kumar, P. Lalith. (2016). *Analysis Of Jack-Up Rig During Wet Tow with Legs Lowered* [master's Thesis]—Indian Institute of Technology Madras Chennai.

LeBlanc, G., Muryanto, B., & Ducourneau, S. (2011, June 7). An Innovative Offshore Fracturing Campaign for a Mature Oil Field: Case Study Offshore West Africa. *All Days*. https://doi.org/10.2118/143565-MS

Londhe, S. N., Shah, S., Dixit, P. R., Nair, T. M. B., Sirisha, P., & Jain, R. (2016). A Coupled Numerical and Artificial Neural Network Model for Improving Location Specific Wave Forecast. *Applied Ocean Research*, *59*, 483–491. https://doi.org/10.1016/j.apor.2016.07.004

Longuet-Higgins, M. S. (1952). On the statistical distributions of the heights of the sea. *Journal of Marine Research*, *11*(3), 245-265.

Lucas, C., & Guedes Soares, C. (2015). On the modelling of swell spectra. *Ocean Engineering*, *108*, 749–759. https://doi.org/10.1016/j.oceaneng.2015.08.017

Mackay, E. B. L. (2012). Resource Assessment for Wave Energy. In Ali Sayigh (Ed.), *Comprehensive Renewable Energy* (Vol. 8, pp. 11–77). Elsevier. https://doi.org/10.1016/B978-0-08-087872-0.00803-9

Manners, W., & Rainey, R. C. T. (1992). Hydrodynamic forces on fixed submerged cylinders. *Proceedings of the Royal Society of London*, 13–32.

Manwell, J. F., Rogers, A., Hayman. G., Avelar, C. T., Mcgowan, J. G., Abdulwahid. U., & Wu, K. (2006). *Hybrid2–a hybrid system simulation model–theory manual*. University of Massachusetts, USA.

McCauley ME, Royal JW, Wylie CD, O'Hanlon JF, & Mackie RR. (1976). *Motion sickness incidence: Exploratory studies of habituation, pitch and roll, and the refinement of a mathematical model. Technical Report No 1733-2. In. Canyon Research Group Inc Goleta Ca Human Factors Research Div*.

Mehn-Andersen, I. (2018). *Time-domain Roll Motion Analysis of a Barge for Transportation of an Offshore Jacket Structure* [master's Thesis, NTNU]. https://ntnuopen.ntnu.no/ntnu-xmlui/bitstream/handle/11250/2564464/18591_FULLTEXT.pdf?sequence=1&isAllowed=y

Neumann, G. (1953). On ocean wave spectra and a new method of forecasting wind-generated sea. *Beach Erosion Board, U. S. Army Corps of Engineers, Tech. Memo.*, *43*, 1–42.

Newman, J. N. (2004). Progress in wave load computations on offshore structures. *In 23rd OMAE Conference*.

Newman, J. N. (2018). *Marine hydrodynamics*. The MIT Press.

Nooij, S. A. (2018). *A review of the effects of motion characteristics on motion sickness incidence. Technical Report No 197*. Max Planck Institute for Biological Cybernetics. Tubingen. https://pure.mpg.de/rest/items/item_3008626_2/component/file_3008627/content

Oberhagemann, J. (2016). *On the prediction of wave-induced loads and vibration of ship structures with finite volume fluid dynamic methods*. PhD thesis, Universität Duisburg-Essen

Ochi, M. K., & Hubble, E. N. (1976). Six-parameter wave spectra. *In: Coastal Engineering Proceedings, 1(15), 17. https://doi.org/10.9753/icce.v15.17*

Ogilvie, T. F., & Tuck, E. O. (1969). *A Rational Theory of Ship Motion Part 1*. MICHIGAN UNIV ANN ARBOR DEPT OF NAVAL ARCHITECTURE AND MARINE ENGINEERING, USA

Ohkusu, M. (1998, August). Validation of theoretical methods for ship motions using experiments. *In Proc. 22nd. Symposium Naval Hydrodynamics*. https://doi.org/doi.org/10.17226/9771

Orji, C. U. (2019). *Motion Analysis of FPSO in Multidirectional Seas: The West African Offshore Region*. PhD Thesis University of Newcastle, UK

Oliver, J. C. (1990). Advanced methods for ship motion and wave load prediction. *In Proc. 22nd. Symposium Naval Hydrodynamics*.

Olugbenga, A. A., Gudmestad, O. T., & Agbakwuru, J. (2017). Swell description for Bonga offshore Nigeria location. *Ocean Systems Engineering*, *7*(4), 345–369. https://doi.org/10.12989/ose.2017.7.4.345

Prevosto, M., Ewans, K., Forristall, G. Z., & Olagnon, M. (2013, June 9). Swell Genesis, Modelling and Measurements in West Africa. *Volume 2B: Structures, Safety and Reliability*. https://doi.org/10.1115/OMAE2013-11201

R. Adrezin, P. Bar-Avi, & H. Benaroya. (1996). Dynamic Response of Compliant Offshore. Journal of Aerospace Engineering, *9*(4), 13156–13173. https://doi.org/10.1061/(ASCE)0893-1321(1996)9:4(114)

Rana, T. , Guedes Soares, C. , & Kumar, R. (2014). Response of Offshore Structures to Long-Period Ocean Waves. *Ocean Engineering*, *87*, 187–197.

Reijers, T. J. A., Petters, S. W., & Nwajide, C. S. (1997). *Chapter 7 The Niger Delta basin* (Vol. 3, pp. 151–172). Elsevier. https://doi.org/10.1016/S1874-5997(97)80010-X

Rijken, O. (2013). Installation Methodologies for a Tension Leg Platform Under Ocean Swell Conditions. *Volume 1: Offshore Technology*, 11381. https://doi.org/10.1115/OMAE2013-11381

Ryabkova, M., Karaev, V., Guo, J., & Titchenko, Yu. (2019). A Review of Wave Spectrum Models as Applied to the Problem of Radar Probing of the Sea Surface. *Journal of Geophysical Research: Oceans*, *124*(10), 7104–7134. https://doi.org/10.1029/2018JC014804

Salvesen, N., Tuck, E. O., & Faltinsen, O. (1970). Ship Motions and Sea Loads. *In Transactions of the Society of Naval Architects and Marine Engineers*, *78*, 250–287.

Sarpkaya, T., & Isaacson, M. (1981). *Mechanics of wave forces on offshore structures*. Van Nostrand Reinhold Company New York.

Sawiji, A. (2020). *The Motion Response Analysis of Floating Jack-Up Rigs in the Operating Condition*. In *Proc. Built Environ., Sci. Technol. Int. Conf.* 191–196. https://doi.org/10.5220/0008908101910196

Schellin, T. E., & Moctar, O. el. (2007). Numerical Prediction of Impact-Related Wave Loads on Ships. *Journal of Offshore Mechanics and Arctic Engineering*, *129*(1), 39–47. https://doi.org/10.1115/1.2429695

Sen, D. T., & Vinh, T. C. (2016). Determination of added mass and inertia moment of marine ships moving in 6 degrees of freedom. *International Journal of Transportation Engineering and Technology*, *2*(1), 8–14.

Shin, S., Kim, I.-H., Kim, J., Nam, J., Hur, D., Lee, H.-S., & Do, K. (2017). *Beach Erosion and Structural Damage by High Swell Waves*. Coastal Dynamics *2017*, 1223-1227.

Stéphanou, A., & Volpert, V. (2016). Hybrid Modelling in Biology: a Classification Review. *Mathematical Modelling of Natural Phenomena*, *11*(1), 37–48. https://doi.org/10.1051/mmnp/201611103

Strekalov, S. S., Tsyploukhin, V. P., & Massel, S. T. (1972). Structure of sea wave frequency spectrum. *In Coastal Engineering*, 307–314.

Torsethaugen, K. (1993, June 22). A Two Peak Wave Spectrum Model. *12th Intl Conf on Offshore Mechanics & Arctic Engng*.

Toualy, E., Aman, A., Koffi, P., Marin, F., & Wango, T. (2015). Ocean swell variability along the northern coast of the Gulf of Guinea. *African Journal of Marine Science*, *37*(3), 353–361. https://doi.org/10.2989/1814232X.2015.1074940

Troesch, A. (1978). Forward Speed Effect on the Sway, Roll and Yaw. Report No. 208, Department of Naval Architecture and Marine Engineering, The University of Michigan. https://deepblue.lib.umich.edu/handle/2027.42/91719

UN Geospatial. (2014, August 1). *Map of Nigeria*.

United Nations. (1982). *United Nations Convention on the Law of the Sea*.

Wang, Y., Gao, Z., & Yang, J. (2019). Study on the response of offshore structures under short-period swell waves. *Ocean Engineering*, 1–13.

Wang, Y., Gao, Z., & Yang, J. (2019). Study on the response of offshore structures under short-period swell waves. *Ocean Engineering*, 1–13

Williams, C. (2011). Research Methods. *Journal of Business & Economics Research (JBER)*, *5*(3). https://doi.org/10.19030/jber.v5i3.2532

Wilson, J. F. (Editor). (2003). *Dynamics of Offshore Structures*. John Wiley & Sons.

Wu, M., & Hermundstad, O. A. (2002). Time-domain simulation of wave-induced nonlinear motions and loads and its applications in ship design. *Marine Structures*, *15*(6), 561–597. https://doi.org/10.1016/S0951-8339(02)00003-5

Xia, J., Wang, Z., & Jensen, J. J. (1998). Non-linear wave loads and ship responses by a time-domain strip theory. *Marine Structures*, *11*(3), 101–123. https://doi.org/10.1016/S0951-8339(98)00008-2

Xiao, X., Jenakumo, T., Ash, C., Bui, H., Fakunle, O., & Weaver, S. (2016, May 2). An Integrated Workflow Combining Seismic Inversion and 3D Geomechanics Modeling - Bonga Field, Offshore Nigeria. *In Offshore Technology Conference*. https://doi.org/10.4043/27108-MS

Yang, J. (1990). *Comparison of added mass modelling for ships* [Masters , University of British Columbia https://open.library.ubc.ca/soa/cIRcle/collections/ubctheses/831/items/1.0098016

Zhang, L., Lu, H., Yang, J., Peng, T., & Xiao, L. (2013). Low-frequency drift forces and horizontal motions of a moored FPSO in bi-directional swell and wind-sea offshore West Africa. *Ships and Offshore Structures*, *8*(5), 425–440. https://doi.org/10.1080/17445302.2012.700564

Zhang, Z., & Li, X.-M. (2017). Global ship accidents and ocean swell-related sea states. *Natural Hazards and Earth System Sciences*, *17*(11), 2041–2051. https://doi.org/10.5194/nhess-17-2041-2017

Appendix 1 – Computer Software ShipX

1 INTRODUCTION

1.1 General

The study of wave induced vessel responses is essential in the design of new ships. To optimize the operability of the vessel in a seaway, it is important to minimize the motions of the ship. If the loads are decreased, the steel weight can be reduced. Further, hydrodynamic loads and motions are important from the standpoint of safety of the ship and its crew. The SHIPX Vessel Responses Plug-In is a SHIPX implementation of the VEssel RESponse program (VERES), which is intended to be a tool which can be used in early design, in defining and evaluating model tests and in obtaining supplementary results. The program calculates:

- Motion transfer functions in six degrees of freedom
- Relative motion transfer functions
- Motion transfer functions at specified points
- Global wave induced loads[1] (forces and moments)
- Short term statistics of the above mentioned
- Long term statistics of the above mentioned
- Postprocessing of slamming pressures
- Operability (operability limiting boundaries, operability diagrams for a given sea state and percentage operability)
- Time simulations of motions and loads including important non-linear effects

Here, *motions* includes both displacements, velocities and accelerations.

Please note that the options you have available will depend on what kind of license you have. Some modules may require an additional license.

All computer programs for calculation of ship motions are based on assumptions and simplifications with respect to theory and hull form representation. In order to use the program in practical design, it is important to be aware of the limitations of the program, and to which extent the results are valid. In theoretical terms the theory applied in the VERES program is said to be based on linear, potential, strip theory. The relevance of these restrictions is that the theory is developed for moderate wave heights inducing moderate motions on a ship with a length which is much larger than the ship breadth and draught. In addition the change in cross-sectional area as function of longitudinal position should be slow. Consequently, large ship motions and large wave heights will restrict the validity of the results. However, ship motions obtained by the program show good correlation with experiments even at wave conditions which are outside the limits of the theory. Hence, the program may be used to investigate a wide range of conditions bearing in mind that the accuracy is reduced as the program is stretched to its limits.

General Introduction on ShipX. Reference is made to (Fathi & Hoff, 2004) *for more information.*

1.3 Overview

The SHIPX Vessel Responses (VERES) program is divided in two major calculation utilities. A Main Program that calculates the transfer functions for motions and loads (frequency domain) as well as performs time simulations, and a Postprocessor which helps you with reporting and data presentation as well as further calculations based on the transfer functions.

Figure 1 shows the steps required to calculate the percentage operability for a vessel when applying frequency-domain calculations.

1. The Main Program calculates the motion transfer functions in six degrees of freedom.
2. The Postprocessor combines the motion transfer functions with the specified wave spectra to obtain the response spectra (short term statistics).
3. The response spectra are combined with the specified seakeeping criteria to obtain operability limiting boundaries.
4. The operability limiting boundaries combined with the specified wave scatter diagram are summed up over the sea states to obtain the percentage operability.

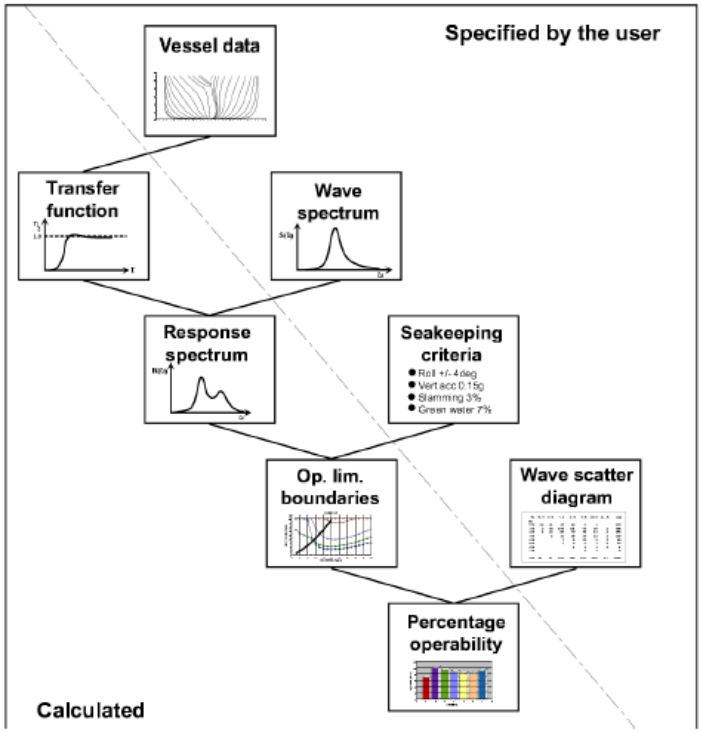

General Overview on ShipX. Reference is made to (Fathi & Hoff, 2004) *for more information.*

Appendix 2 – Derivation of Gamma (γ)

Asabo Field

Derivation of Gammer for the Series of HS & Tp - Asabo

HS	Tp	Hs^-0,5	Tp* Hs^-0,5	Gamma	Remarks
0,50	6	1,414	8,485	1	PM Zone
1,00	6	1,000	6,000	1	PM Zone
1,50	6	0,816	4,899	1,4	JONSWAP
2,00	6	0,707	4,243	2,5	JONSWAP
2,25	6	0,667	4,000	3,1	JONSWAP
0,50	8	1,414	11,314	1	PM Zone
1,00	8	1,000	8,000	1	PM Zone
1,50	8	0,816	6,532	1	PM Zone
2,00	8	0,707	5,657	1	PM Zone
0,50	10	1,414	14,142	1	PM Zone
1,00	10	1,000	10,000	1	PM Zone
1,50	10	0,816	8,165	1	PM Zone
2,00	10	0,707	7,071	1	PM Zone
0,50	10,2	1,414	14,425	1	PM Zone
1,00	10,2	1,000	10,200	1	PM Zone
1,50	10,2	0,816	8,328	1	PM Zone
2,00	10,2	0,707	7,212	1	PM Zone
2,30	10,2	0,659	6,726	1	PM Zone
0,58	12	1,313	15,757	1	PM Zone
0,80	12	1,118	13,416	1	PM Zone
1,30	12	0,877	10,525	1	PM Zone
1,9	12	0,725	8,706	1	PM Zone
1,40	14	0,845	11,832	1	PM Zone
1,80	14	0,745	10,435	1	PM Zone
2,00	14	0,707	9,899	1	PM Zone
1,5	16,1	0,816	13,146	1	PM Zone
1,8	16,1	0,745	12,000	1	PM Zone
2,2	16,1	0,674	10,855	1	PM Zone

Legend:	Analysed Spectra

Table 4-5: 0.5-2.5m H_s & 6s-17s T_p for Asabo Field Offshore Nigeria. Adapted from (A. A. Jasper et al., 2020)

H_s (m)	0.5 – 2.25	0.5-2.0	0.5-2.0	0.5-2.3	0.58-1.9	1.4-2.0	1.6-2.2	1.52-2.1
T_p (s)	6	8	10	10.2	12	14	16	16.1

$$\gamma = \begin{cases} 5 & \text{for } Tp/\sqrt{Hs} \leq 3.6 \\ e^{5.75-1.15T_p/\sqrt{H_s}} & \text{for } 3.6 \leq Tp/\sqrt{Hs} \leq 5 \\ 1 & \text{for } 5 \leq Tp/\sqrt{Hs} \end{cases}$$

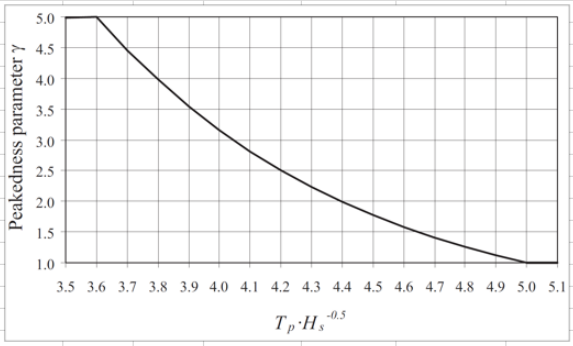

Forcados Field

Derivation of Gammer for the Series of HS & Tp - Asabo

HS	Tp	Hs^-0,5	Tp* Hs^-0,5	Gamma	Remarks
0,50	6	1,414	8,485	1	PM Spectrum
1,00	6	1,000	6,000	1	PM Spectrum
1,52	6	0,811	4,867	1,2	JONSWAP
0,50	8	1,414	11,314	1	PM Spectrum
1,00	8	1,000	8,000	1	PM Spectrum
1,50	8	0,816	6,532	1	PM Spectrum
2,00	8	0,707	5,657	1	PM Spectrum
0,50	10	1,414	14,142	1	PM Spectrum
1,00	10	1,000	10,000	1	PM Spectrum
1,50	10	0,816	8,165	1	PM Spectrum
2,00	10	0,707	7,071	1	PM Spectrum
0,50	12	1,414	16,971	1	PM Spectrum
1,00	12	1,000	12,000	1	PM Spectrum
1,50	12	0,816	9,798	1	PM Spectrum
2,00	12	0,707	8,485	1	PM Spectrum
2,20	12	0,674	8,090	1	PM Spectrum
1,80	14	0,745	10,435	1	PM Spectrum
2,20	14,1	0,674	9,506	1	PM Spectrum
1,80	14,4	0,745	10,733	1	PM Spectrum

Legend: Analysed Spectra

Table 4-6: 0.5-2.2m H_s & 6s-14.4s T_p for Asabo Field Offshore Nigeria. Adapted from (A. A. Jasper et al., 2020)

H_s (m)	0.5 – 1.52	0.5-2.0	0.5-2.0	0.5-1.8	0.54-2.2	1.7-1.8	1.8-2.2	1.7-1.8
T_p (s)	6	8	10	10.2	12	14	14.1	14.4

$$\gamma = \begin{cases} 5 & \text{for } Tp/\sqrt{Hs} \le 3.6 \\ e^{5.75-1.15Tp/\sqrt{Hs}} & \text{for } 3.6 \le Tp/\sqrt{Hs} \le 5 \\ 1 & \text{for } 5 \le Tp/\sqrt{Hs} \end{cases}$$

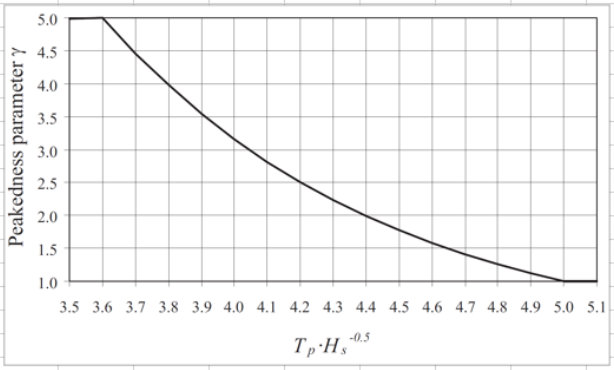

Bonga Field

Derivation of Gammer for the Series of HS & Tp - Bonga Field

HS	Tp	Hs^-0,5	Tp* Hs^-0,5	Gamma	Remarks
0,50	12	1,414	16,971	1	PM Spectrum
0,75	12	1,155	13,856	1	PM Spectrum
0,50	13	1,414	18,385	1	PM Spectrum
1,00	13	1,000	13,000	1	PM Spectrum
1,50	13	0,816	10,614	1	PM Spectrum
0,50	14	1,414	19,799	1	PM Spectrum
1,00	14	1,000	14,000	1	PM Spectrum
1,90	14	0,725	10,157	1	PM Spectrum
0,50	17	1,414	24,042	1	PM Spectrum
1,00	17	1,000	17,000	1	PM Spectrum
1,80	17	0,745	12,671	1	PM Spectrum
0,50	18	1,414	25,456	1	PM Spectrum
1,00	18	1,000	18,000	1	PM Spectrum
1,50	18	0,816	14,697	1	PM Spectrum
2,00	18	0,707	12,728	1	PM Spectrum
0,50	20	1,414	28,284	1	PM Spectrum
1,00	20	1,000	20,000	1	PM Spectrum
1,50	20	0,816	16,330	1	PM Spectrum
2,00	20	0,707	14,142	1	PM Spectrum
0,50	21	1,414	29,698	1	PM Spectrum
1,00	21	1,000	21,000	1	PM Spectrum
1,80	21	0,745	15,652	1	PM Spectrum
0,50	22	1,414	31,113	1	PM Spectrum
1,00	22	1,000	22,000	1	PM Spectrum
1,90	22	0,725	15,960	1	PM Spectrum
1,00	23	1,000	23,000	1	PM Spectrum
1,80	23	0,745	17,143	1	PM Spectrum
0,50	24	1,414	33,941	1	PM Spectrum
0,50	25	1,414	35,355	1	PM Spectrum
0,60	26	1,291	33,566	1	PM Spectrum

Legend: Analysed Spectra

Table 4-7: 0.5-2.2m H_s & 6s-14.4s T_p for Bonga Field Offshore Nigeria. Adapted from (Olugbenga et al., 2017)

H_s (m)	0.5 – 0.75	0.5-1.5	0.5-1.9	0.5-1.8	0.5-2.0	0.5-2.25	0.5-2.0	0.5-1.8
T_p (s)	12	13	14	17	18	19	20	21
H_s (m)	0.5-1.9	1- 1.8	0.25-0.5	0.4-0.5	0.4-0.6			
T_p (s)	22	23	24	25	26			

$$\gamma = \begin{cases} 5 & \text{for } Tp/\sqrt{Hs} \le 3.6 \\ e^{5.75-1.15Tp/\sqrt{Hs}} & \text{for } 3.6 \le Tp/\sqrt{Hs} \le 5 \\ 1 & \text{for } 5 \le Tp/\sqrt{Hs} \end{cases}$$

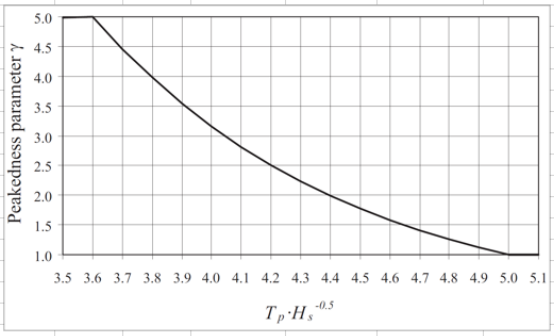

JONSWAP Spectrum Classification

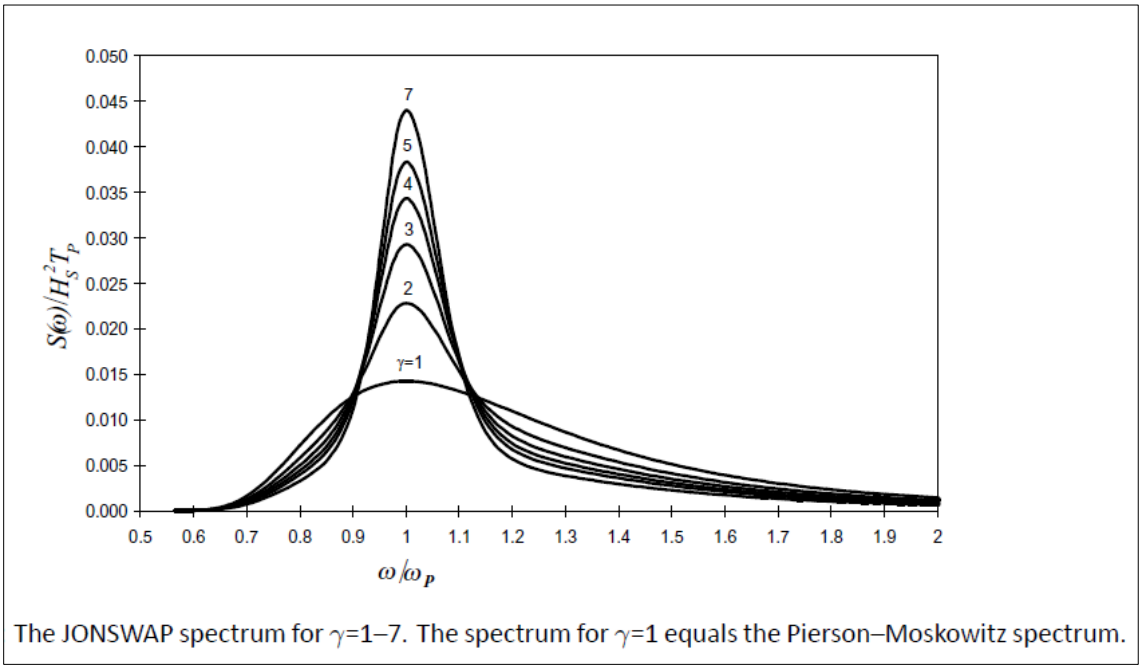

The JONSWAP spectrum for γ=1–7. The spectrum for γ=1 equals the Pierson–Moskowitz spectrum.

Spectrum Classification based on Peak Parameter. Source: (Fathi & Hoff, 2004)

Appendix 3 – Selected Results

RESPONSE AMPLITUDE OPERATORS	ENCL. a)
	REPORT
	DATE 2023
	REF

DISPLACEMENTS

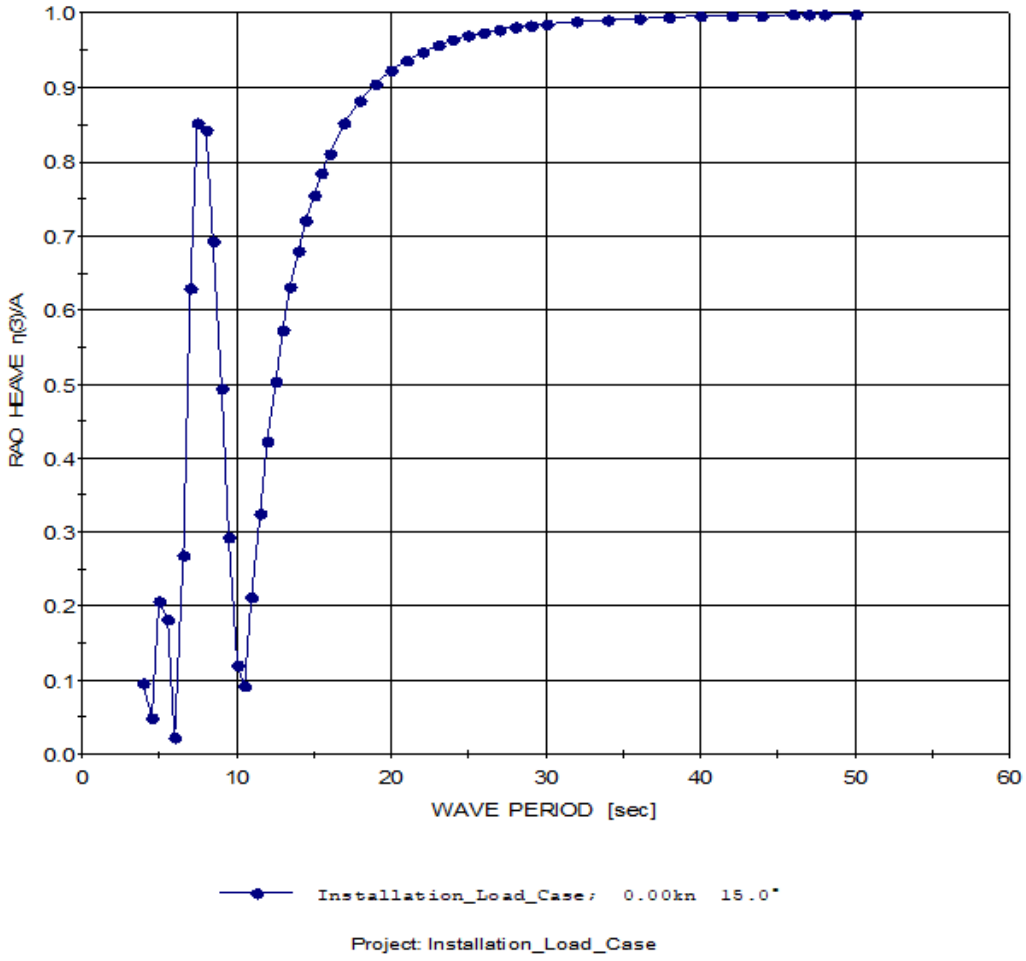

ShipX - 19.05.2023 - 15:19:48 - Licensed to: Boa Management AS (Trondheim)

ENCL.	b)
REPORT	
DATE	2023-05
REF	

RESPONSE AMPLITUDE OPERATORS

DISPLACEMENTS

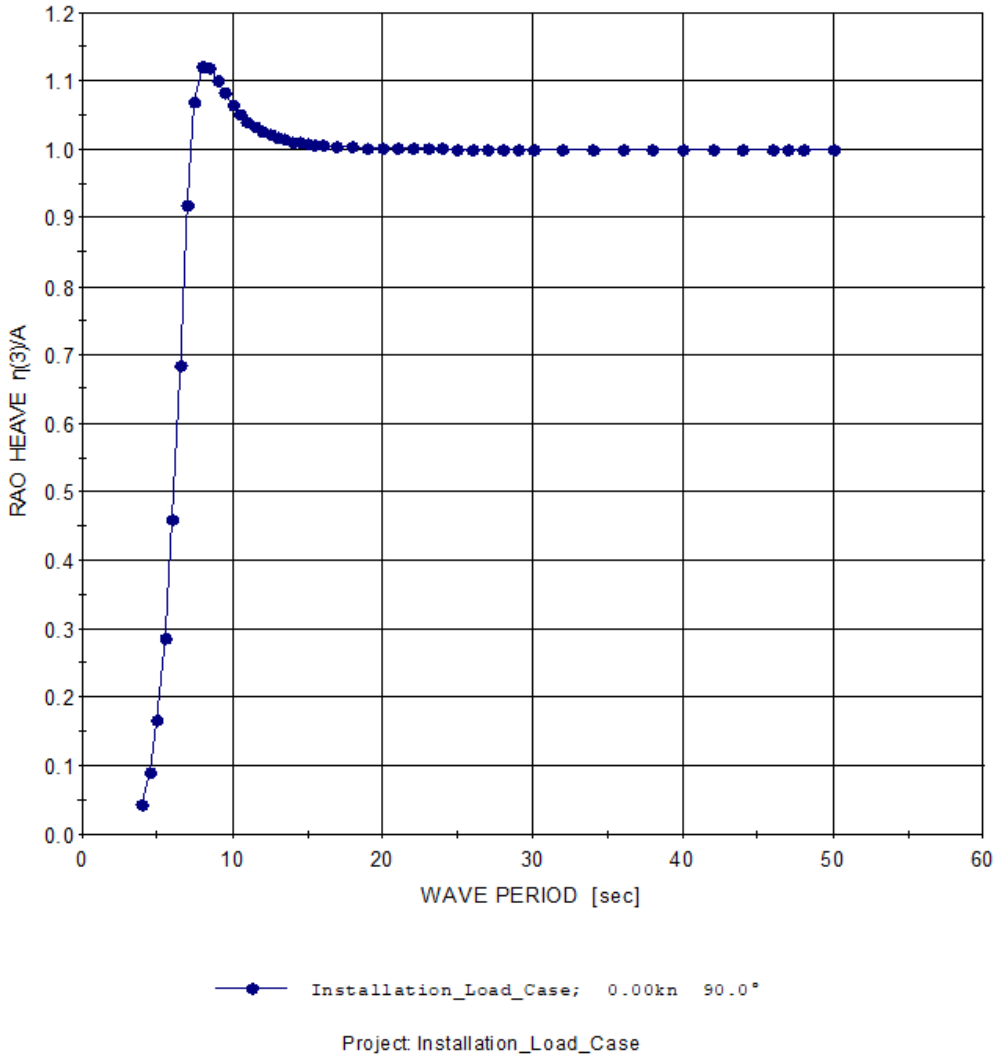

Project: Installation_Load_Case

ShipX - 19.05.2023 - 15:39:23 - Licensed to: Boa Management AS (Trondheim)

RESPONSE AMPLITUDE OPERATORS	ENCL. c)
	REPORT
	DATE 2023-05-
	REF

DISPLACEMENTS

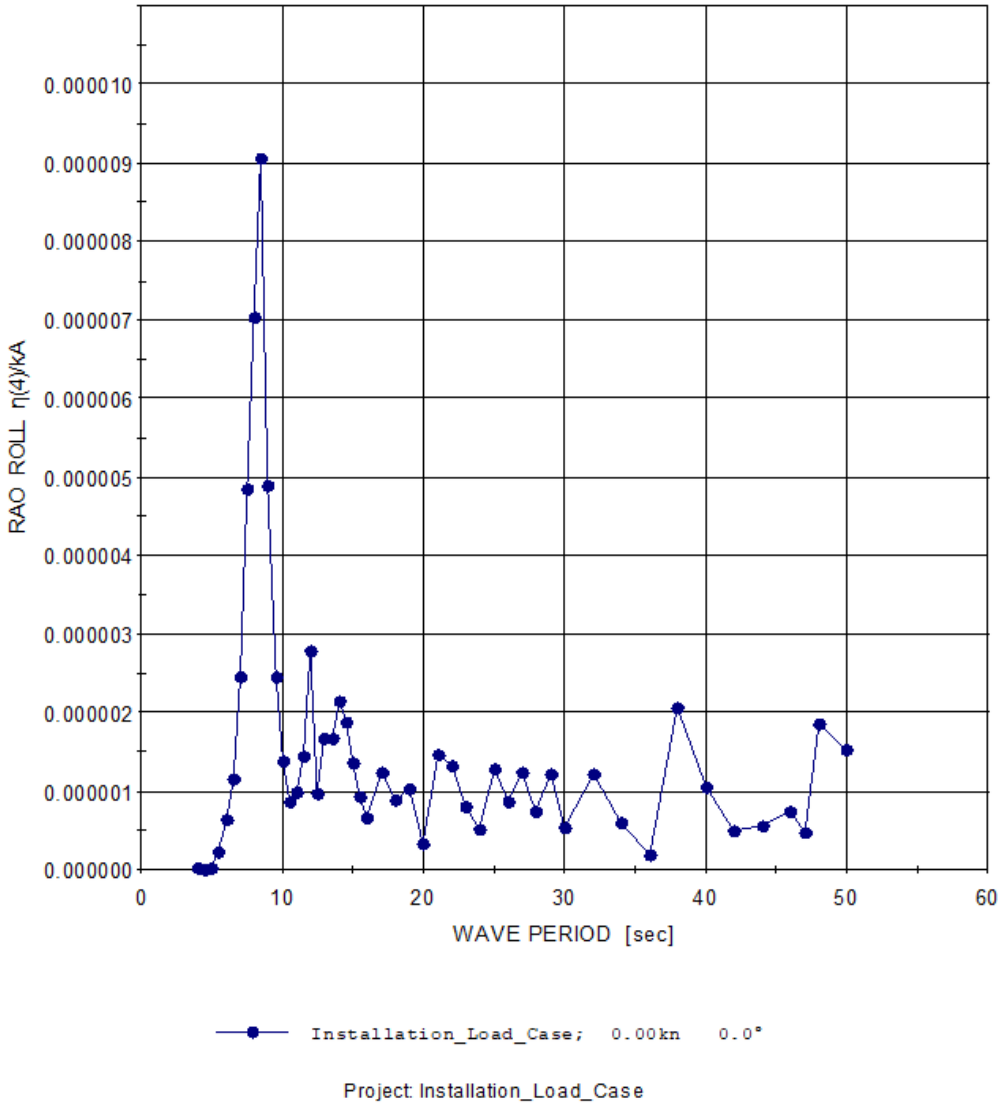

Project: Installation_Load_Case

ShipX - 19.05.2023 - 15:45:49 - Licensed to: Boa Management AS (Trondheim)

RESPONSE AMPLITUDE OPERATORS	ENCL. d)
	REPORT
	DATE 2023-05
	REF

DISPLACEMENTS

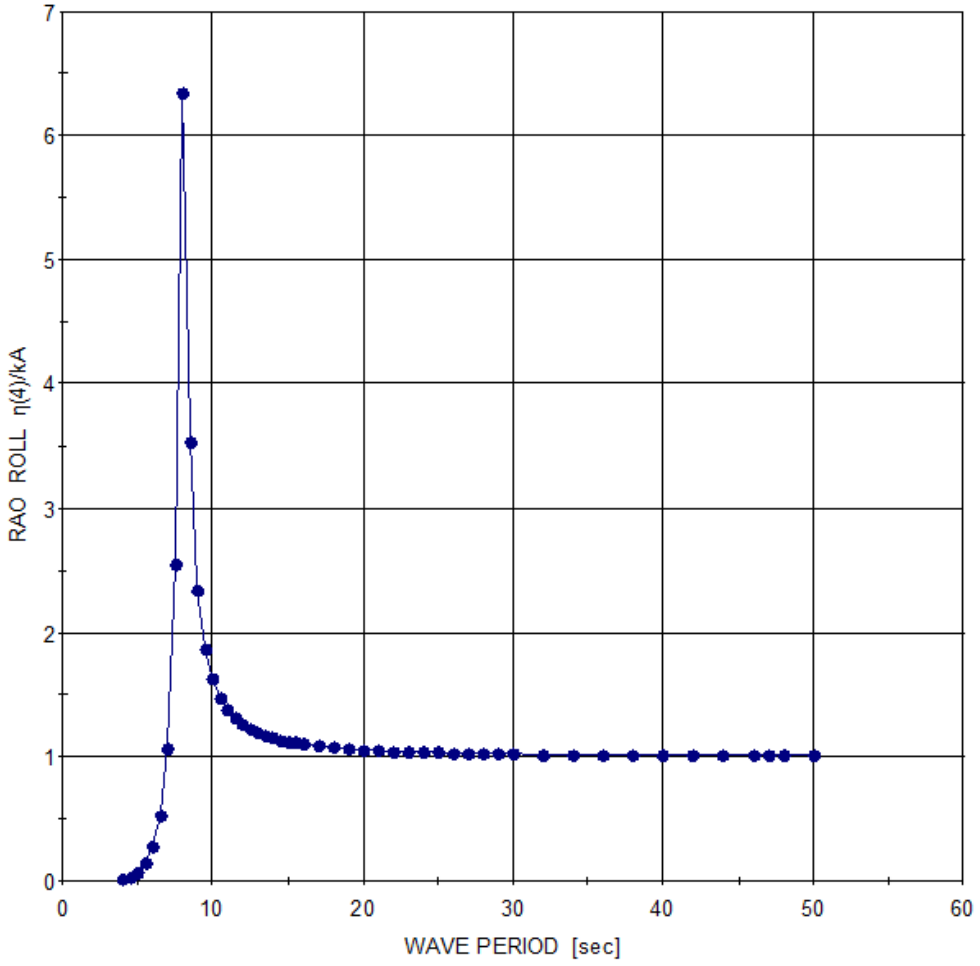

Project: Installation_Load_Case

ShipX - 19.05.2023 - 16:03:05 - Licensed to: Boa Management AS (Trondheim)

RESPONSE AMPLITUDE OPERATORS	ENCL. e)
	REPORT
	DATE 2023-05-28
	REF

DISPLACEMENTS

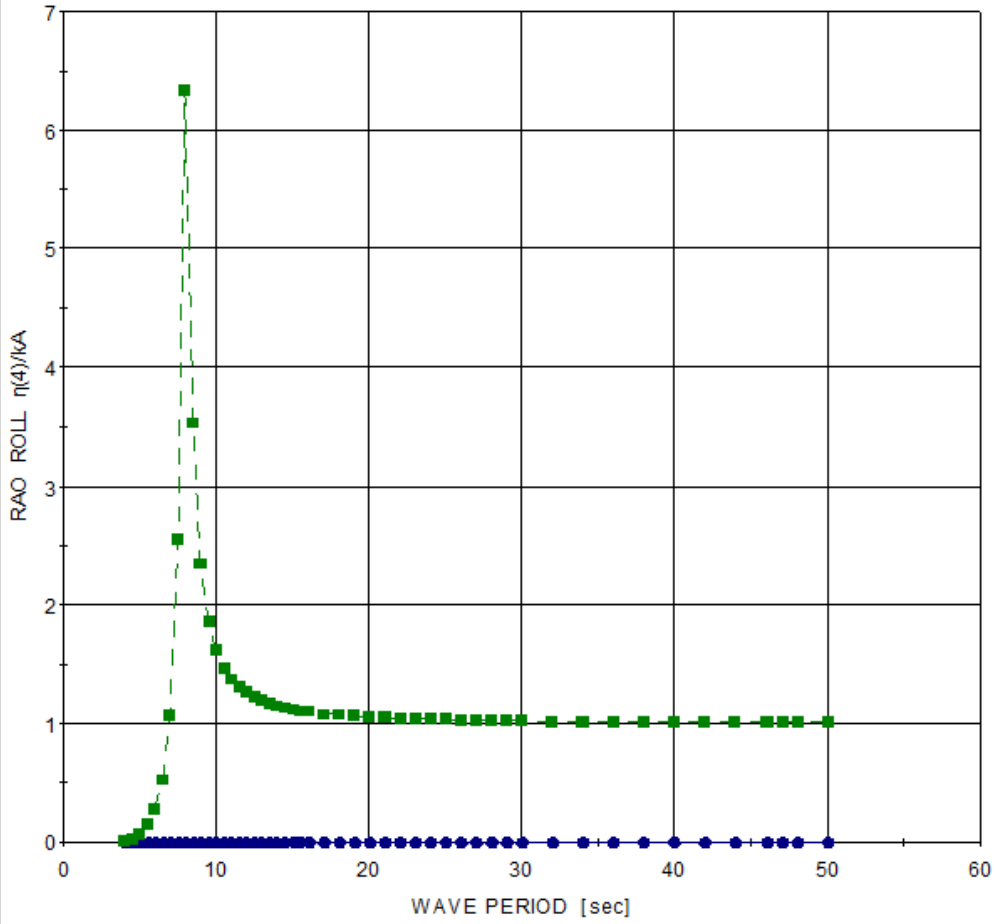

Project: Installation_Load_Case

ShipX - 19.05.2023 - 16:06:00 - Licensed to: Boa Management AS (Trondheim)

SPECTRAL ANALYSIS	ENCL. f)
	REPORT
	DATE 2023-0
	REF

Installation_Load_Case; 0.00kn 15.0°
HEAVE DISPLACEMENTS - FORCADOS, FEILD

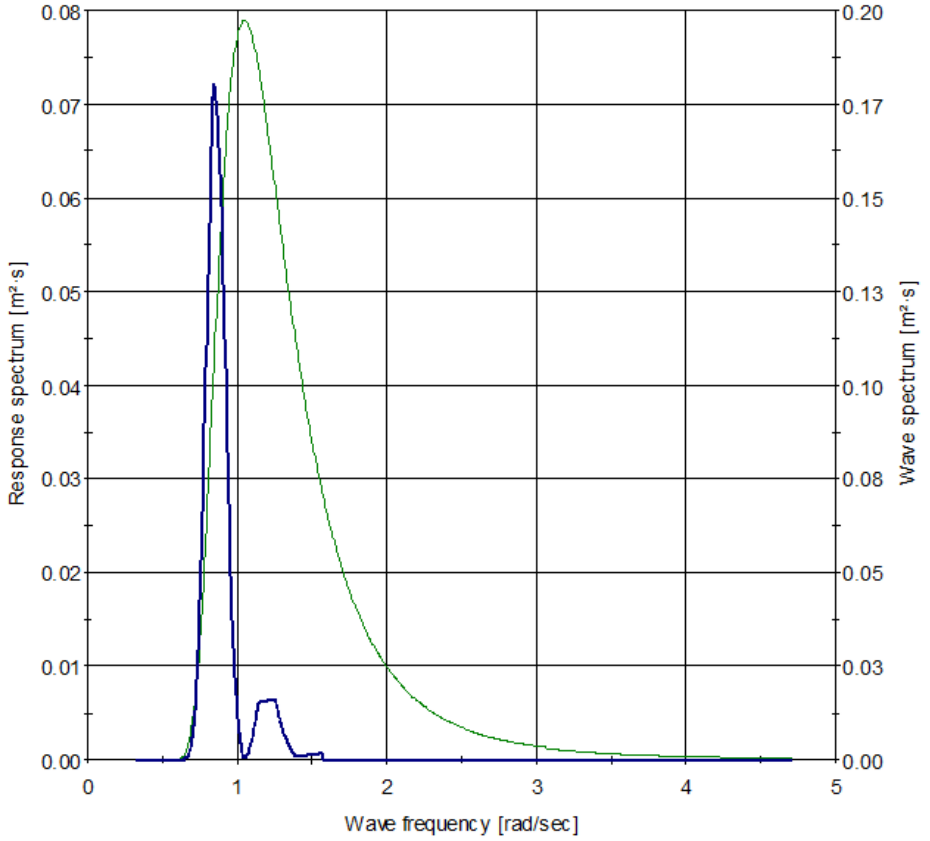

Response spectrum; m0 = 0.0125 m1 = 0.0112 m2 = 0.0103 ; Std.dev = 0.1119 m
Wave spectrum ; m0 = 0.1440 m1 = 0.1932 m2 = 0.2942 ; Hm0 = 1.52 m

Project: Installation_Load_Case
Wave spectrum Pierson-Moskowitz Hs = 1.52 m Tp = 6.0 sec
Long-crested seas

ShipX - 21.05.2023 - 16:13:22 - Licensed to: Boa Management AS (Trondheim)

SPECTRAL ANALYSIS	ENCL. g)
	REPORT
	DATE 2023
	REF

Installation_Load_Case; 0.00kn 0.0°
ROLL DISPLACEMENTS - BONGA FIELD

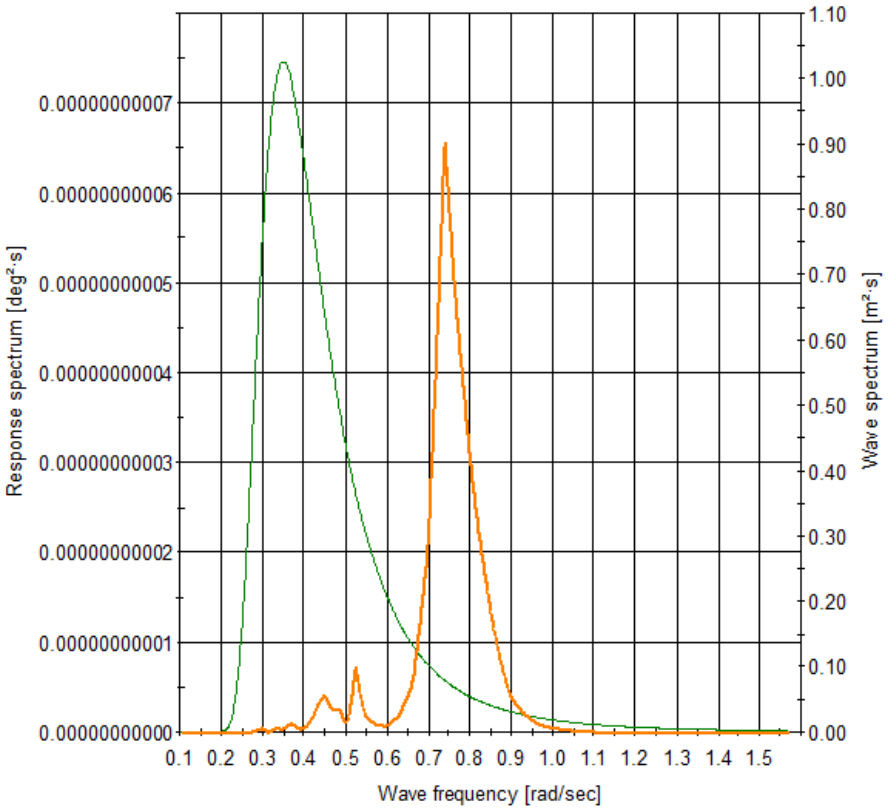

Response spectrum; m0 = 0.0000 m1 = 0.0000 m2 = 0.0000 ; Std.dev = 0.0000 deg
Wave spectrum ; m0 = 0.2492 m1 = 0.1115 m2 = 0.0566 ; Hm0 = 2.00 m

Project: Installation_Load_Case
Wave spectrum Pierson-Moskowitz Hs = 2.00 m Tp = 18.0 sec
Long-crested seas

ShipX - 21.05.2023 - 20:10:21 - Licensed to: Boa Management AS (Trondheim)

SPECTRAL ANALYSIS	ENCL. (686)
	REPORT
	DATE 2023-05-27
	REF

Installation_Load_Case; 0.00kn 30.0°
ROLL DISPLACEMENTS

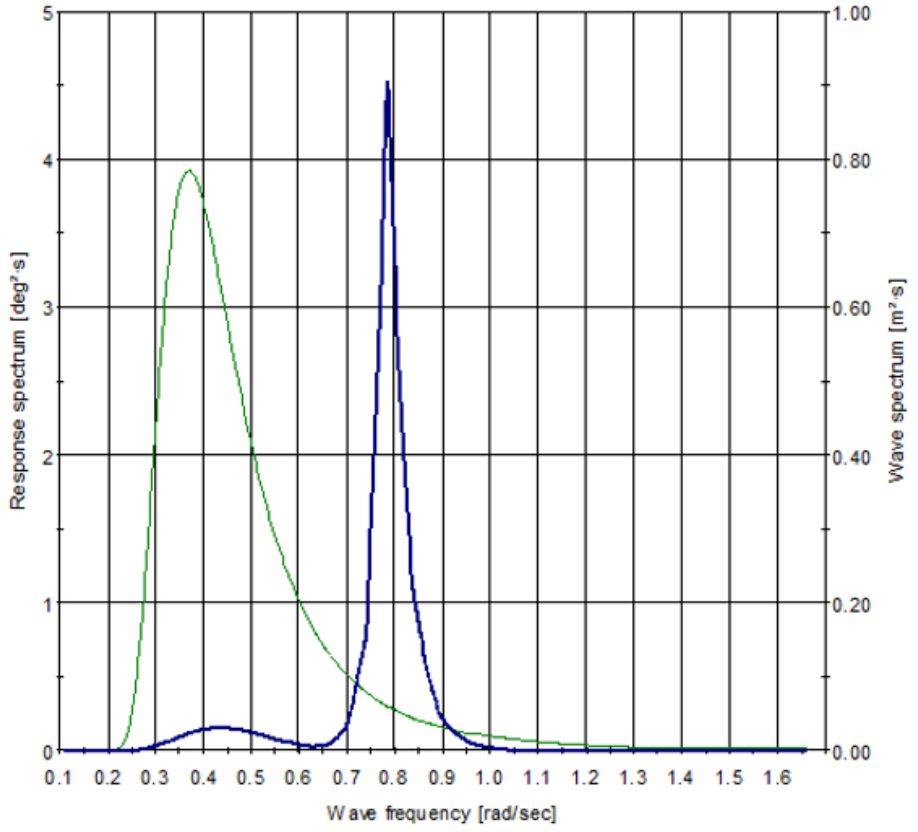

Response spectrum; m0 = 0.3509 m1 = 0.2680 m2 = 0.2091 ; Std.dev = 0.5924 deg
Wave spectrum ; m0 = 0.2019 m1 = 0.0956 m2 = 0.0514 ; Hm0 = 1.80 m

Project Installation_Load_Case
Wave spectrum Pierson-Moskowitz Hs = 1.80 m Tp = 17.0 sec
Long-crested seas

SPECTRAL ANALYSIS	ENCL. (761)
	REPORT
	DATE 2023-05-27
	REF

Installation_Load_Case; 0.00kn 30.0°
ROLL VELOCITIES

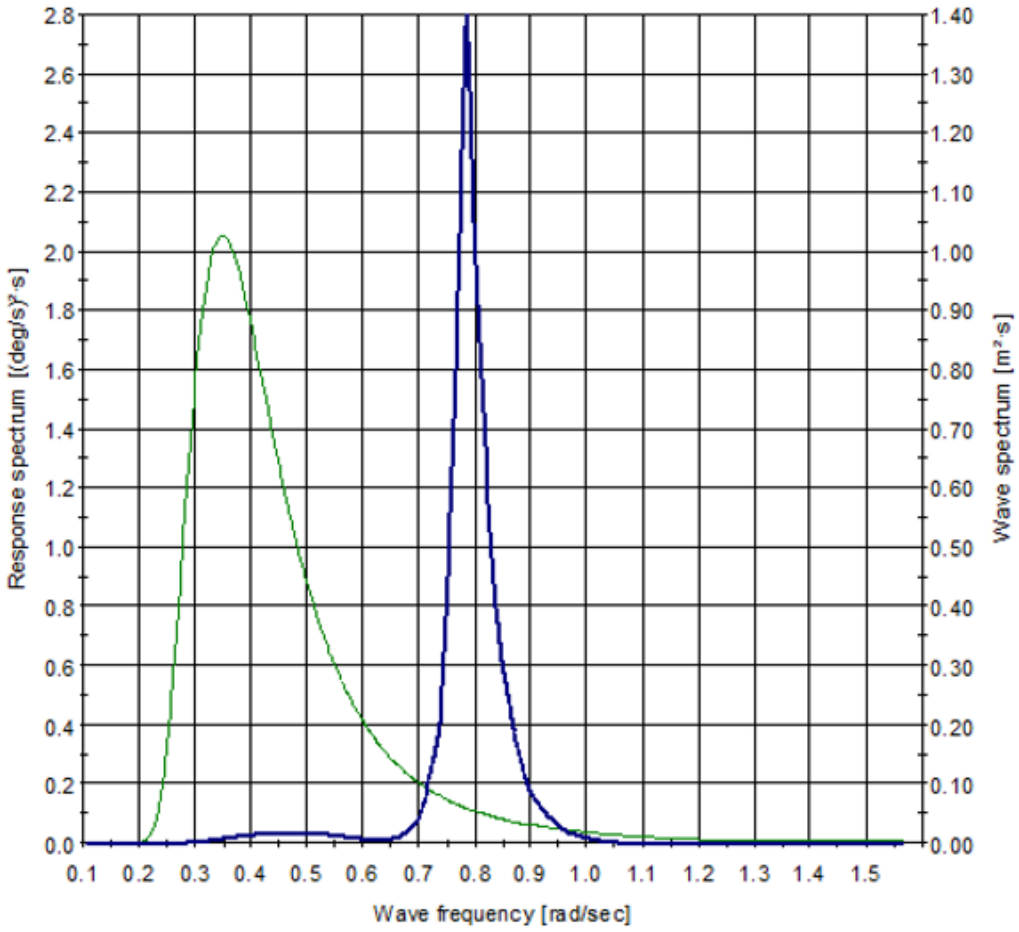

Response spectrum; m0 = 0.2087 m1 = 0.1647 m2 = 0.1313 ; Std.dev = 0.4569 deg/s
Wave spectrum ; m0 = 0.2492 m1 = 0.1115 m2 = 0.0566 ; Hm0 = 2.00 m

Project Installation_Load_Case
Wave spectrum Pierson-Moskowitz Hs = 2.00 m Tp = 18.0 sec
Long-crested seas

SPECTRAL ANALYSIS	ENCL. (801)
	REPORT
	DATE 2023-05-2
	REF

Installation_Load_Case; 0.00kn 90.0°
ROLL VELOCITIES

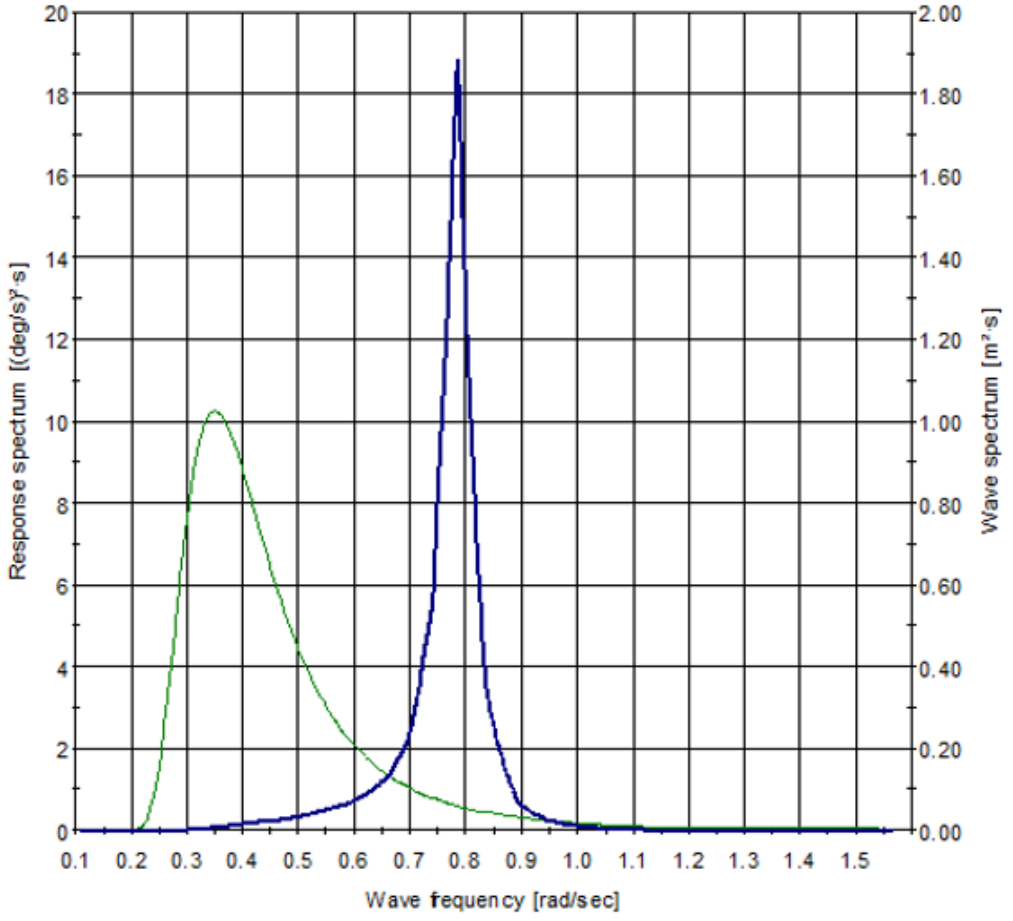

Response spectrum; m0 = 1.5684 m1 = 1.1971 m2 = 0.9252 ; Std.dev = 1.2524 deg/s
Wave spectrum ; m0 = 0.2492 m1 = 0.1115 m2 = 0.0566 ; Hm0 = 2.00 m

Project Installation_Load_Case
Wave spectrum Pierson-Moskowitz Hs = 2.00 m Tp = 18.0 sec
Long-crested seas

SPECTRAL ANALYSIS	ENCL. (453)
	REPORT
	DATE 2023-05-27
	REF

Installation_Load_Case; 0.00kn 90.0°
ROLL ACCELERATIONS - FORCADOS FIELD

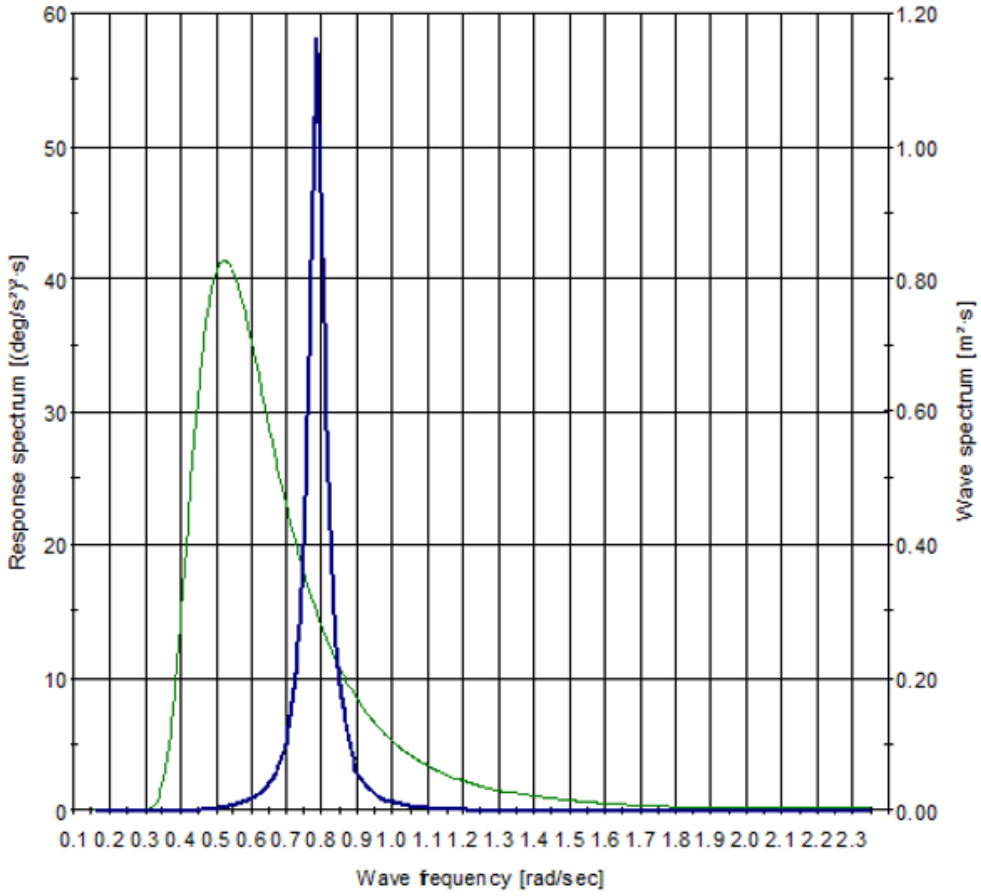

Response spectrum; m0 = 4.5511 m1 = 3.5867 m2 = 2.8480 ; Std.dev = 2.1333 deg/s²
Wave spectrum ; m0 = 0.3016 m1 = 0.2023 m2 = 0.1541 ; Hm0 = 2.20 m

Project Installation_Load_Case
Wave spectrum Pierson-Moskowitz Hs = 2.20 m Tp = 12.0 sec
Long-crested seas